Modeling Polymerization-based Amplification

by

Ji Sam Wong

B.S. Chemical Engineering
Cornell University, 2010

Submitted to the Department of Chemical Engineering
in partial fulfillment of the requirements for the degree of

Doctor of Philosophy in Chemical Engineering

at the

MASSACHUSETTS INSTITUTE OF TECHNOLOGY

June 2016

Signature of Author . . . . . .
Ji Sam Wong
Department of Chemical Engineering
Program in Polymers and Soft Matter
May 19, 2016

Certified by . . . . . .
Hadley D. Sikes
Assistant Professor of Chemical Engineering
Thesis Supervisor

Accepted by . . . . . .
Richard D. Braatz
Edwin R. Gilliland Professor of Chemical Engineering
Chairman, Committee for Graduate Students

Modeling Polymerization-based Amplification

by

Ji Sam Wong

Submitted to the Department of Chemical Engineering on May 19, 2016
in partial fulfillment of the requirements for the degree of
Doctor of Philosophy in Chemical Engineering

Abstract

Eosin, a photoreducible xanthene derivative, acts as a Type II photoinitiator of free radical polymerizations when used in combination with alcohols or amines as co-initiators. Previous work utilizing eosin in polymerizations focused on high concentrations of initiators but it has recently been gaining use in bio-applications at lower concentrations due to its ability to initiate polymerizations when illuminated by harmless visible light even in the presence of orders-of-magnitude larger amounts of dissolved oxygen which acts as an inhibitor.

We investigated the mechanism behind eosin's role in the polymerization process and its ability to initiate polymerization at concentrations lower than that of oxygen. A series of model simulation studies that systematically examined the effects of including additional elementary reactions based on proposed reactions in published literature into the classical free radical polymerization scheme without fitting any unknown parameters to experimental results were performed and analyzed.

The first study examined the effect on having an eosin regeneration reaction between the reduced eosin radical which is formed during the photogeneration of free radicals, and the peroxy radical formed by inhibiting reactions of propagating radicals with oxygen. This reaction results in an unreactive hydroperoxy species and the regeneration of ground state eosin which can then produce even more radicals that undergo propagation. The simulation results indicated that the additional eosin regeneration reaction did explain eosin's ability to initiate polymerization at lower concentrations than oxygen, but the best predicted times required for the formation of polymer was larger than experiments by an order of magnitude, suggesting that the reaction scheme was incomplete.

We subsequently incorporated an amine chain peroxidation reaction into the overall reaction scheme and determined the effects of such a change. The amine chain peroxidation reaction involves the peroxy radical extracting a hydrogen atom from the

tertiary amines present in the reaction mixture, forming an unreactive hydroperoxide species and an amino-radical that can further undergo propagation. The addition of this reaction greatly increased the rate of oxygen consumption and reduced the predicted polymerization times to an order of magnitude lower than experiments.

In addition to purely kinetic studies on the overall reaction scheme, a one-dimensional reaction-diffusion model was also created to understand the effects of having a continuously diffusing oxygen flux on the overall polymerization process. The time course of polymerization and spatial variations when using the various reaction schemes were analyzed and contrasted. The models predicted the formation of a reaction front which forms at the onset of polymerization and slowly moves towards the closed surface, tracking the diffusion of oxygen back into the reaction system. A surface region of higher eosin concentrations was also simulated to model the effects of binding events occurring in polymerization-based amplification (PBA). The addition of a small amount of eosin on the surface resulted in slightly faster predicted polymerization times close to the surface, similar to experimental observations where a surface polymer is first formed before the whole solution polymerizes where binding events have occurred.

Thesis Supervisor: Hadley D. Sikes
Title: Assistant Professor of Chemical Engineering

Contents

List of Schemes

List of Figures

List of Tables

Chapter 1. Introduction

1.1 Free radical polymerization

Free radical polymerizations have been utilized in many different industries to generate useful polymeric products such as coatings, films and resins[1–4]. Its products are ubiquitous throughout modern society, being utilized in a variety of applications such as packaging material, protective equipment, structural support, conduits, coatings and adhesives. These varied uses are all on dependent the mechanical and chemical properties of the polymeric material, which are in turn contingent on the chemical structure as well as processing conditions during the synthesis of the polymer. Understanding the kinetics of the polymerization process is therefore crucial for controlling the properties of the end product obtained.

In free radical polymerizations, reactive free radicals produced from initiators are able to add to a monomer molecule's C=C double bond to form a new radical center that can also undergo the same reaction. When this addition of monomers to the radical is successively repeated, a long chain polymer is formed as the reactive center is propagated along the length of the chain. Polymer chain growth can be hampered or terminated by reaction with other reactants in the mixture, and the relative rates of propagation, termination and chain transfer are all dependent on the type of reactive radical center as well as the reaction conditions during the various stages of polymerization. The types and relative concentrations of monomers or any other compounds used in the polymerization mixture can thus affect the final properties of the resulting polymer as the distribution of polymer lengths and type of polymer formed determines the properties of the subsequent product.

Free radical photopolymerizations are a subset of the general class of polymerizations initiated by free radicals. Major advantages of using photopolymerizations are that the reactions are rapid and are able to proceed at room temperature instead of requiring higher temperatures for reasonable polymerization

times when using thermal initiated polymerizations. Another significant benefit to using photoinitiators instead of traditional thermal decomposition initiators is that formation of the final polymer product can be easily controlled by manipulating the duration, intensity and direction of the light source as well as by selecting the appropriate photoinitiator to be used based on its absorptivity and reactivity at the wavelength of the light source[4–6]. Depending on the end use, various combinations of monomer and photoinitiator systems that produce free radicals can be utilized, with the final properties of the product, which are determined chiefly by the degree of polymerization, controlled through manipulation of reaction conditions during the processing steps. The formation of polymer product can be temporally controlled through the choice of light wavelength, intensity, and exposure time while spatial control is obtained by utilizing photomasks, optics, or initiator concentration gradients.

However, despite all these benefits of free radical polymerizations, a critical complicating factor for free radical polymerizations is the need to prevent inhibition of reactions by inhibitors such as oxygen[7–12]. Oxygen is a potent inhibitor of free radical polymerization reactions as it reacts quickly with carbon-centered free radicals at diffusion-limited rates, forming peroxy radical species that are less reactive towards C=C double bonds as compared to the original carbon radicals, thus creating an inhibition time whereby double bond conversion is negligible and slowing down the overall rate of polymerization. Common methods used to overcome this problem are to either saturate the polymerization mixture with initiators, or purge the system with an inert gas to drive out oxygen before proceeding with the polymerization[11] reduce the inhibition time, but incur additional processing time, cost and effort.

1.1.1 Kinetics of free radical polymerizations

The kinetics of classical free radical polymerizations are well-studied, with the overall chain reaction consisting of three steps in sequence to generate a polymer: initiation, propagation and termination. The initiation step involves the production of a free radical from the initiating species, after which this initiator radical adds to the first monomer to produce the initial chain radical. This chain radical can then successively add more monomers during the propagation step, gradually increasing in chain length. At some

point during the polymerization process, the growing chain radical can undergo chain termination, where the radical centers are annihilated through a bimolecular reaction between two radical species. One dead polymer chain from the chain radical is formed from this reaction, with the other product from termination, depending on radical species it is derived from, also becoming unreactive as a radical as well.

Modeling of complex chemical reaction schemes are often performed in order to understand the reaction mechanisms and study in detail the effects of changing the reaction conditions. Free radical polymerizations in bulk or solutions have been studied extensively for many years[3,13–15], and various models having been successfully applied to systems concerning free radical polymerizations in bulk and solutions[3,5,13–17]. These models for free radical polymerization generally consist of initiation, propagation and termination reactions that are taken as irreversible. The pseudo-steady state assumption and terminal or penultimate models are also used to simplify the rate equations[18]. Further extensions of these simple kinetic rate-equation models have also modeled radical trapping[19] as well as helped provide evidence for reaction-diffusion[20] during polymerization of multifunctional monomers. In many of these cases, the models are attempting to match with experimental results[21–23] where a large degree of conversion is desired, as that is the point at which the mechanical or surface properties of the polymer become suitable for their various applications.

For example, Goodner & Bowman[24] proposed a model that includes diffusion-controlled kinetics through free volume considerations for the free radical photopolymerization of millimeter-thick films used as coatings, with the paper focusing mainly on the high conversion rates for bulk polymerization of solvent-free monomers and the auto-acceleration effect. In these cases, the goal is usually to create a model that is able to determine the conversion profile from bulk or solution polymerizations at different starting conditions whereby the inhibition effects of oxygen are kept under control either by purging the system to remove any oxygen present or by adding large amounts of 5 wt% or more initiators in order to consume all the oxygen present in the system.

On the other hand, Kizilel & Kizilel[25] modeled the surface-initiated photopolymerization of PEGDA and VP to track the polymerization progress as cross-links form and begin to form a gel structure. In their comprehensive model, they obtained estimates of some unknown kinetic parameters through fitting their model to their experimental data and modeled the spatial dependence of the change in cross-link density and gel thickness with time as polymerization proceeds.

1.2 Polymerization-based Amplification (PBA)

Early diagnosis of diseases has been shown to be a vital factor in the effective and successful treatment of the resulting medical condition. Thus, the detection of minute quantities of various target biomolecules that indicate the presence of disease has become a major goal in the field of medical diagnostics. Due to the extremely low concentrations of certain biomarkers in the body, there is a need to distinguish between the actual signal and random background noise; signal amplification is therefore required in order to detect ultralow concentrations of analytes that would otherwise go unnoticed when using direct readout methods. Different tests for various types of biomarkers have since been developed, and polymerization-based amplification (PBA) has been proposed as a method that is well-suited for compact molecular diagnostic devices due to its high sensitivity and simple operation.

The PBA system generally consists of three major parts: a binding event where a surface-attached molecule binds to the analyte of interest, a second binding event where a photoinitiator-labeled species (macrophotoinitiator) is used to detect the complex, and finally a free radical copolymerization reaction to form a gel layer only where the complex is bound to the surface. It has been shown to be reproducible, sensitive, tolerant to complex fluids and relatively easy to perform, making it one of the most promising method of producing a signal from very small amounts of target molecules[9]. The specific binding of DNA[26], antigens and antibodies[27], nuclear membrane receptors and ligands[28] or an avidin-initiator conjugate to a biotin-biomolecule[29] conjugate allows for the detection of tiny amounts of target analytes through the copolymerization of monomers only at specific sites where the binding

interactions are occurring. The higher concentrations of initiator at the binding sites result in a detectable change as a visible polymer film forms at these specific areas before the whole bulk solution is able to polymerize. This general concept behind PBA has been shown to work well in a number of cases[28,30], and the ideas are starting to be employed in ever more applications.

PBA in its current form utilizes free radical polymerization as opposed to other types of polymerizations such as living polymerizations or metathesis polymerizations due to its simplicity and fast reaction times; surface-initiated free radical polymerizations are able to form micron-thick polymer films in minutes as compared to hours for nanoscale films for living polymerizations. Thus, when the exact properties of a polymer film are not critical and only the presence of a thick film is of any significance, the speed and flexibility afforded by using free radical polymerizations without requiring special reagents make it a good fit for use in diagnostic applications.

1.2.1 Eosin as a visible light photoinitiator for PBA

With recent burgeoning interest in biomaterials and its applications in healthcare, eosin, a photoreducible xanthene dye, has recently garnered much attention as a photoinitiator that works using harmless visible light to produce useful biopolymers. With a peak absorption wavelength of about 525 nm and a peak molar absorptivity of around 12,000 cm^{-1} M^{-1}, eosin can be easily promoted to a photoexcited state using visible green LED lights. When used in combination with tertiary amines as a co-initiator, eosin has been shown to initiate polymerization of acrylate monomers[5,31–33] that result in micron-scale hydrogel films under inert gas-purged conditions. Furthermore, low micromolar concentrations of xanthene dye derivatives, which eosin is an example, have also been shown to have an improved ability to reduce the effects of oxygen inhibition without the need for purging[10,34], making it a useful initiating system for applications containing biologically sensitive species as in PBA[9,26,27,35]. This ability of low concentrations of eosin, in combination with tertiary amines in the presence of light, to overcome inhibition by millimolar concentrations of dissolved oxygen and initiate rapid aqueous polymerization of vinyl pyrrolidone (VP) and poly(ethylene glycol) diacrylate (PEGDA) was not observed when other photoinitiators such as

benzophenones[34] and Irgacure 2959[34] were used as substitutes. This particular combination of monomers and initiators is of particular interest as it has been utilized in various applications of PBA and found to be an important component of the whole process[10].

1.2.2 Eosin's resistance to oxygen inhibition

The presence of inhibitors in the reaction mixture has a major effect on the PBA response, with dissolved oxygen shown to influence inhibition time and delay the onset of polymerization[10]. Using eosin in combination with triethanolamine (TEA) in the monomer solution allows for the polymerization of acrylate monomers to form hydrogels without purging with inert gases, even as a constant influx of oxygen from open air[10,34,36,37] is diffusing in. However, Kaastrup & Sikes[10] have since shown that adding only sub-micromolar concentrations of extra free eosin to the amplification solution, in addition to eosin which was already conjugated to the macrophotoinitiators bound to the surface, can reduce the inhibiting effects of oxygen during the PBA process without affecting the sensitivity. This new formulation for amplification solutions[10,36,38–40] containing eosin in addition to the usual amounts of monomers have been found to help in simplifying PBA procedures while also accelerating the speed of polymerization.

Despite the successes in getting PBA to perform well experimentally, there is a lack of theoretical understanding about the processes behind the amplification response of PBA. Because of PBA's relatively short history, systematic experimental investigations of the diverse parameters of the system have yet to take off, and further optimizations of the PBA procedures to improve sensitivity and signal response are still possible. Similarly, mathematical analysis of the PBA system is also lacking in the literature, and many aspects of the PBA system have yet to be explored in great detail. Various models have been proposed for free radical polymerizations using different types of initiators and the effect of a reaction system open to oxygen has also previously been modeled in the literature, but few polymerization models have explored the mechanisms and trends of photoinitiation systems with amounts of photoinitiators smaller than that of the concentration of dissolved oxygen.

1.2.3 Modeling efforts

Previous numerical models[23,25] incorporating the eosin-tertiary amine initiation system assumed oxygen was absent as much prior experimental work[26,32,33] focused on the ability of the initiation system to polymerize acrylate monomers under inert gas-purged conditions. Thus, theoretical contributions towards the elucidation of the mechanism behind eosin's ability to initiate polymerization in the presence of a large excess of oxygen are lacking as these models also estimated the unknown rate constants associated with initiation by using them collectively as a fitting parameter to match model results with experimentally measured conversion profiles. In those cases, the effect of the regeneration of eosin was also insignificant due to the absence of inhibiting oxygen as opposed to PBA reactions where eosin concentrations are purposefully kept low to prevent non-specific polymerizations while also operating in open air with a constant replenishment of oxygen from the open surface.

Two characteristics that are of significance in our eosin-based PBA system are the remarkable ability of eosin to readily overcome oxygen inhibition, and the requirement that a polymer film should first form at the surface where binding events are occurring before the bulk solution begins to polymerize and render the signal response indistinguishable from the background. Based on their experimental results, Avens & Bowman[34] have proposed a cyclic dye regeneration mechanism that could explain the effectiveness of eosin in overcoming inhibition caused by the dissolved oxygen. In their proposed mechanism, eosin radicals, created by hydrogen transfer from a tertiary amine to eosin, can react with peroxy radicals which were formed by the reaction of polymer radicals with oxygen, thereby regenerating eosin which can further initiate polymerization. This study was a recent first step in trying to explain the reason behind eosin's exceptional ability to initiate free radical polymerizations in the presence oxygen even at very low concentrations, but the field is still wide open for further investigations into the exact mechanism of eosin regeneration.

As the eosin-tertiary amine initiation system gets utilized in more applications requiring visible-light initiated polymerizations in open air, a greater understanding of the effects of oxygen diffusion and its resulting trends on the polymerization process would be greatly useful in optimizing reaction conditions in order to control and obtain the final

product that we want. There is a lack of understanding on the principles behind the interfacial polymerization response at specific sites in PBA, and modeling approaches which consider plausible mechanisms that cause such responses would be useful in helping to optimize reaction conditions for the best possible outcome. With such a unique initiation system, there has been a lack of models that investigate the polymerization process utilizing this eosin-tertiary amine initiator system. Thus, modeling the PBA system is projected to be a fruitful endeavor as a deeper understanding of the mechanism and polymerization process can provide a basis for modifying current implementations to improve performance while also driving further deployment of PBA to other systems.

1.3 Thesis Overview

The main objective of this thesis is to develop a working model for eosin-tertiary amine initiated photopolymerizations in the context of PBA. I investigated the chemical mechanism underlying the ability of the eosin-tertiary amine system to initiate polymerization in the presence of excess oxygen using a systematic approach whereby the reaction kinetics are first understood by solving the set of ordinary differential equations (ODE) using kinetic rate equations derived from the overall reaction scheme. Considering that it is always possible to match experimental conversion profiles with a model by treating unknown rate constants or collections of rate constants as fitting parameters, this customary modeling approach cannot be used as evidence to support a proposed mechanism. Thus, we have taken a different approach whereby we build upon the classical model of free radical polymerization by systematically adding reactions that support the trends obtained from experiments while using established kinetic rate constants from literature for well-known reactions. Sensitivity analyses were performed on uncertain kinetic rate constants for the new proposed reactions in order to examine the effects of its inclusion into the reaction scheme. Starting with the relatively simpler system of ODEs allows us to determine how the various reactions are interdependent on one another before moving on to the more complex reaction-diffusion models. The system of kinetic rate equations was then extended into reaction-diffusion

models that allowed for the diffusion of molecular species and incorporated the replenishment of oxygen through the addition of an oxygen flux boundary condition.

Chapter 2 describes the effects of a proposed peroxy radical mediated eosin regeneration reaction on the overall polymerization process. In Chapter 3, a reaction-diffusion model incorporating this eosin regeneration reaction was numerically solved at various eosin concentrations pertinent to PBA and subsequent simulation results analyzed, focusing on the effects of the replenishment and diffusion of oxygen on the spatial profiles during polymerization. Chapter 4 then summarizes the impact amine chain peroxidation has on the overall reaction kinetics. Chapter 5 follows up on work done in Chapters 3 and 4 by studying the impacts of including amine chain peroxidation on the reaction-diffusion model with a continuous oxygen flux at one end. In addition, a surface region of higher eosin concentration modeling the binding events occurring for positive test results in PBA was also simulated and its effects on the progress of polymerization investigated. In Chapter 6, two different reactions expected to slow down oxygen consumption and its effects on polymerization were briefly modeled and investigated. Finally, we conclude in Chapter 7 with a summary of the main findings and some suggestions for future follow-up work.

Chapter 2. Significance of peroxy radical mediated regeneration of eosin

Portions of this chapter are reproduced from Wong, J.; Kaastrup, K.; Aguirre-Soto, A.; Sikes, H. D. Polymer (Guildf). 2015, 69, 169–177.

Abstract

Eosin, a photoreducible xanthene, reacts with tertiary amines and initiates the free radical photopolymerization of aqueous solutions of acrylate monomers. This reaction proceeds even in the presence of a large excess (~1000X) of inhibiting oxygen via a mechanism that has not been established conclusively. This chemistry has proven useful in the area of biosensing, where the formation of a hydrogel on the time scale of seconds serves as a macroscopic, amplified signal that can be connected to molecular recognition events. In this work, we built a kinetic model to quantitatively explore a mechanism in which eosin is regenerated through the reaction of eosin-based radicals with peroxy- radicals formed from oxygen-inhibition reactions. To determine whether the predictions of this model are consistent with conversion profiles measured using real-time FTIR, we refrained from fitting rate constants or other unknown parameters associated with individual steps in the mechanism to the conversion profile. Rather, we considered physical upper bounds and performed sensitivity analyses spanning several orders of magnitude to predict the reactivity of the system. We explored the effects of the peroxy- mediated regeneration rate constant, kregen, and the initial eosin concentration on the irradiation time that is required to reach a C=C bond conversion of 0.2 ($t_{0.2}$). At this C=C bond conversion, the aqueous monomer solutions studied herein have become hydrogels. The predictions of the model capture several trends that we have observed experimentally. However, even when the rate constants associated with eosin regeneration via reaction with peroxy- species are set at the physical upper bounds, the values of $t_{0.2}$ predicted by the model are much larger than those that we observed experimentally. The results presented herein motivate and provide a framework for future work to more fully elucidate the mechanism of this interesting and useful photopolymerization reaction.

2.1 Introduction

Free radical photopolymerization chemistry[2,3,5] is used routinely in several well-established industries to generate polymeric products such as coatings, films and adhesives[41,42], and intense efforts are underway to use similar chemistry for emerging applications such as regenerative medicine[43–45] and molecular diagnostics[38,46–48]. These polymerization reactions proceed rapidly at room temperature with a variety of radical-producing photoinitiator systems[6], with the formation of the polymer product temporally controlled by choice of wavelength, intensity and exposure time[49], and spatially controlled by using photomasks[46,50], optics[4,51], or local concentration gradients of initiators[10,35,52,53]. However, a critical issue precluding exploitation of the full potential of radical polymerization reactions is oxygen inhibition[7–11]. Because dioxygen reacts with carbon-centered radicals at diffusion-limited rates and the resulting peroxy- radical species react slowly with carbon-carbon double bonds, oxygen serves as a potent inhibitor of acrylate polymerization reactions that proceed through chain-growth mechanisms.

Common strategies to overcome oxygen inhibition include saturating the polymerization mixture with initiators so that initiators are more abundant than oxygen, and purging the system with an inert gas to drive out oxygen before proceeding with the polymerization[11]. These methods significantly reduce the inhibition time, but incur additional processing cost and effort. Newer polymer synthesis techniques such as Activator Generated by Electron Transfer Atom Transfer Radical Polymerization (AGET ATRP)[54] and thiol-ene[55] polymerizations have been shown to proceed in air. However, the controlled nature of ATRP reactions makes them slow for some practical purposes, and the step-growth nature of thiol-ene polymerizations is not well suited to some applications.

One such practical application is polymerization-based amplification[9,10,26,56,57] (PBA), a recently developed biosensing technique where polymer films are grown *in situ* by the user in order to detect and quantify molecules in bodily fluids that indicate health or disease. In this technique, initiator molecules are localized near a surface as a function

of molecular recognition events. An amplification solution containing monomers is supplied to the system along with a suitable input of energy, and polymer films form if a sufficient number of binding events have occurred. Air-tolerant polymerization reactions simplify PBA procedures; however, the use of AGET ATRP for PBA is not ideal as it requires hours to achieve nanometer-thick films that cannot be easily detected[56,57], making it unsuitable for diagnostic tests that require rapid response times. Conversely, eosin, a photoreducible xanthene dye, has been shown to initiate polymerization reactions that result in micron-scale hydrogel films in thirty-five seconds to two minutes in air in this context[10,36,38], making it a suitable choice as a photoinitiator for PBA when rapid response times are required.

Previous experimental work[26,32,33] using eosin in combination with a tertiary amine focused on the ability of the initiation system to polymerize acrylate monomers under inert gas-purged conditions to form hydrogels localized at interfaces. Recent experimental evidence shows that inclusion of sub-micromolar concentrations of eosin in the monomer solution allows the reaction to proceed without purging using inert gases and in the presence of a constant influx of oxygen from air[10,34,36], but theoretical contributions towards the elucidation of the mechanism behind eosin's ability to initiate polymerization in the presence of a large excess of oxygen are lacking. Previous numerical models[23,25] incorporating the eosin-tertiary amine initiation system assumed oxygen was absent and estimated the unknown rate constants associated with initiation by using them collectively as a fit parameter to match model results with experimentally measured conversion profiles. This approach was well justified and informative in past studies where the focus was to support the use of these hydrogels as biomaterials for cell and tissue engineering; polymer properties such as crosslink density and film thickness were well described using these models. In contrast, our focus herein is to investigate the chemical mechanism underlying the ability of the eosin-tertiary amine system (Scheme 2-1) to initiate polymerization in the presence of excess oxygen. Since treating unknown rate constants or collections of rate constants as fit parameters ensures that a model will match experimental conversion profiles, this approach cannot be used as evidence consistent with or inconsistent with a proposed mechanism. Thus, we have taken a different approach in this work.

Scheme 2-1. Chemical structures of photoinitiation system and monomers

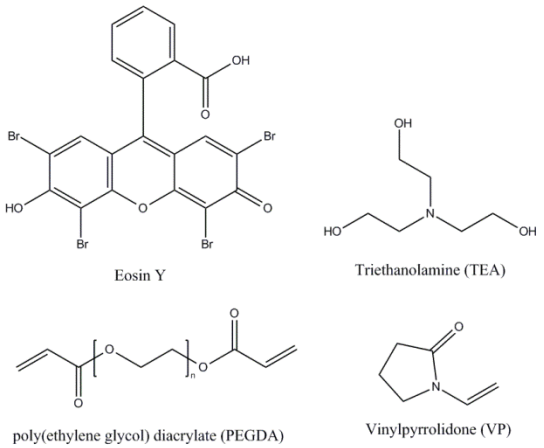

As a starting point for mechanistic investigation, Avens and Bowman[34] provided convincing experimental evidence that pathways exist for the regeneration of eosin after the following simplified overall photo-initiation reaction (1) occurs, where E is eosin and TEA is triethanolamine:

$$E + TEA \xrightarrow{h\nu} EH\bullet + TEA\bullet \quad (1)$$

Of the two products of this reaction, the amine-derived radical is much more reactive towards C=C bonds and thus serves as the initiating species in acrylate polymerizations. Avens and Bowman studied this initiation reaction in the presence of oxygen and also in the presence of (2,2,6,6-Tetramethyl-1-piperidinyl)oxy (TEMPO) inhibitor.[34] They used variable reaction stoichiometries and real-time FTIR measurements to *i.)* establish that a cyclic eosin regeneration mechanism underlies the resistance of this system to oxygen inhibition and *ii.)* show increased termination in the eosin system in comparison with termination in an analogous polymerization reaction initiated using a cleavage-type initiator. Avens and Bowman ruled out mechanisms which include eosin absorbing a single photon and triggering a chain reaction that generates many radicals, and concluded that the following eosin regeneration mechanism is one probable explanation that is qualitatively consistent with the kinetic data:

$EH\bullet + P_nOO\bullet \rightarrow E + P_nOOH$ (2)

where $P_nOO\bullet$ is the product of the reaction of any propagating radical species with dioxygen. The goal of this work is to quantitatively investigate this mechanism using kinetic modeling. Does the proposed regeneration mechanism quantitatively predict the experimentally observed inhibition periods as the eosin concentration is varied in the 0.1-10 μM range with 0.5 mM dissolved oxygen? This concentration of dissolved oxygen is typical for aqueous solutions equilibrated with the atmosphere. If not, what is the magnitude of alternative or additional regeneration reactions for eosin that must be elucidated? To answer these mechanistic questions, we refrain from introducing adjustable parameters or fitting data to a model that represents an assumed mechanism. Rather, we have listed a system of elementary reactions, formulated the ordinary differential equations that describe the kinetics of each reaction, and used well-established rate constants and known reactant concentrations to simultaneously numerically solve the resulting system of equations. In cases of unknown rate constants for reactions involving radical species of low molecular weight, we have used diffusion-limited values representative of the upper limit of physical possibility and we have performed sensitivity analyses to account for the possibility of lower values.

2.2 Model development

We integrated the elementary reactions associated with the proposed eosin regeneration mechanism into a classical model of free radical polymerization consisting of initiation, propagation, and termination reactions. The overall reaction scheme with the corresponding rate equation for each elementary reaction is summarized in Scheme 2-2, with a particular focus on the critical reactions in this scheme that have not been examined previously from a quantitative perspective. These reactions center on the regeneration of eosin (Eq. 19). As proposed by Avens & Bowman[34], peroxy- species $\mathrm{P_nOO\cdot}$ can react with the photoreduced eosin intermediate $\mathrm{EH\cdot}$ formed in Eq. 5 to yield an unreactive species $\mathrm{P_nOOH}$ and eosin that is able to further initiate radical formation.

2.2.1 Reaction mechanisms

In our system, the photoinitiator eosin (E) is first activated by light to give an excited state eosin in its triplet state (E*) as in Eq. 3, where ε is the molar absorptivity of eosin, I_0 is the light intensity, [E] is the concentration of eosin and E' is the energy content per mole of photons that the eosin absorbs. The excited photoinitiator can then be deactivated through various nonreactive processes such as fluorescence and vibrational relaxation, which are lumped into k_{deact} as an overall rate constant in Eq. 4.

Scheme 2-2. Overall reaction scheme utilized in the kinetic rate model

Photogeneration of radicals:

$$\mathrm{E} \xrightarrow{\mathrm{hv}} \mathrm{E}^* \qquad \text{Rate} = \frac{\varepsilon\, I_0\, [\mathrm{E}]}{E'} \qquad (3)$$

$$\mathrm{E}^* \xrightarrow{k_{deact}} \mathrm{E} \qquad \text{Rate} = k_{deact}\,[\mathrm{E}^*] \qquad (4)$$

$$\mathrm{E}^* + \mathrm{TEA} \xrightarrow{k_i} \mathrm{EH}\bullet + \mathrm{TEA}\bullet \qquad \text{Rate} = k_i[\mathrm{E}^*][\mathrm{TEA}] \qquad (5)$$

Initiation:

$$\mathrm{TEA}\bullet + \mathrm{PEGDA} \xrightarrow{k_{p,A}} \mathrm{P_n}\bullet \qquad \text{Rate} = k_{p,A}[\mathrm{TEA}\bullet][\mathrm{PEGDA}] \qquad (6)$$

$$\mathrm{TEA}\bullet + \mathrm{VP} \xrightarrow{k_{p,B}} \mathrm{P_n}\bullet \qquad \text{Rate} = k_{p,B}[\mathrm{TEA}\bullet][\,\mathrm{VP}] \qquad (7)$$

$$\mathrm{P_nO}\bullet/\mathrm{TEA}-\mathrm{O}\bullet + \mathrm{PEGDA} \xrightarrow{k_{p,A}} \mathrm{P_n}\bullet \qquad \text{Rate} = k_{p,A}[\mathrm{P_nO}\bullet][\mathrm{PEGDA}] \qquad (8)$$

$$\mathrm{P_nO}\bullet/\mathrm{TEA}-\mathrm{O}\bullet + \mathrm{VP} \xrightarrow{k_{p,B}} \mathrm{P_n}\bullet \qquad \text{Rate} = k_{p,B}[\mathrm{P_nO}\bullet][\,\mathrm{VP}] \qquad (9)$$

Propagation:

$$\mathrm{P_n}\bullet + \mathrm{PEGDA} \xrightarrow{k_{p,A}} \mathrm{P_n}\bullet \qquad \text{Rate} = k_{p,A}[\mathrm{P_n}\bullet][\mathrm{PEGDA}] \qquad (10)$$

$$\mathrm{P_n}\bullet + \mathrm{VP} \xrightarrow{k_{p,B}} \mathrm{P_n}\bullet \qquad \text{Rate} = k_{p,B}[\mathrm{P_n}\bullet][\,\mathrm{VP}] \qquad (11)$$

Radical terminations:

$$\mathrm{P_n}\bullet + \mathrm{TEA}\bullet \xrightarrow{k_t} \mathrm{P_{n+1}} \qquad \text{Rate} = k_t[\,\mathrm{P_n}\bullet][\mathrm{TEA}\bullet] \qquad (12)$$

$$\mathrm{P_n}\bullet + \mathrm{P_n}\bullet \xrightarrow{k_t} \mathrm{P_{n+n}} \qquad \text{Rate} = k_t[\,\mathrm{P_n}\bullet][\mathrm{P_n}\bullet] \qquad (13)$$

$$\mathrm{P_n}\bullet + \mathrm{P_nO}\bullet/\mathrm{TEA}-\mathrm{O}\bullet \xrightarrow{k_t} \mathrm{P_{n+n}} \qquad \text{Rate} = k_t[\,\mathrm{P_n}\bullet][\mathrm{P_nO}\bullet] \qquad (14)$$

Radical quenching:

$$\mathrm{P_nO}\bullet/\mathrm{TEA}-\mathrm{O}\bullet + \mathrm{TEA}\bullet \xrightarrow{k_t} \mathrm{P_{n+n}} \qquad \text{Rate} = k_t[\,\mathrm{P_nO}\bullet][\mathrm{TEA}\bullet] \qquad (15)$$

$$2\mathrm{P_nO}\bullet/\mathrm{TEA}-\mathrm{O}\bullet \xrightarrow{k_t} \mathrm{P_{n+n}} \qquad \text{Rate} = k_t[\,\mathrm{P_nO}\bullet][\mathrm{P_nO}\bullet] \qquad (16)$$

Inhibition by oxygen:

$$\mathrm{TEA}\bullet + \mathrm{O_2} \xrightarrow{k_{inh}} \mathrm{P_nOO}\bullet \qquad \text{Rate} = k_{inh}[\mathrm{TEA}\bullet][\,\mathrm{O_2}] \qquad (17)$$

$$\mathrm{P_n}\bullet + \mathrm{O_2} \xrightarrow{k_{inh}} \mathrm{P_nOO}\bullet \qquad \text{Rate} = k_{inh}[\mathrm{P_n}\bullet][\,\mathrm{O_2}] \qquad (18)$$

Regeneration of eosin:

$$\mathrm{P_nOO}\bullet + \mathrm{EH}\bullet \xrightarrow{k_{regen}} \mathrm{POOH} + \mathrm{E} \qquad \text{Rate} = k_{regen}\,[\mathrm{P_nOO}\bullet][\,\mathrm{EH}\bullet] \qquad (19)$$

Peroxy radical reactions:

$$\mathrm{P_nOO}\bullet + \mathrm{TEA}\bullet \xrightarrow{k_{peroxide}} \mathrm{POO-TEA} \qquad \text{Rate} = k_{peroxide}\,[\mathrm{P_nOO}\bullet][\mathrm{TEA}\bullet] \qquad (20)$$

$$\mathrm{P_nOO-TEA} \xrightarrow{k_{dis}} \mathrm{P_nO}\bullet + \mathrm{TEA}-\mathrm{O}\bullet \qquad \text{Rate} = k_{dis}[\mathrm{P_nOO-TEA}] \qquad (21)$$

The next step involves the reaction of the activated eosin with co-initiator triethanolamine (TEA). This reaction generates TEA free radicals (TEA·) and non-initiating eosin-based radicals (EH ·) as products, as in Eq. 5, with the rate of this reaction governed by the kinetic rate constant for initiation, k_i. The value of k_i was taken

to be the rate of reaction of triplet eosin with itself as that was the best available experimental data on the kinetics of hydrogen transfer for activated eosin.

The TEA free radical can then react with either of two monomers (PEGDA or VP) to form polymer radicals ($\mathrm{P_n}\cdot$), as shown in Eqs. 6 & 7. These polymer radicals can propagate and grow in length upon reaction with either PEGDA or VP as in Eqs. 10 & 11, with rate constants $k_{p,A}$ and $k_{p,B}$ respectively. In the presence of oxygen, alkoxy radicals such as $\mathrm{P_nO}\cdot$ and $\mathrm{TEA-O}\cdot$ generated from the sequence of radical reactions with oxygen during the polymerization can also react and reinitiate with both monomers as in Eqs. 8 & 9. In the model, the value of propagation rate constants used was presumed to only be dependent on the type of monomer being added to the reactive propagating radicals, with the length and type of propagating radical assumed to have negligible effect due to the monomers' small size and relatively high diffusivity. Thus, TEA free radicals, polymer radicals and alkoxy radicals were all modeled to react with PEGDA with a rate constant of $k_{p,A}$ and with VP with a rate constant of $k_{p,B}$.

Termination reactions occur when a primary free radical reacts with a propagating polymer radical to form a dead polymer (P) as in Eq. 12, or when two polymer radicals react through combination to form one polymer chain, as shown in Eq. 13. These termination reactions were modeled to proceed at a rate that is dependent on the termination rate constant k_t which in turn is affected by the kinetic chain length of the propagating radicals.

In our system, the reaction of primary and propagating radicals with oxygen inhibits the overall polymerization process by creating the less reactive polymer peroxy species $\mathrm{P_nOO}\cdot$ that propagates much more slowly. These inhibition reactions are governed by the inhibition rate constant k_{inh}, as shown in Eq. 17 & 18. Similar to propagation, the inhibition rate constant was also assumed to be independent from the type and length of the reactive radicals reacting with oxygen due to oxygen's small size and relatively high diffusivity.

The regeneration of eosin was modeled using the proposed mechanism where the peroxy radical ($\mathrm{P_nOO}\cdot$) reacts with the eosin intermediate radical ($\mathrm{EH}\cdot$) at a rate

constant k_{regen} to form an unreactive $\mathrm{P_nOOH}$ and a regenerated eosin that can undergo further initiation. As the reaction between two uncharged radicals is expected to be very fast, the time required for the two radicals to meet becomes the limiting factor and $k_{regen}$was therefore assumed to be diffusion-limited. No other eosin regeneration reaction was included as the focus of this study was to determine if the proposed eosin regeneration alone is able to produce the same simulation results as the experimental data.

The other major reaction involving the peroxy radical is that of TEA· reacting with $\mathrm{P_nOO\cdot}$ at a rate constant of $k_{peroxide}$ to form a peroxide $\mathrm{P_nOO-TEA}$, as shown in Eq. 20. The reaction between $\mathrm{P_nOO\cdot}$ and $\mathrm{P_n\cdot}$ was assumed to be unimportant as it involves a reaction between two long radicals that diffuse slowly as compared to a small mobile TEA· reacting with a long chain radical. This peroxide can then dissociate with a rate constant k_{dis} to form more reactive alkoxy radicals $\mathrm{TEA-O\cdot}$ and $\mathrm{P_nO\cdot}$, as shown in Eq. 21. These alkoxy radicals can further propagate with both monomers or react with other reactive radical species in a termination reaction.

Chain transfer reactions were not considered in our reaction scheme as chain transfer does not generate new radicals and our propagation rate constants were already assumed to be independent of the propagating chain length. The addition of chain transfer reactions to our model is therefore not expected to greatly affect the time required for polymerization to begin.

2.2.2 Equations and numerical model details

Species balances

The species balance equations for our system are derived from the conservation of chemical species, with the term on the left representing the accumulation of chemical species over time, while the term on the right is a source term that accounts for the net generation of species by various reactions:

$$\frac{\mathrm{dc}_i}{\mathrm{dt}} = \sum_j \mathrm{a}_{ij}\mathrm{R}_j \tag{22}$$

where the subscript *i* refers to any of the species described earlier, $\mathrm{c_i}$ represents the concentration of the respective species, *j* denotes the running index for all of the elementary reactions, a_{ij} is the stoichiometric coefficient for the corresponding *i* species in the *j*th elementary reaction, and R_j is the rate equation for the respective *j*th elementary reaction described in the earlier section. Table 2-1 shows all the overall equations used for each reaction species.

Energy balance

The energy balance equation is derived from the law of conservation of energy, with the first term representing the accumulation of energy over time, while the second term is a source term that accounts for the generation of heat by reaction:

$$\rho \mathrm{C_p}\frac{\mathrm{dT}}{\mathrm{dt}} = \Delta\mathrm{H}\frac{\mathrm{dM}}{\mathrm{dt}}|_{\mathrm{rxn}} \tag{23}$$

where ρ is the density, $\mathrm{C_p}$ is the heat capacity, $\Delta\mathrm{H}$ is the heat of reaction, and $\frac{\mathrm{dM}}{\mathrm{dt}}|_{\mathrm{rxn}}$ is the rate of consumption of monomers for all reactions. Heat generated from light absorption of photoinitiators is expected to be minor due to the weak light intensity used and is hence neglected. Similarly, the thermal and physical properties in the system are assumed to be constant while the reaction proceeds because water, with its high heat capacity, is in excess as the solvent and does not participate in any of the reactions.

Assuming no heat loss to the surroundings, the maximum temperature change is limited by the amounts of monomers present in the solution, and is calculated to be:

$$\Delta T_{max} = \frac{\Delta\mathrm{H}([\mathrm{PEGDA}]_0 + [\mathrm{VP}]_0)}{\rho \mathrm{C_p}} = 12\ K \tag{24}$$

This temperature rise of 12 K is negligible and temperature is therefore not expected to have a major effect on the value of the rate constants.

Model parameters

The values of the parameters used in our simulations are specific to the aqueous co-polymerization of PEGDA and VP, with eosin as the initiator and TEA as the co-initiator.

Table 2-1. Summary of species balance equations solved in polymerization model

Species	Overall species balance equation
E	$\frac{\mathrm{d[E]}}{\mathrm{dt}} = -\frac{\varepsilon\, I_0\, [\mathrm{E}]}{E'} + k_{regen}[\mathrm{P_nOO\bullet}][\,\mathrm{EH\bullet}] + k_{deact}[\mathrm{E^*}]$
$\mathrm{E^*}$	$\frac{\mathrm{d[E^*]}}{\mathrm{dt}} = \frac{\varepsilon\, I_0\, [\mathrm{E}]}{E'} - k_i[\mathrm{E^*}][\,\mathrm{TEA}] - k_{deact}[\mathrm{E^*}]$
EH•	$\frac{\mathrm{d[EH\bullet]}}{\mathrm{dt}} = k_i[\mathrm{E^*}][\mathrm{TEA}] - k_{regen}[\mathrm{P_nOO\bullet}][\,\mathrm{EH\bullet}]$
TEA•	$\frac{\mathrm{d[TEA\bullet]}}{\mathrm{dt}} = k_i[\mathrm{E^*}][\mathrm{TEA}] - k_{p,A}[\mathrm{TEA\bullet}][\,\mathrm{PEGDA}] - k_{p,B}[\mathrm{TEA\bullet}][\,\mathrm{VP}]$ $- k_t[\mathrm{TEA\bullet}]([\mathrm{P_nA\bullet}] + [\mathrm{P_nB\bullet}] + [\mathrm{TEA\bullet}] + [\mathrm{P_nO\bullet}])$ $- k_{inh}[\mathrm{TEA\bullet}][\,\mathrm{O_2}] - k_{peroxide}[\mathrm{TEA\bullet}][\,\mathrm{P_nOO\bullet}]$
TEA	$\frac{\mathrm{d[TEA]}}{\mathrm{dt}} = -k_i[\mathrm{E^*}][\mathrm{TEA}]$
PEGDA	$\frac{\mathrm{d[PEGDA]}}{\mathrm{dt}} = -k_{p,A}[\mathrm{PEGDA}]([\mathrm{TEA\bullet}] + [\mathrm{P_nA\bullet}] + [\mathrm{P_nB\bullet}] + [\mathrm{P_nO\bullet}])$
VP	$\frac{\mathrm{d[VP]}}{\mathrm{dt}} = -k_{p,B}[\,\mathrm{VP}]([\mathrm{TEA\bullet}] + [\mathrm{P_nA\bullet}] + [\mathrm{P_nB\bullet}] + [\mathrm{P_nO\bullet}])$
$\mathrm{P_n}$	$\frac{\mathrm{d[P_n]}}{\mathrm{dt}} = k_t([\mathrm{TEA\bullet}] + [\mathrm{P_nA\bullet}] + [\mathrm{P_nB\bullet}])([\mathrm{TEA\bullet}] + [\mathrm{P_nA\bullet}] + [\mathrm{P_nB\bullet}])$ $+ k_{regen}[\mathrm{P_nOO\bullet}][\,\mathrm{EH\bullet}]$
$\mathrm{P_nA\bullet}$	$\frac{\mathrm{d[P_nA\bullet]}}{\mathrm{dt}} = k_{p,A}[\mathrm{PEGDA}]([\mathrm{TEA\bullet}] + [\mathrm{P_nB\bullet}] + [\mathrm{P_nO\bullet}]) - k_{p,B}[\mathrm{VP}][\mathrm{P_nA\bullet}]$ $- k_t[\mathrm{P_nA\bullet}]([\mathrm{TEA\bullet}] + [\mathrm{P_nA\bullet}] + [\mathrm{P_nB\bullet}] + [\mathrm{P_nO\bullet}])$ $- k_{inh}[\mathrm{P_nA\bullet}][\,\mathrm{O_2}]$
$\mathrm{P_nB\bullet}$	$\frac{\mathrm{d[P_nB\bullet]}}{\mathrm{dt}} = k_{p,B}[\mathrm{VP}]([\mathrm{TEA\bullet}] + [\mathrm{P_nA\bullet}] + [\mathrm{P_nO\bullet}]) - k_{p,A}[\mathrm{PEGDA}][\mathrm{P_nB\bullet}]$ $- k_t[\mathrm{P_nB\bullet}]([\mathrm{TEA\bullet}] + [\mathrm{P_nA\bullet}] + [\mathrm{P_nB\bullet}] + [\mathrm{P_nO\bullet}])$ $- k_{inh}[\mathrm{P_nB\bullet}][\,\mathrm{O_2}]$
$\mathrm{P_nOO\bullet}$	$\frac{\mathrm{d[P_nOO\bullet]}}{\mathrm{dt}} = k_{inh}[\,\mathrm{O_2}]([\mathrm{TEA\bullet}] + [\mathrm{P_nA\bullet}] + [\mathrm{P_nB\bullet}]) - k_{regen}[\mathrm{P_nOO\bullet}][\,\mathrm{EH\bullet}]$ $- k_{peroxide}[\mathrm{TEA\bullet}][\,\mathrm{P_nOO\bullet}]$
$\mathrm{O_2}$	$\frac{\mathrm{d[O_2]}}{\mathrm{dt}} = -k_{inh}[\,\mathrm{O_2}]([\mathrm{TEA\bullet}] + [\mathrm{P_nA\bullet}] + [\mathrm{P_nB\bullet}])$
$\mathrm{P_nOO-TEA}$	$\frac{\mathrm{d[P_nOO-TEA]}}{\mathrm{dt}} = k_{peroxide}[\mathrm{TEA\bullet}][\,\mathrm{P_nOO\bullet}] - k_{dis}[\mathrm{P_nOO-TEA}]$

$P_nO\bullet/\,TEA-O\bullet$	$\frac{d[P_nO\bullet]}{dt} = 2\,k_{dis}[P_nOO-TEA] - k_{pA}[PEGDA][P_nO\bullet] - k_{pB}[VP][P_nO\bullet]$ $- k_t[PO\bullet]([P_nA\bullet] + [P_nB\bullet] + [TEA\bullet]) - 2k_t[P_nO\bullet][P_nO\bullet]$

All values were either well-established literature values that have been validated, or obtained by physical reasoning, with none of the parameters fitted to our experimental FT-NIR results for monomer conversion.

Physical properties of the system and experimental conditions are listed in Table 2-2. The values follow from our chosen experimental conditions where reactants are initially at room temperature (25˚C) with water as the solvent.

Table 2-2. Physical properties and experimental conditions

Parameter	Default Value [units]	Remarks	Source
ε	36148 [L mol^{-1} cm^{-1}]	Absorptivity of eosin at 500 nm in ethanol	http://omlc.org/spectra/PhotochemCAD/data/061-abs.txt last accessed 30 Jan 2015
I_0	1.25 [mW cm^{-2}]	Light intensity	Experimental condition[34]
E'	239253 [J mol^{-1}]	Energy of photons at wavelength of 500 nm	Calculated value
$[TEA]_0$	150×10^{-3} [mol L^{-1}]	TEA concentration	Experimental condition[34]
$[PEGDA]_0$	420×10^{-3} [mol L^{-1}]	PEGDA concentration	Experimental condition[34]
$[VP]_0$	35×10^{-3} [mol L^{-1}]	VP concentration	Experimental condition[34]
$[E]_0$	4×10^{-6} [mol L^{-1}]	Eosin bulk concentration	Experimental condition[34]
$[O_2]_0$	0.5×10^{-3} [mol L^{-1}]	Dissolved oxygen in pure water at 1 atm, 25 ˚C	http://water.usgs.gov/software/DOTABLES last accessed 30 Jan 2015
T_0	298.15 [K]	Room temperature	
ρC_p	4.17×10^{6} [J m^{-3} K^{-1}]	Water's value at 25 ˚C	CRC Handbook of Chemistry and Physics Section 6: Thermophysical Properties of Water and Steam
ΔH	-5.78×10^{4} [J mol^{-1}]	Heat of reaction of C=C bond	Goodner & Bowman[24]

A list of kinetic parameters obtained from existing literature is shown in Table 2-3. These kinetic rate constants are either acquired from experimental studies of the same reactants as our system or from analogous reactants with very similar structures. The typical polymerization rate constants for our system $k_{p,A}$, $k_{p,B}$, k_{t0}, and k_{inh}, were previously studied in detail and thus literature values for those same reactions were used. On the other hand, rate constants k_i and k_{deact} involve photochemical reactions that are not included in traditional polymerization schemes. The values for these parameters were therefore obtained from photochemical experiments, with k_i estimated to be similar to the hydrogen transfer reaction between two triplet eosins[58], which is also of the same order-of-magnitude as the quenching rate of amines with eosin[59], while k_{deact} was obtained directly from a measurement of the overall rate at which triplet eosin relaxes to its ground state. Similarly, the rate of dissociation for t-butyl peroxide, a typical peroxide used in polymerizations, was used as an order-of-magnitude estimate for k_{dis}, which encompasses multiple possible peroxide species of various lengths due to the chain growth process of free radical polymerizations.

Table 2-3. Kinetic constants obtained from the literature

Parameter	Default Value [units]	Remarks	Source
k_i	1×10^{8} [L mol^{-1} s^{-1}]	Rate of hydrogen transfer of triplet eosin reacting with another triplet eosin	Kashe & Lindqvist[58]
$k_{p,A}$	2.165×10^{4} [L mol^{-1} s^{-1}]	PEGDA-PEGDA propagation rate constant	Beuermann et al.[60]
$k_{p,B}$	7.66×10^{4} [L mol^{-1} s^{-1}]	VP-VP propagation rate constant	Stach et al.[61]
k_{t0}	0.755×10^{6} [L mol^{-1} s^{-1}]	PEGDA-PEGDA termination rate constant	Anseth et al.[20]
k_{inh}	4.9×10^{9} [L mol^{-1} s^{-1}]	Reaction rate of tertiary amine radical with oxygen	Maillard, Ingold & Scaiano[62]
k_{deact}	540 [s^{-1}]	Triplet eosin to unexcited eosin rate constant	Kashe & Lindqvist[58]
k_{dis}	1×10^{-5} [s^{-1}]	Order-of-magnitude estimate from t-butyl peroxide dissociation	Huyser & VanScoy[63]

The kinetic parameters for the proposed reactions that are the focus of this work are listed in Table 2-4. These parameters, which are not available in the literature or readily accessible experimentally, were treated using physical arguments. For k_{regen} and $k_{peroxide}$, both of these reactions involve two uncharged radicals reacting together with negligible activation energy. Here, with a small highly mobile radical as one of the reacting species, the diffusion-limited value was taken to be the best estimate, and the following relation for bimolecular diffusion-limited reactions utilized to approximate its value:

$$k_{diffusion-limited} \approx \frac{8RT}{3\eta} \tag{22}$$

where η is the viscosity of the solvent. Using the viscosity of pure water as the minimum viscosity for our more viscous solution mixture, the values for k_{regen} and $k_{peroxide}$ were thus estimated to be of the order of 10^9 [L mol^{-1} s^{-1}]. We also performed a sensitivity analysis to determine the influence of this value on the reactivity of the system.

Table 2-4. Kinetic constants treated with upper bounds based on diffusion limits

Parameter	Default Value [units]	Remarks
k_{regen}	1×10^9 [L mol^{-1} s^{-1}]	Order-of-magnitude estimate for diffusion-limited value
$k_{peroxide}$	1×10^9 [L mol^{-1} s^{-1}]	Order-of-magnitude estimate for diffusion-limited value

Chain-length dependent termination

The termination rate constant is expected to decrease while the polymerization proceeds as polymer chains grow longer and can no longer terminate as quickly due to their increasing size. This influence of chain-length on the termination reactions is modeled according to the following equation:

$$k_t = k_{t0}\, {X_n}^{-0.5} \tag{25}$$

where X_n is number-averaged degree of polymerization as determined using Eq. 26:

$$X_n = \frac{[\mathrm{PEGDA}_{reacted}] + [\mathrm{VP}_{reacted}]}{[\mathrm{TEA}\bullet_{total}]} \quad (26)$$

with $[\mathrm{PEGDA}_{reacted}]$, $[\mathrm{VP}_{reacted}]$ and $[\mathrm{TEA}\bullet_{total}]$ being the total concentration of PEGDA reacted, VP reacted and $\mathrm{TEA}\bullet$ generated respectively. The form of the equation linking termination to chain-length is based on the expectation that termination becomes diffusion-limited due to the low activation energy and rapid rate of reaction between two radicals. The Stokes-Einstein equation states that diffusion of particles scales inversely with its radius:

$$D = \frac{k_B T}{6\pi\eta r} \quad (27)$$

From polymer physics, the hydrodynamic radius of an ideal polymer chain is found to scale with chain length to a power of 0.5:

$$r \sim {X_n}^{0.5} \quad (28)$$

Combining equations 27 and 28, the termination rate constant between polymer chain radicals is therefore assumed to effectively scale with chain length to a power of -0.5, as in Eq. 25.

Model assumptions and limitations

This study presents a kinetic model of photo-initiated, chain growth polymerization with the goal of understanding the mechanism underlying the reduced effect of oxygen inhibition for a xanthene dye initiator. Chain transfer reactions were not included as chain transfer is very slow compared to propagation and thus, expected to have little effect on the polymerization within our stated goal. As a simplification, an LED source is assumed be a monochromatic light source. The kinetic parameters are presumed to be unchanged with conversion because of the low concentrations of monomer used with water as a solvent. The large heat capacity of water justifies this assumption as a temperature increase of at most 12 K was calculated assuming an adiabatic system (Eq. 24). In addition, the model generally assumes that it is the species which reacts with any reactive radical that determines the appropriate rate constant to use for that

reaction; the structure of a reactive radical is expected to have less influence on the reaction kinetics when compared to the type of molecule being added to the radical. Thus, all radicals react with oxygen at the same rate constant k_{inh}, and the initiation and propagation reactions are assumed to depend only on the monomer species that is to be added, independent of the monomer at the propagating end. All rate constants, with the exception of the termination rate constant as discussed in Eq. 25, are assumed to be chain-length independent and do not change as the polymerization progresses.

Numerical solution

The ParametricNDSolve function in Mathematica 9 software was used to numerically solve the model using the LSODA approach with a maximum step size of 1 second. Plots were generated from the resulting data using Plot and ContourPlot functions in Mathematica 9.

2.3 Results and Discussion

Numerically solving the system of kinetic equations in Table 2-1 with known experimental conditions, rate constants and parameter estimates based on physical upper bounds (Tables 1 to 3) as inputs, we can predict double bond conversion profiles as a function of time. We are most interested in the early stages of the reaction because of the importance of avoiding bulk polymerization when PBA reactions are used in clinical diagnostics[9,10,26,35,38] (Scheme 2-3). Here, bulk polymerization is defined as the formation of a hydrogel throughout the entire monomer and co-initiator solution rather than only in the interfacial region near the surface. The illumination time required to reach a C=C bond conversion of 0.2 is of special significance when eosin and tertiary amines are used to initiate PBA reactions.

2.3.1 The significance of $t_{0.2}$ in PBA reactions

In PBA, the analyte of interest (i.e. a protein, nucleic acid or other biological molecule), in a solution that also includes many other components, specifically binds to a surface that has been pre-functionalized with a binding partner for the analyte[12,20,31]. The other components are then washed away, after which a solution containing eosin-

conjugated binding molecules are added. The eosin-conjugated binding molecules bind to the analyte, creating a surface region of high eosin concentration. The surface is then rinsed to remove non-specifically bound molecules, after which the surface is contacted with an amplification solution containing monomers, co-initiators, and a sub-micromolar concentration of free eosin. Free eosin (i.e. not coupled to any biomolecule) is included in the amplification solution in order to overcome the inhibiting effects of oxygen; experiments without it fail to produce interfacial polymers when the system is open to air even when interfacial molecular recognition events have occurred.[20] The surface in contact with a droplet of amplification solution is then illuminated in order to initiate polymerization only if the analyte was captured at the surface. The presence of a higher concentration of eosin near the surface due to eosin-conjugated binding molecules that recognized the analyte results in polymerization initially confined to the surface once t_{PBA} has elapsed, but if illumination is not stopped after the interfacial region polymerizes, the whole droplet will also polymerize due to the eosin in the monomer solution, masking the results of the surface polymerization as depicted in the bottom row of Scheme 2-3.

Scheme 2-3. Interfacial polymerization versus bulk polymerization

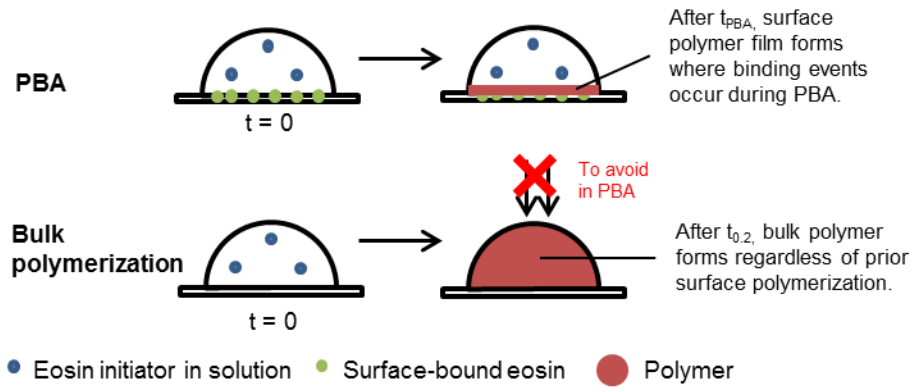

The amount of time required to polymerize the entire droplet of amplification solution thus indicates the maximum time available to distinguish between the desired surface-localized polymerization amplification response associated with binding events and the non-specific bulk polymerization. After this time, the response associated with binding events, if present, becomes obscured by the formation of bulk polymer and the amount

of polymer is no longer related to the number of binding events. In addition, if the test was a true negative, the presence of a bulk polymer introduces false positive results. In the analysis of our results, this bulk polymerization time is defined to be the duration required for conversion to reach 0.2 after the initiating light is turned on ($t_{0.2}$). At this stage, the solution begins to solidify[64] and is resistant to rinsing.

2.3.2 The effect of k_{regen} on the conversion profile

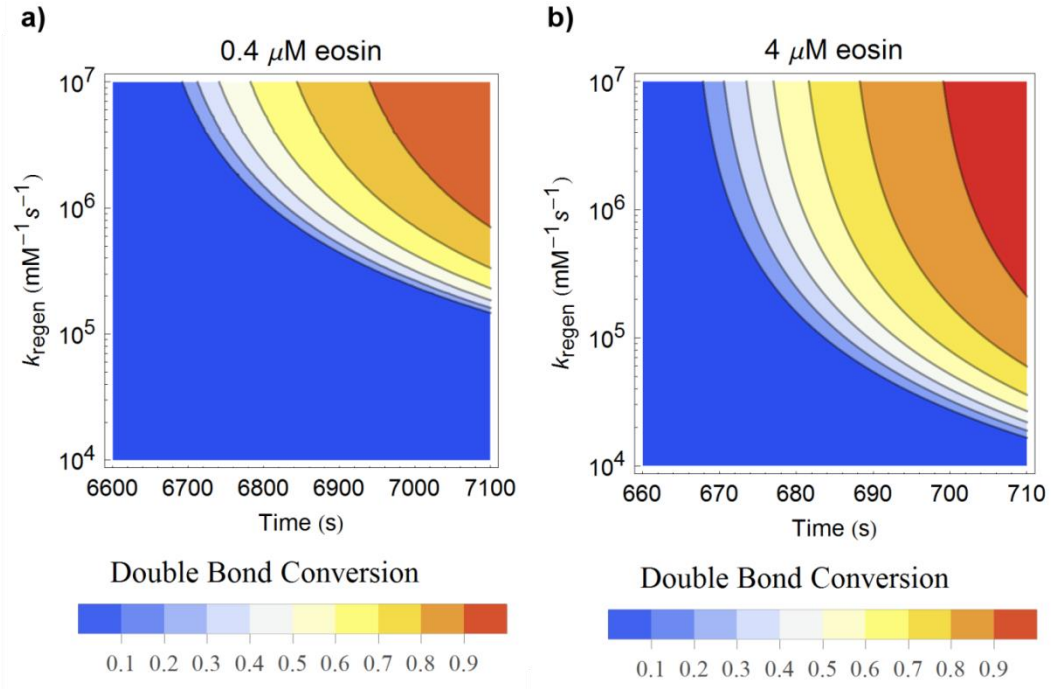

Figure 2-1. Contour plots obtained from model simulations around the onset of polymerization showing how the value of k_{regen} affects conversion, with time as x-axis, k_{regen} as y-axis and conversion as the contours. Two different starting eosin concentrations are shown: (a) 0.4 μM eosin with the conversion profile plotted between 6600 and 7100 seconds; (b) 4 μM eosin with the conversion profile plotted between 660 and 710 seconds.

We first explored the model's sensitivity to the unknown value of k_{regen} when the system has 0.5 mM of dissolved oxygen initially present (Figure 2-1). At a starting eosin concentration of 0.4 μM, a k_{regen} value below ~10^5 $mM^{-1}s^{-1}$ predicts an onset of polymerization after 7100 s with the time required for polymerization to begin gradually decreasing to about 6850 s if k_{regen} was as high as 10^6 $mM^{-1}s^{-1}$ (the diffusion limit). When the eosin concentration is increased to 4 μM, polymerization begins at around 700 seconds for all values of k_{regen} higher than 10^4 $mM^{-1}s^{-1}$, with a relatively small increase in polymerization time if k_{regen} goes as low as 10^4 $mM^{-1}s^{-1}$. This sensitivity

analysis demonstrates that regeneration is an important reaction that influences the conversion profile for very low concentrations of eosin; if the value of k_{regen} is below the diffusion-limited value, the onset of polymerization is delayed. Conversely, for the higher starting eosin concentration of 4 μM, the analysis shows that even if the value of k_{regen} is significantly less than the diffusion-limited value of 10^6 $mM^{-1}s^{-1}$, it will not drastically affect the predicted onset time as there is little variance in the conversion profile around the diffusion-limited value.

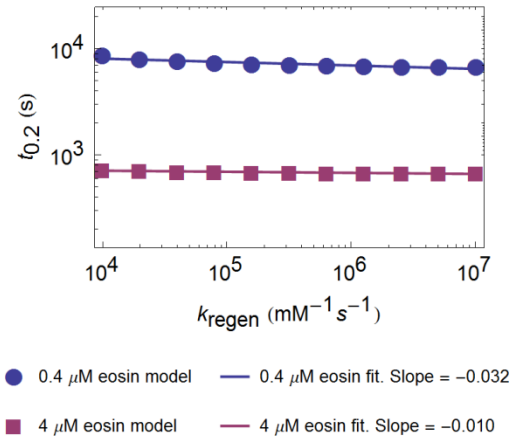

Figure 2-2. Log-log plot of $t_{0.2}$ when k_{regen} is varied over 3 orders of magnitude as obtained from model simulations. Data points are values of $t_{0.2}$ obtained from various k_{regen} values in Figure 2-1 while the lines are the best-fit lines for the corresponding data points.

The predicted $t_{0.2}$ as a function of k_{regen} obtained from the model simulations presented in Figure 2-1 are plotted on a log scale in Figure 2-2. When k_{regen} is increased by three orders of magnitude from 10^4 to 10^7 $mM^{-1}s^{-1}$, the predicted values of $t_{0.2}$ for the 0.4 μM eosin case decrease from 7200 to 6600 seconds, while $t_{0.2}$ for the 4 μM eosin case range from 720 to 670 seconds, a decrease of ~8% for both cases. Despite the large differences in the magnitude of the value of $t_{0.2}$ for these eosin concentrations, the best-fit lines for both concentrations are similarly almost horizontal, with insignificant slopes of values -0.032 and -0.010 for 0.4 μM and 4 μM eosin respectively. The log-log plot thus suggests that the regeneration reaction is not the limiting reaction at the experimental conditions, and that the value of k_{regen} does not have a large effect on the order-of-magnitude of the estimated time required for bulk polymerization. Taken

together, these results illustrate that uncertainty in the estimate of 10^6 $mM^{-1}s^{-1}$ for k_{regen} would not drastically affect the predicted reactivity of the system.

2.3.3 Sensitivity analyses of other rate constants

$k_{peroxide}$ sweep

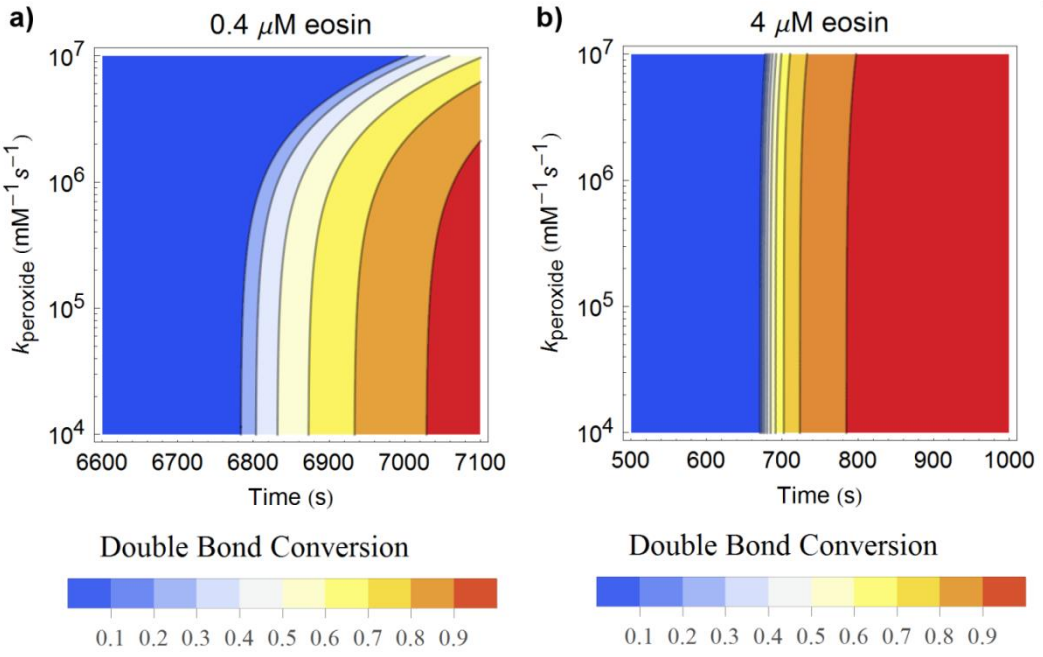

Figure 2-3. Contour plots from model simulations spanning 500 seconds around the onset of polymerization showing how the value of $k_{peroxide}$ affects conversion, with time as x-axis, $k_{peroxide}$ as y-axis and conversion as the contours. Two different starting eosin concentrations are shown: (a) 0.4 μM eosin with the conversion profile plotted between 6600 and 7100 seconds; (b) 4 μM eosin with the conversion profile plotted between 500 and 1000 seconds.

We also studied the effect of having a different estimate for $k_{peroxide}$ in a similar manner as was performed for k_{regen}. When the eosin concentration is at 0.4 μM, polymerization is predicted to begin only after about 6780 seconds has elapsed when $k_{peroxide}$ is smaller than 10^6 $mM^{-1}s^{-1}$, with the onset of polymerization predicted to take longer as $k_{peroxide}$ is increased above that. On the other hand, at the higher eosin concentration of 4 μM, polymerization begins in less than 700 seconds, with only a slight increase in polymerization time when $k_{peroxide}$ is increased, implying that the onset of polymerization is less sensitive to the estimated value of $k_{peroxide}$ when the eosin concentration is higher. Taken together, this sensitivity analysis suggests that the estimated value for $k_{peroxide}$ is not as important for the overall reaction scheme as three

orders-of-magnitude less than the diffusion-limited value still results in very little difference in the predicted polymerization time.

k_i sweep

We also studied the effect of having a different estimate for k_i on polymerization. From the contour plots, we find that the value of k_i has little effect on the time required for polymerization to begin; only at the lower eosin concentration does the onset of polymerization occur later if the value of k_i is about two orders-of-magnitude lower at $2X10^{-3}$ $mM^{-1}s^{-1}$. This sensitivity analysis thus suggests that k_i has little impact on the overall polymerization process and that the reaction scheme is not very sensitive to the estimated value of k_i.

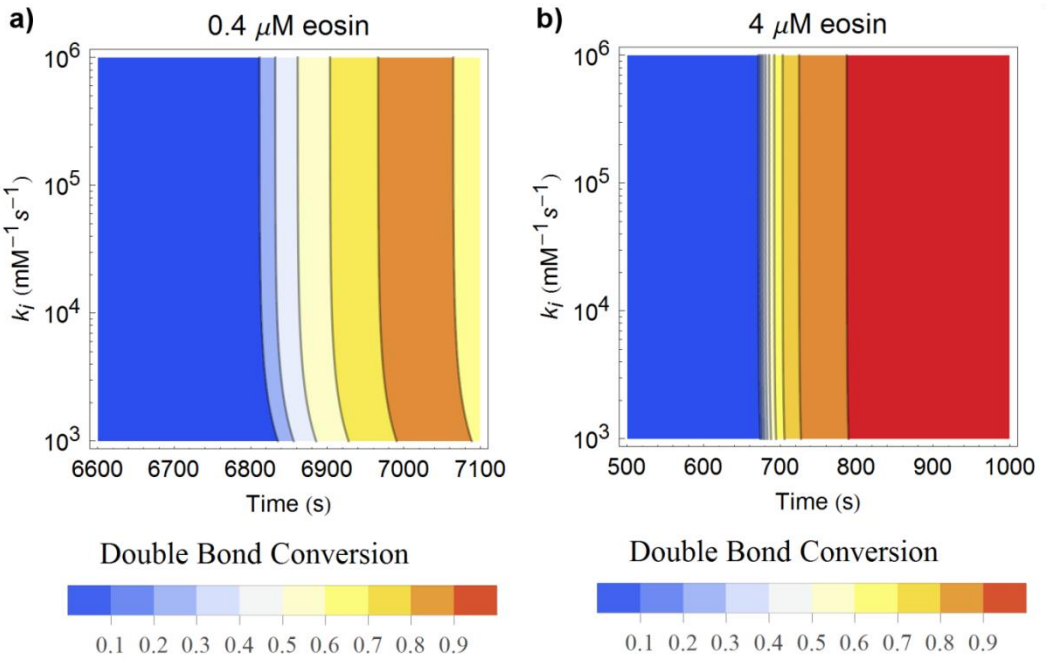

Figure 2-4. Contour plots from model simulations spanning 500 seconds around the onset of polymerization showing how the value of k_i affects conversion, with time as x-axis, k_i as y-axis and conversion as the contours. Two different starting eosin concentrations are shown: (a) 0.4 μM eosin with the conversion profile plotted between 6600 and 7100 seconds; (b) 4 μM eosin with the conversion profile plotted between 500 and 1000 seconds.

k_{pA} sweep

We also studied how k_{pA} affects the polymerization reaction in the model. From the contour plots, we find decreasing that the value of k_{pA} from the default value increases

the time for polymerization to begin as well as changes the conversion profile with time. On the other hand, increasing the value of k_{pA} has relatively little effect on when polymerization starts to occur. Thus, results using the default estimate for the value of k_{pA} would provide a reasonable approximation for the shortest time required for the onset polymerization when the other parameters are at their default values.

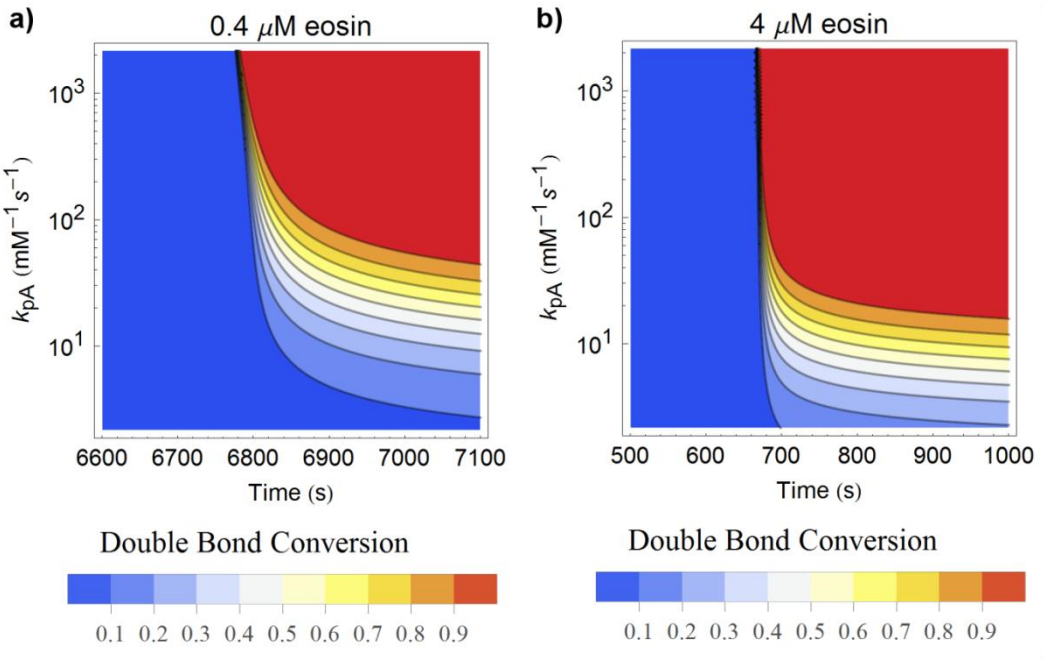

Figure 2-5. Contour plots from model simulations spanning 500 seconds around the onset of polymerization showing how the value of k_{pA} affects conversion, with time as x-axis, k_{pA} as y-axis and conversion as the contours. Two different starting eosin concentrations are shown: (a) 0.4 µM eosin with the conversion profile plotted between 6600 and 7100 seconds; (b) 4 µM eosin with the conversion profile plotted between 500 and 1000 seconds.

k_{pB} sweep

The effect of different values of k_{pB} on the polymerization process was also studied. We see from the contour plots that the value of k_{pB} has little effect on the time required for the onset of polymerization, and that the conversion profile with time only changes a little as k_{pB} is decreased, with the sensitivity of the polymerization response greater at lower eosin concentrations. This analysis thus suggests that that the reaction model is not very sensitive to k_{pB} as varying k_{pB} by an order-of-magnitude around its default value has relatively little effect on the polymerization kinetics.

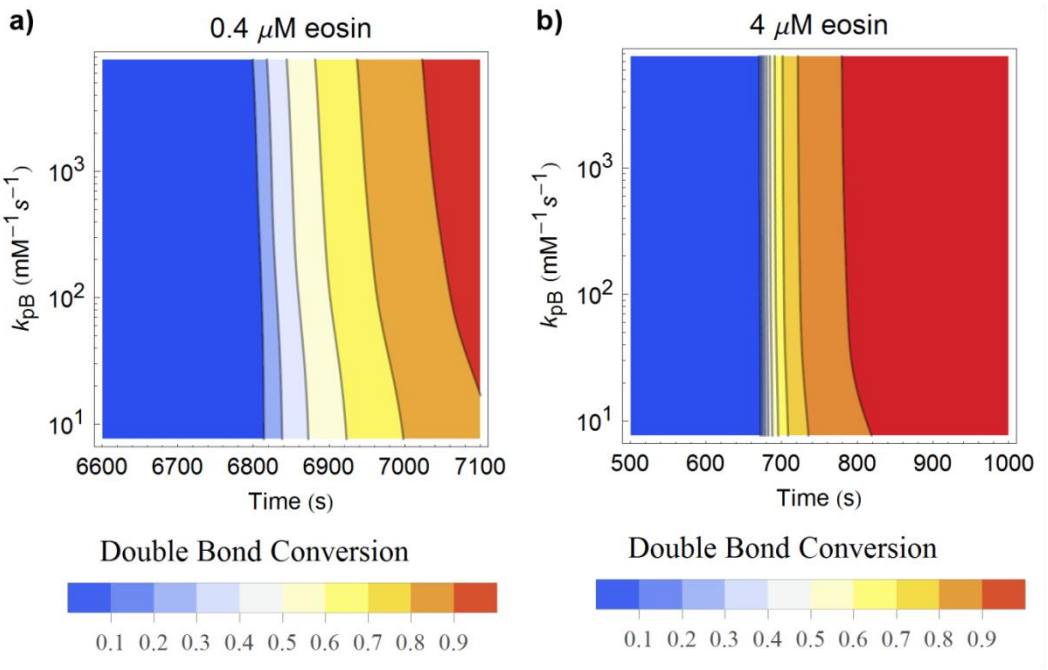

Figure 2-6. Contour plots from model simulations spanning 500 seconds around the onset of polymerization showing how the value of k_{pB} affects conversion, with time as x-axis, k_{pB} as y-axis and conversion as the contours. Two different starting eosin concentrations are shown: (a) 0.4 μM eosin with the conversion profile plotted between 6600 and 7100 seconds; (b) 4 μM eosin with the conversion profile plotted between 500 and 1000 seconds.

k_{t0} sweep

We also studied the effect of having a different estimate for k_{t0} on the polymerization kinetics. The contour plots show that the value of k_{t0} has a great effect on the time required for polymerization to begin as its value is increased. This is to be expected as the termination reactions prevent the radicals from propagating and consuming monomers to increase conversion. On the other hand, having a lower k_{t0} value below ~10^3 $mM^{-1}s^{-1}$ for 0.4 μM eosin and ~5X10^3 $mM^{-1}s^{-1}$ for 4 μM eosin does not have a large effect on the onset of polymerization although the polymerization profiles are affected. Thus, despite the increased time required for polymerization as k_{t0} is increased, results using the default value of 0.7X10^3 $mM^{-1}s^{-1}$ for k_{t0} would still give a reasonable approximation for the shortest $t_{0.2}$ using the model when the other parameters are at their default values.

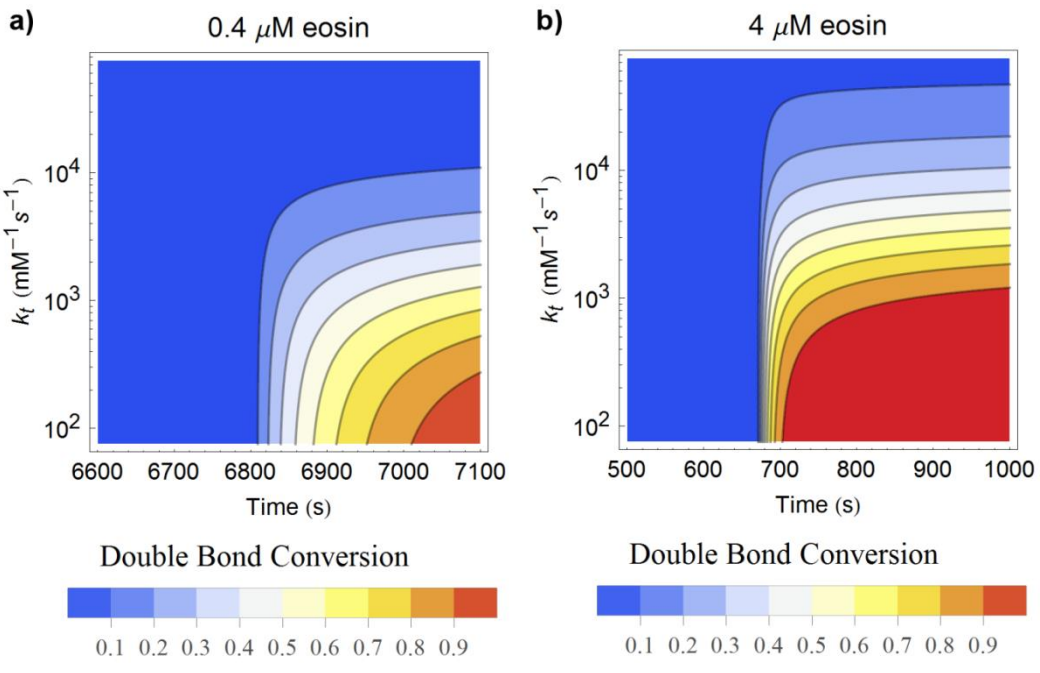

Figure 2-7. Contour plots from model simulations spanning 500 seconds around the onset of polymerization showing how the value of k_{t0} affects conversion, with time as x-axis, k_{t0} as y-axis and conversion as the contours. Two different starting eosin concentrations are shown: (a) 0.4 μM eosin with the conversion profile plotted between 6600 and 7100 seconds; (b) 4 μM eosin with the conversion profile plotted between 500 and 1000 seconds.

k_{inh} sweep

The influence of k_{inh} on the polymerization profiles in the model was also investigated. From the contour plots, we find that k_{inh} has little effect on polymerization at the higher 4 μM eosin concentration, but having a lower value for k_{inh} results in a slower onset of polymerization at the lower eosin concentration of 0.4 μM. This is somewhat surprising as we would expect a faster inhibition to slow down polymerization instead. However, at these concentrations of eosin which are much less than the oxygen concentration, the regeneration of eosin becomes a limiting aspect of the reaction scheme that allows for the subsequent production of more free radicals for polymerization. This regeneration reaction is dependent on the concentration of peroxy radicals which are produced from the inhibition reaction, thus when k_{inh} is too small, inhibition becomes a limiting factor and delays the onset of polymerization. Furthermore, inhibition competes with termination for free radicals to consume, so when k_{inh} is small, more free radicals undergo termination and become dead chains without being able to

regenerate eosin, further reducing the amount of eosin that can be regenerated. In spite of this, the default estimated value for k_{inh} still gives simulation results that overestimate $t_{0.2}$ and having a different value of k_{inh} alone would not account for the discrepancy between the model and experimental data.

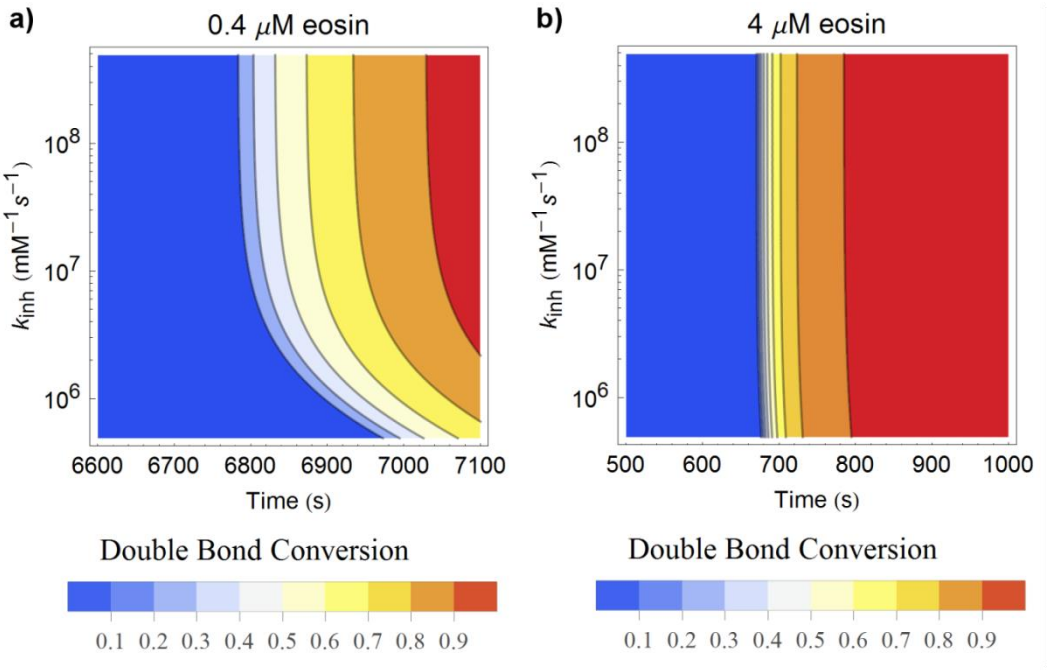

Figure 2-8. Contour plots from model simulations spanning 500 seconds around the onset of polymerization showing how the value of k_{inh} affects conversion, with time as x-axis, k_{inh} as y-axis and conversion as the contours. Two different starting eosin concentrations are shown: (a) 0.4 μM eosin with the conversion profile plotted between 6600 and 7100 seconds; (b) 4 μM eosin with the conversion profile plotted between 500 and 1000 seconds.

kdis sweep

We also studied how k_{dis} affects the polymerization reaction in the model. As observed from the contour plots, k_{dis} is found to have little effect on the polymerization kinetics, with the contour lines appearing almost vertical. At the lower eosin concentration of 0.4 μM, increasing k_{dis} results in a decreased time for the onset of polymerization, but the change is only of the order of 0.1% when k_{dis} changes three orders of magnitude. This result thus suggests that k_{dis} has a negligible impact on the reaction model and any uncertainty in its actual value would not drastically affect the results from the simulations.

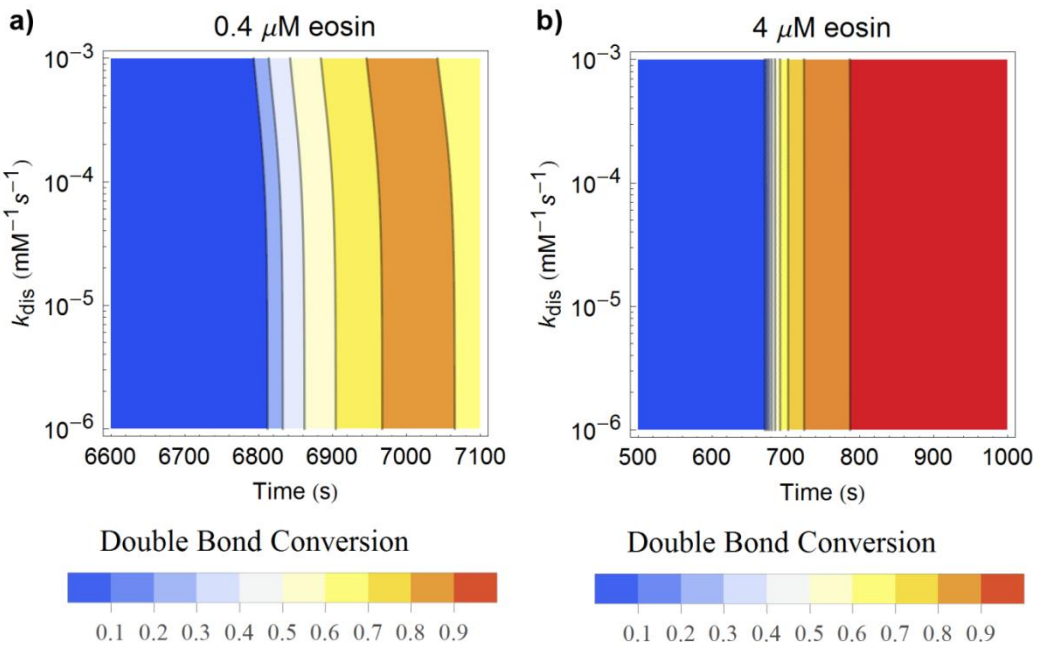

Figure 2-9. Contour plots from model simulations spanning 500 seconds around the onset of polymerization showing how the value of k_{dis} affects conversion, with time as x-axis, k_{dis} as y-axis and conversion as the contours. Two different starting eosin concentrations are shown: (a) 0.4 μM eosin with the conversion profile plotted between 6600 and 7100 seconds; (b) 4 μM eosin with the conversion profile plotted between 500 and 1000 seconds.

Initial concentration of dissolved oxygen sweep

We also investigated the effect of the initial concentration of dissolved oxygen ($[O_2]_0$) on the polymerization process. As expected, the amount of oxygen in the system drastically affects the time required for the onset of polymerization. When oxygen concentration is increased by an order of magnitude, the time required for polymerization to begin is also increased by an order of magnitude. This shows that the polymerization process is very sensitive to the initial oxygen content, which matches experiments where polymerization under nitrogen-purged conditions occurred much faster than experiments conducted in open air. As the value for the initial oxygen concentration in our model is that of pure water, it underestimates the actual oxygen concentration of our monomer solution which contains organic compounds that increase the solubility of oxygen. We measured the oxygen concentration in our monomer solution using a dissolved oxygen meter to be 0.58 mM, which is slightly larger than the model estimate of 0.5 mM. This sensitivity analysis thus further supports our conclusion

that the proposed regeneration alone is unable to explain the ability of eosin to initiate polymerizations quickly in air.

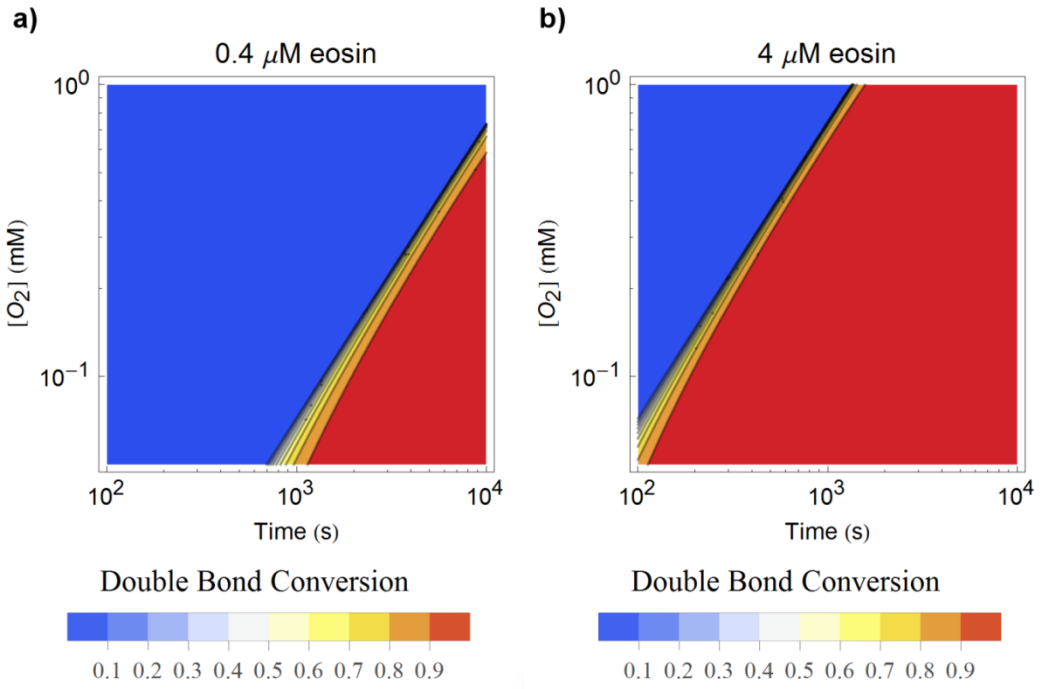

Figure 2-10. Contour plots from model simulations spanning from 100 to 10000 seconds around the onset of polymerization showing how the value of initial concentration of dissolved oxygen affects polymerization, with time as x-axis, $[O_2]_0$ as y-axis and conversion as the contours. Two different starting eosin concentrations are shown: (a) 0.4 μM eosin; (b) 4 μM eosin.

2.3.4 The effect of initial concentration of eosin on the conversion profile

The starting eosin concentration in the system is one initial condition that is expected to have the most influence on the onset of polymerization as it is directly related to free radical production. Its effect on the progress of the polymerization was explored by plotting the conversion profiles obtained from model simulations at eosin concentrations varying from 0.1 μM to 10 μM (Figure 2-11). Increasing the eosin concentration reduces the inhibition time from ~2000 seconds with an initial concentration of 1 μM eosin to ~270 seconds with 10 μM eosin. At higher concentrations of eosin, this inhibition time becomes shorter due to the rapid consumption of oxygen as larger amounts of primary free radicals are generated. At low eosin concentrations below ~1 μM, the inhibition time of thousands of seconds is much longer, which can be explained by oxygen reacting preferentially with free radicals, thereby preventing polymerization until almost all oxygen has been consumed.

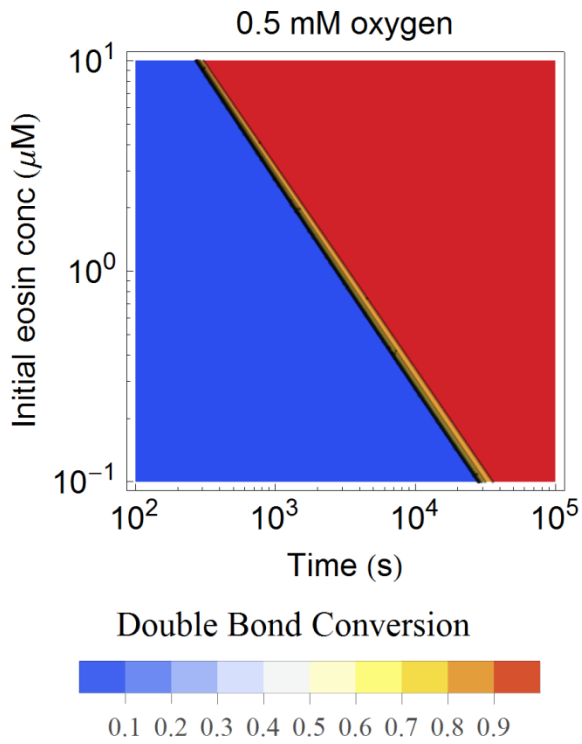

Figure 2-11. Contour plots obtained from model simulations showing how conversion as a function of time is affected by the starting eosin concentration

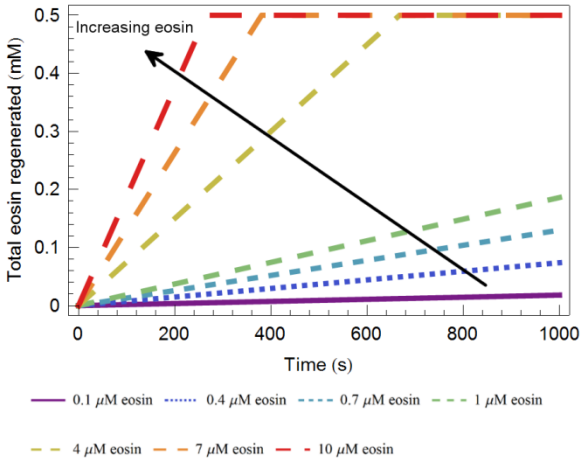

Figure 2-12. Plots obtained from model simulations showing the total cumulative amounts of eosin that is regenerated with time as the starting eosin concentration is varied.

To further illustrate the predictions of the model, Figure 2-12 presents the amount of eosin regenerated as a function of time with various starting eosin concentrations. The total cumulative amount of eosin that is regenerated increases with time for all concentrations. The overall rate at which eosin is regenerated is increased when more

eosin is initially present as implied by the steeper slope when the starting eosin concentration is higher. This faster eosin regeneration rate is due to the higher concentrations of photoreduced eosin intermediates ($EH\cdot$) available to participate in regeneration when more eosin is added to the reaction system. Additionally, the total eosin regenerated plateaus around 0.5 mM as that is the point where oxygen has been completely consumed and further production of peroxy radicals, required for regeneration of eosin, is not possible.

2.3.5 Comparison between theoretical upper-bound conversion profiles and experimental conversion profiles

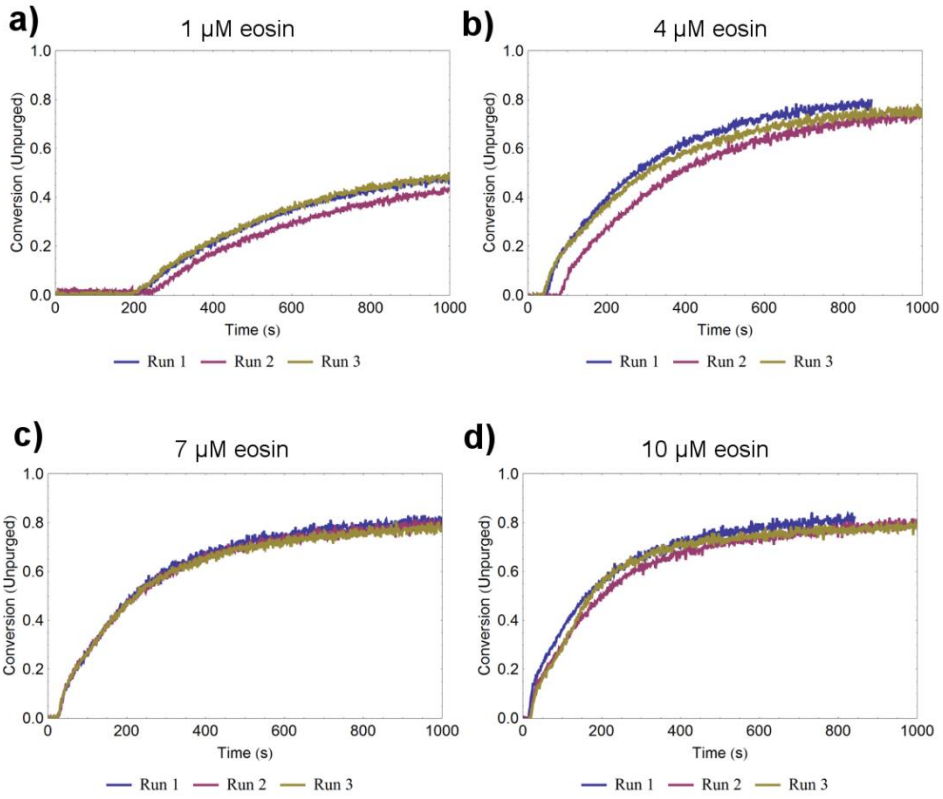

Figure 2-13. Experimental conversion profiles for (a) 1 μM eosin; (b) 4 μM eosin; (c) 7 μM eosin; (d) 10 μM eosin in unpurged conditions.

The experimental conversion data with time for the various initial eosin concentrations in unpurged conditions with the reaction system equilibrated with open air are shown in Figure 2-13. The double bond conversion is calculated by dividing the peak area at wavenumbers between 6229 cm^{-1} to 6128.8 cm^{-1} during each time point

with the original unreacted peak area as obtained from the IR spectrometer. The values for $t_{0.2}$ of each run were obtained by finding the earliest time at which the average conversion of three consecutive data points exceeds 0.2 and taking the earliest time in that group of three data points. The mean value of three runs for each initial condition was then taken to be the value of $t_{0.2}$ for that respective data set.

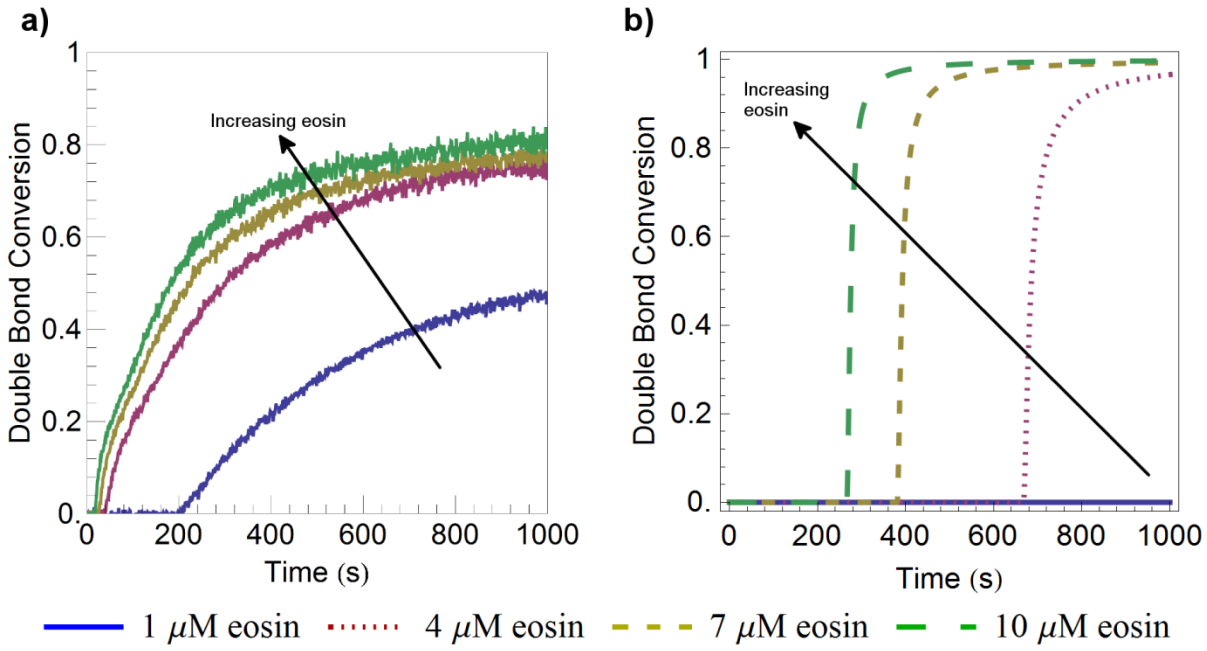

Figure 2-14. Representative conversion profiles as a function of time for various starting eosin concentrations obtained (a) experimentally and (b) from simulations using diffusion-limited values of rate constants related to regeneration of eosin due to reaction of $EH\cdot$ with peroxy- species.

With the effects of changing parameters in the model that are pertinent to peroxy-mediated regeneration of eosin explored and analyzed, we examined the conversion versus irradiation time profile for various starting eosin concentrations with the rate constants related to eosin regeneration set at diffusion-limited values. Figure 2-14 compares experimental data with model predictions. The model results show a rapid increase in conversion during the initial stages of the reaction that later slows down and plateaus, similar to the profiles obtained from the experiments. In contrast with experimental conversion profiles, the model predicts a much slower onset of polymerization and a much sharper transition from no conversion to almost full conversion. The experimental data shows an inhibition time of about 200 seconds for the 1 μM eosin case, with shorter times of less than 50 seconds observed for 4, 7 & 10

μM eosin. The model predicts much longer inhibition times for all of the concentrations, with inhibition times increasing from about 270 seconds with 10 μM eosin to more than 2000 seconds for the 1 μM eosin case. The differences in the shape and slope of the conversion plots with time could be due to the simplified termination reactions in the model and the assumption of unchanging rate constants; the effects of increasing viscosity due to crosslinking in the reaction mixture was not accounted for in the model. The uncertainties in the values of the rate constants used in the model were found to have little effect on $t_{0.2}$ as sensitivity analyses performed earlier for all of the rate constants showed that none of them significantly reduced $t_{0.2}$ even when their values were varied over more than an order-of-magnitude. In fact, deviating away from the current set of parameters used in the model simulations generally resulted in a slower onset of polymerization and larger predicted values of $t_{0.2}$.

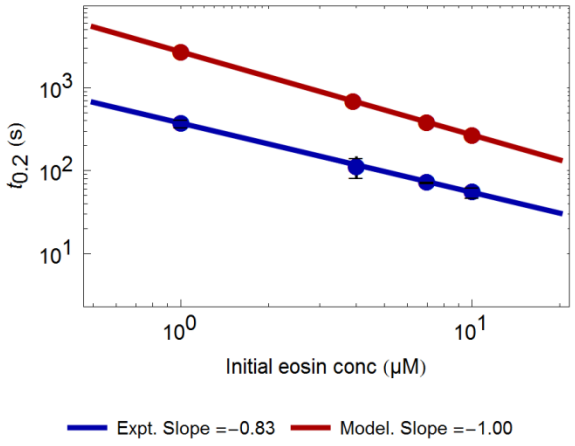

Figure 2-15. Log-log plot obtained from model simulations comparing $t_{0.2}$ obtained from simulations with experimental data. Data points are values of $t_{0.2}$ obtained from experiments at various eosin concentrations in Figure 2-5 or calculated from the model simulations. The lines are best-fit lines to their corresponding data points. Error bars represent one standard deviation about the mean of three independent experimental trials.

Figure 2-15 presents the effect of changing the starting eosin concentration on $t_{0.2}$. When the starting eosin concentration is increased, the model predicts that $t_{0.2}$ decreases according to a power law of slope -1.00, with the effects of oxygen inhibition being reduced at the higher eosin concentrations due to the increased capacity to generate free radicals for polymerization. Similar to the trend obtained from the model predictions, the experimental results also show $t_{0.2}$ decreasing in a power-law manner

with a slope of -0.83 as eosin concentration is increased. Thus, as the model and experimental results show, eosin is a limiting reagent at these low concentrations and its concentration has a large effect on $t_{0.2}$. As such, in PBA applications where binding events at the surface would create a higher local concentration of initiators, this difference in $t_{0.2}$ could be one explanation for the formation of a thin film on the surface before the bulk starts to polymerize. Furthermore, we find that the slopes for both the model and experimental results are similar, thus indicating that the proposed regeneration mechanism captures some, but not all, of the relevant trends of the initial stages of the polymerization process in the presence of oxygen.

The model for peroxy- mediated cyclic regeneration of eosin predicts a much longer $t_{0.2}$ as compared to experiments performed at the corresponding eosin concentrations. In order to predict the $t_{0.2}$ that were observed experimentally, the model would require that more eosin is initially present, with the required fold increase ranging from 5 to 7 as compared to experimental values (Table 2-5). This finding implies that the experimental eosin concentrations correspond to eosin concentrations that are effectively much higher than those predicted by the model based only on peroxy- mediated regeneration. Therefore, other reactions are required to explain the faster polymerization times that are observed experimentally, and the analysis above suggests that such reactions must regenerate eosin, consume oxygen, or produce other initiating radicals.

Table 2-5. Comparison of eosin concentrations required to get the same $t_{0.2}$ between experimental data and model predictions.

Experimental [eosin] (μM)	Experimental $t_{0.2}$	Model [eosin] to get same $t_{0.2}$ (μM)	[Eosin] fold increase
1	380 ± 40	7	7
4	110 ± 30	24	6
7	74 ± 1	37	5
10	57± 8	48	5

With eosin regeneration reactions shown to be important in eosin-tertiary amine initiated polymerizations, this model serves as a starting point for further extensions to understand the effects of oxygen or other inhibitors on the polymerizations. Even with

unknown parameters in the model set to the maximum values as dictated by diffusion limitations, the consistently larger values of $t_{0.2}$ predicted for polymerizations with oxygen present in the system indicate that the proposed regeneration mechanism alone is insufficient to account for the high reactivity of the eosin-tertiary amine initiation system. In future work, we intend to further explore the mechanism with spectroscopic techniques in order to more fully understand the factors that make this initiation system function well in the presence of excess oxygen.

2.4 Conclusions

The modeling results presented herein predict that eosin concentrations of at least two orders of magnitude smaller than the initial oxygen concentration are able to overcome the inhibiting effects of oxygen in the system. In addition, the current model provides a useful first description of the bulk polymerization process for the eosin-tertiary amine initiation system in the presence of oxygen. Comparison of simulation results with experimental data provides support for the deduced trends for $t_{0.2}$. Given that the trends obtained from simulations when a peroxy- mediated mechanism for cyclic regeneration of eosin is incorporated into the reaction scheme are consistent with experimental observations, our analysis thus suggests that this mechanism is plausible. It is, however, insufficient to fully explain the reduced inhibition times and the diminished inhibitory effect of oxygen on photopolymerization reactions initiated by eosin in combination with tertiary amines. This finding motivates future spectroscopic studies, ongoing in our lab, to reveal the identities of species that are involved in the more rapid consumption of oxygen and/or regeneration of eosin that must occur for consistency with experimental observations. Such work supports the larger goal of understanding how to rationally choose and modify reactive systems for PBA and how the times for interfacial polymerization versus polymerization of the entire solution may be controlled and tuned.

2.5 Appendix: Experimental details

Real-time FT-NIR Monitoring

Monomer solutions were prepared with 420 mM poly(ethylene glycol) diacrylate 575 (PEGDA), 35 mM vinylpyrrolidone (VP), 210 mM triethanolamine (TEA), and between 1 and 10 μM Eosin Y. A multi-wavelength light emitting diode (LED) box containing a green, 500 nm LED with a FWHM of 20 nm (FC8-LED, Prizmatix, Southfield, MI) was used to excite eosin to its singlet state. Irradiance or power density was controlled with a potentiometer and measured with a radiometer (6253, International Light Technologies, Peabody, MA) within the 400-700 nm range. Irradiance was 1.25 mW/cm^2. Each condition was tested in triplicate.

A fiber optic coupled FT-IR spectrometer (Nicolet Magna-IR Series II, Thermo Scientific, West Palm Beach, FL) was used to track the vinyl group concentration via the quantification of the peak area between 6229 and 6128.8 cm^{-1} for the first overtone of the =C-H bond(s) associated with the acrylate group centered at ~6160 cm^{-1}. A path length of 2 mm was used for the NIR spectroscopy to avoid saturation by the O-H bands from the water. FT-IR settings were set to 8 scans, a resolution of 8, a gain of 1, and an optical aperture of 10. Acquisition time for the FT-NIR remained between 0.5 and 3 seconds.

PMMA cuvettes with a cross-section of 10 x 2 mm (UVette, Eppendorf, Hauppauge, NY) were used inside an adaptor with custom-made optical apertures. Sample volume was 50 μL, which lead to sample dimensions of 2 mm x 10 mm x 2.5 mm, where the latter is the thickness in the direction of the excitation light from the LED. Samples were placed inside a CUV-ALL-UV 4-Way Cuvette Holder (Ocean Optics, Dunedin, FL) with SMA connectors for fiber optic integration. Fiber optic cables were connected for FT-NIR analysis. For the FT-NIR, two 1000 nm fibers were used to feed the IR light from the spectrometer to the sample, and from the sample back into the InGaAs detector.

Chapter 3. Impact of oxygen replenishment from open air

Portions of this chapter are reproduced from Wong, J.; Sikes, H. D. Macromol. Theory Simulations 2016, in press, DOI: 10.1002/mats.201500098

Abstract

Eosin, a photosensitizer dye which can exist in multiple oxidation states, has been shown to initiate visible-light photopolymerizations of acrylates in open air when used in combination with tertiary amines. The exact mechanism behind this reactivity with micromolar concentrations of eosin in aqueous monomer solutions initially containing millimolar concentrations of oxygen has not been conclusively established, although pathways for regeneration of eosin in the presence of oxygen certainly play a role. In this work, we built a reaction-diffusion model incorporating a peroxy-mediated eosin-regeneration mechanism to explore the effects of oxygen diffusing into the system as the light-activated reaction proceeds. We used an oxygen concentration-dependent flux boundary condition to model the continuous replenishment of oxygen at the surface open to air as it is consumed by reaction. The model predicts the formation of a free radical concentration front that initially forms closer to the open surface and gradually moves towards the closed surface, with polymer film thickness increasing and the time required for polymerization to begin decreasing as the initial eosin concentration is increased. These results suggest that oxygen's dual role as both a free radical inhibitor and a precursor of the oxidizing species required for regeneration of eosin brings about interesting spatial variations when the reaction is carried out in a thin film geometry that is exposed to open air. In this case, an assumption of a well-mixed system is not appropriate and the kinetics of the reaction and conversion as a function of position are likely to depend on the geometry of the system.

3.1 Introduction

Eosin, a type of xanthene dye, has been shown to readily participate in many photochemical reactions when activated by light to its excited states.[65–67] Thus, eosin has found uses in many applications such as photoredox catalysis in organic synthesis[68,69] and photoinitiation of free radical polymerizations.[3,5,59] Interest in the photochemistry of eosin spans numerous decades, and many studies[58,68–70] have proposed various radical and charged eosin species in order to explain its reactivity. In addition, eosin has recently been gaining attention as a useful photoinitiator due to its ability to initiate free radical photopolymerizations in the presence of visible light instead of biologically harmful UV light, making it suitable for use in biomaterial applications or *in-situ* polymerizations of living cells and tissues[43,71]. However, as with all free radical polymerizations, the presence of oxygen can substantially slow down the polymerization process[7–9,11] as it can react with carbon-centered radicals to form peroxy radicals that are less reactive towards further propagation reactions, thereby inhibiting the chain-growth process of free radical polymerization.

As such, oxygen inhibition is an important factor to consider during the polymerization process, especially when reactions are performed under atmospheric conditions where oxygen can readily diffuse into the monomer solution and inhibit free radical polymerization. When used in combination with tertiary amines as a co-initiator, even monolayers of eosin, a photoreducible xanthene dye, have been shown to initiate polymerization of acrylate monomers, resulting in micron-scale hydrogel films under inert gas-purged conditions,[26,32,33,72] and recent experiments show that including sub-micromolar concentrations of eosin into the monomer solution allows the polymerization to proceed under oxygen-containing air without purging using inert gases.[10,36] Furthermore, eosin regeneration reactions have been proposed[34] to account for eosin's ability to initiate polymerizations at such low concentrations, and a recent study has shown that oxygen participates in the regeneration of eosin[73] in these aqueous eosin/tertiary amine-initiated free radical polymerizations. Thus, it is anticipated that for polymerizations in open air, the diffusion of oxygen would play an important role in determining the spatial profiles of reactive species in the overall process.

Various models have been proposed for radical polymerizations using different types of initiators[74–76] and the effect of a reaction system open to oxygen[17,77] has also previously been modeled in the literature, but few polymerization models have explored the mechanisms and trends of photoinitiation systems with amounts of photoinitiators smaller than that of the concentration of dissolved oxygen.[78] Moreover, previous numerical models of eosin/tertiary amine-initiated polymerizations assumed oxygen was absent[23,25] or not replenished through diffusion from the open surface[78] and did not consider the possibility of the regeneration of eosin in their kinetic reaction schemes.[23,25] As the eosin/tertiary amine initiation system is particularly useful in applications requiring visible-light initiated polymerizations[79,80] in open air, a greater understanding of the effects of oxygen diffusion on the polymerization process is desirable to support rational reaction engineering.

Herein, we developed and used a reaction-diffusion model to investigate the influence of an eosin regeneration reaction on the time required for polymerization to begin when oxygen continuously diffuses into the reaction system at the surface open to air. We incorporated a previously proposed kinetic reaction scheme[78] which was shown to qualitatively match trends obtained from experiments along with corresponding kinetic rate constants into a reaction-diffusion model that accounts for the flux of oxygen at the open-air surface and the spatial distributions caused by this boundary condition. This reaction-diffusion model was numerically solved at the micromolar eosin concentrations that we have recently studied experimentally,[73,78] allowing analysis of subsequent simulation results with a focus on the effects of oxygen diffusion on the spatial profiles of various pertinent species during polymerization.

3.2 Reaction-diffusion model

We extended the previously described model that incorporated a proposed eosin regeneration reaction[78] to include the effects of diffusion, paying particular attention to the consequences of having one end of the reaction system open to air whereby oxygen can readily dissolve into the reaction mixture. Scheme 3-1 shows an overview of the reaction-diffusion model, with an oxygen flux at the open surface of one end diffusing

into a one-dimensional spatial coordinate as a simplification of the thin-film geometry. The film thickness of 1 mm is discretized in the model into a mesh with a maximum of 1 µm mesh spacing allowed. In the reaction-diffusion model, the conservation equation that is numerically solved at each mesh point is that of the species balance equation:

$$\frac{\partial[i]}{\partial t} = \frac{\partial}{\partial z}\left(D_i \frac{\partial[i]}{\partial z}\right) + R_i \qquad (1)$$

where *[i]* is the concentration of the *i* species, *t* is time, *z* is the spatial position, D_i is diffusion constant of the *i* species, and $[R_i]$ is the reaction term of the *i* species. Every chemical species in the reaction scheme has its own corresponding species balance equation to solve, with the reaction terms obtained from the rate equations in the kinetic reaction scheme previously summarized in Scheme 2-2. To describe a reaction mixture that is open to air on one side where oxygen continuously dissolves and diffuses into the mixture as it is consumed by reaction, the boundary condition for oxygen species only was set to a local oxygen concentration-dependent flux while the standard no-flux boundary condition was used to model the gas-liquid interface of the reaction mixture for all other species. At the opposite end, a solid glass surface on which the aqueous reaction mixture rests was modeled as a no-flux boundary condition whereby diffusion through the surface is not possible.

Scheme 3-1. Overview of reaction-diffusion model.

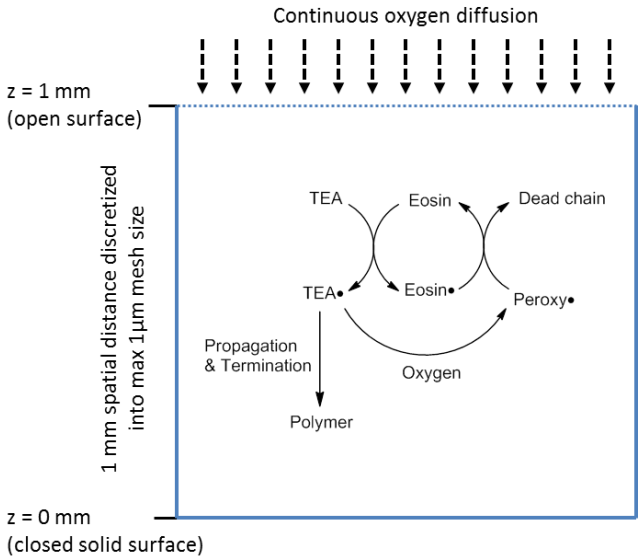

The corresponding rate equation utilized in the reaction-diffusion model for each elementary reaction in the overall reaction scheme is summarized in Scheme 2-2. The lists of kinetic parameters and initial conditions used for the model are also previously provided in Tables 2-2, 2-3 & 2-4, while the diffusion constants are listed in Table 3-1. For the rate constants k_{regen} and $k_{peroxide}$ which have not been experimentally determined, it was assumed as in past work[78] that their values were the diffusion-limited value of 10^9 L mol^{-1} s^{-1} as both reactions involve one small mobile radical reacting with another radical with minimal activation energy required, and is therefore not expected to be kinetically limited. The intensity was also increased by an order of magnitude to 12.5 mW cm^{-2} as initial simulation results at the lower intensity of 1.25 mW cm^{-2} used in Chapter 2 did not produce any noticeable changes in conversion profiles when oxygen replenishment is added into the model.

Table 3-1. Diffusion constants

Parameter	Default Value [units]	Remarks	Source
D_E D_{E*} $D_{E\cdot}$	0.55×10^{-9} [m^2 s^{-1}]	Fluorescein value in water/sterile medium	De Beer et al.[81]
D_{TEA} $D_{TEA\cdot}$	0.7043×10^{-9} [m^2 s^{-1}]	Triethanolamine in water at 25 ºC	Yaws[82]
D_{VP}	0.9013×10^{-9} [m^2 s^{-1}]	N-methyl-2-pyrrolidone in water at 25 ºC	Yaws[82]
D_{PEGDA}	0.9013×10^{-9} [m^2 s^{-1}]	Used VP value	Yaws[82]
D_{O2}	1.96×10^{-9} [m^2 s^{-1}]	Oxygen in water at 25 ºC	Han & Bartels[83]

The system of reaction-diffusion equations and boundary conditions were modeled in COMSOL and numerically solved using BDF and PARDISO solvers. The simulations were run with a maximum time step of 1 second for total reaction times of up to 500 seconds, with the reaction rates and species concentrations exported at 1 second intervals and then plotted as contour plots with blue color corresponding to a low value and red as a high value. As in our previous work[78], $t_{0.2}$ was defined to be the duration

required for the local conversion of the mesh element to reach a value of 0.2 that represents the formation of a hydrogel.

3.3 Results and Discussion

3.3.1 The effect of oxygen diffusing in from the open surface

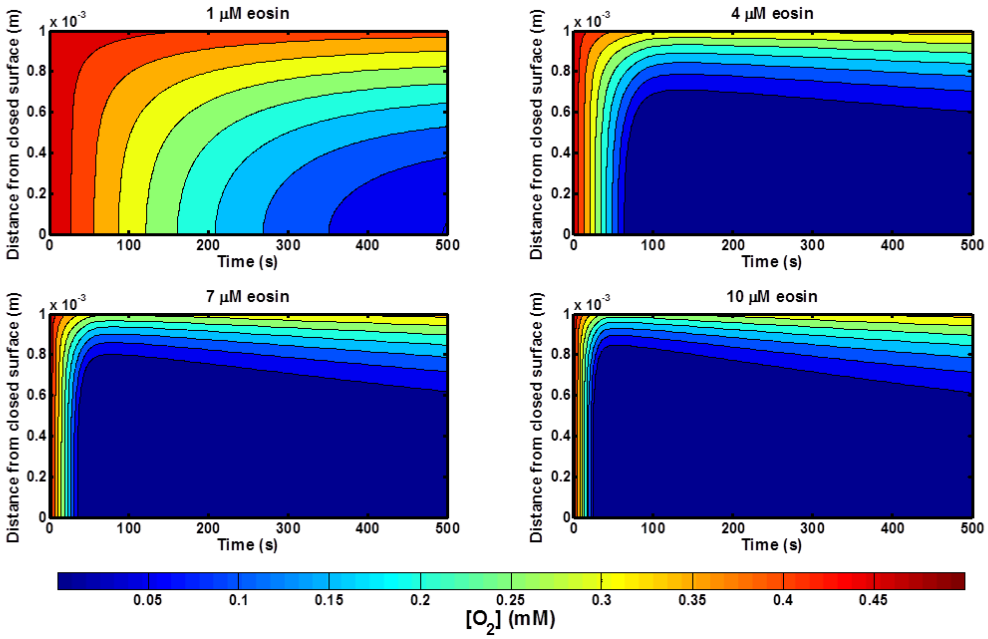

Figure 3-1. Contour plots of oxygen concentrations as the contours with time as the x-axis and distance from the surface open to air as the y-axis at different initial eosin concentrations.

As the presence of oxygen has a strong inhibitory effect on radicals that might otherwise propagate, it is informative to be aware of the spatial and temporal dependence of the oxygen concentration when a reactive solution is exposed to air and illuminated. The effect of a continuous flux of oxygen diffusing from the air into the polymerization mixture was simulated in our reaction-diffusion model containing the proposed eosin regeneration reaction, with the contour plots of oxygen concentration plotted as a function of time and distance from the closed surface at various initial eosin concentrations in Figure 3-1. As deduced from the curvature of the contour lines, all of the plots show a slightly faster depletion of oxygen nearer the closed surface when compared to the open surface where oxygen is replenished from air. The time required for the oxygen concentration to drop one order-of-magnitude is heavily dependent on

the initial eosin concentration, with higher concentrations needing a shorter period of time. Similarly, the oxygen concentration profiles for higher initial eosin concentrations also show the region of lower oxygen concentrations reaching further away from the closed surface. In addition, a threshold initial eosin concentration between 1 μM and 4 μM is required for the rapid depletion of oxygen as the contour plots for 4 μM of initial eosin are similar to those at higher initial eosin concentrations while the oxygen profile for 1 μM of initial eosin exhibits a much slower reduction in oxygen concentration with time. After the rapid initial consumption of oxygen, all of the plots also show gradual movements of higher oxygen concentration towards the closed surface with time, implying that the continuous replenishment of oxygen from open air is now dominating over oxygen consumption through the inhibition reaction. Furthermore, at such low eosin concentrations, if regeneration of eosin was not occurring, negligible changes in the oxygen profile would develop from the initial uniform concentration as very little oxygen would be consumed due to the low concentrations of free radicals being generated.

The competition between diffusion of oxygen towards to the closed surface and its participation in inhibition reactions can be studied by analyzing the Damkohler number of oxygen (Da_{O2}):

$$Da_{O2} = \frac{rate\ of\ reaction\ of\ O_2}{rate\ of\ diffusion\ \ of\ \ O_2} = \frac{k_{inh}[TEA\cdot]}{D_{O2}/L^2} \quad (2)$$

where k_{inh} is inhibition rate constant, $[TEA\cdot]$ is the concentration of TEA radicals, D_{O2} is the diffusion constant of oxygen and L is the distance from the open surface to the closed surface. This dimensionless number serves to indicate the regions in space where reaction is dominating over diffusion when Da_{O2} is more than one, or where diffusion is much faster than reaction when Da_{O2} is less than one.

Contour plots of Da_{O2} as a function of time and space are presented in Figure 3-2. In all cases, the magnitude of Da_{O2} is more than 1, indicating that reaction of oxygen is faster than diffusion. However, in the case of 1 μM initial eosin where the low concentration of eosin results in low production of free radicals and hence less reaction of oxygen, the magnitude of Da_{O2} stays very close to 1 with very little spatial and

temporal variation. Conversely, at the higher concentrations of eosin (>4 μM), Da_{O2} profiles show a broad band of high values being formed that slowly reaches towards the closed surface as time progresses, with a thinner band and further penetration away from the closed surface as eosin concentration increases. This suggests that the initial eosin concentrations affect the influence of oxygen diffusion from the open air boundary which ultimately controls the overall progress of polymerization.

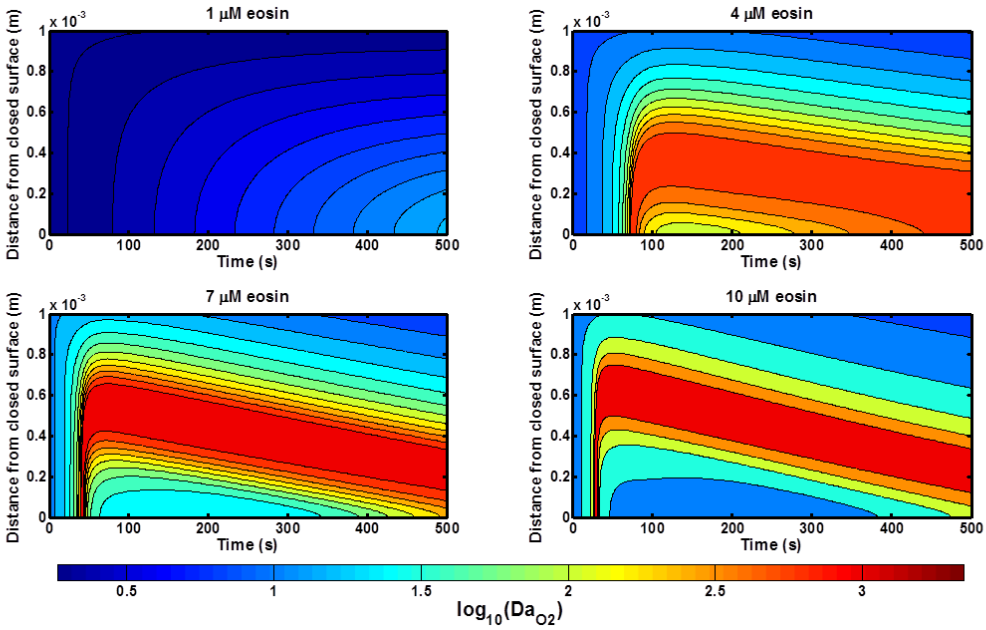

Figure 3-2. Contour plots of $\log_{10}$ of the Damkohler number of oxygen as the contours with time as the x-axis and distance from the surface open to air as the y-axis at different initial eosin concentrations.

3.3.2 Tertiary amine (TEA) radical concentrations

The overall polymerization process is heavily dependent on the production of free radicals in the initiation process as the radicals are the reactive species that react with monomers and propagate to form the polymer. It is therefore useful to visualize the spatial and temporal profiles of the TEA radicals in order to understand the regions where most of the radicals are building up and can undergo propagation. The contour plots of TEA· concentrations at various initial eosin concentrations are thus presented in Figure 3-3. As shown, both the depth of penetration away from the closed surface and the magnitude of the increase in TEA· increase as the initial eosin concentration is increased. Furthermore, all of the plots show a broad band of high TEA· concentrations

moving towards the closed surface that follows the same spatial trends as that of the regions with the largest oxygen Damkohler number values, highlighting the regions of a front where most of the reactive free radicals are produced as oxygen diffuses back into the mixture. This is not unexpected as the regions with high oxygen Damkohler numbers suggest that oxygen is being consumed at the highest rates and thus the regions where free radicals are being generated at the highest rates. At higher initial eosin concentrations, the production rate of TEA radicals is increased and oxygen is depleted more quickly, resulting in a higher peak TEA· concentrations and further penetration away from the closed surface as the flux of oxygen from the air is unable to diffuse that far before reacting with the radicals. These results suggest that peak radical concentrations in our model follow the diffusion front of oxygen as it moves towards the closed surface, contrary to expectations that radical concentrations should remain high at regions near the closed surface where oxygen replenishment is the slowest.

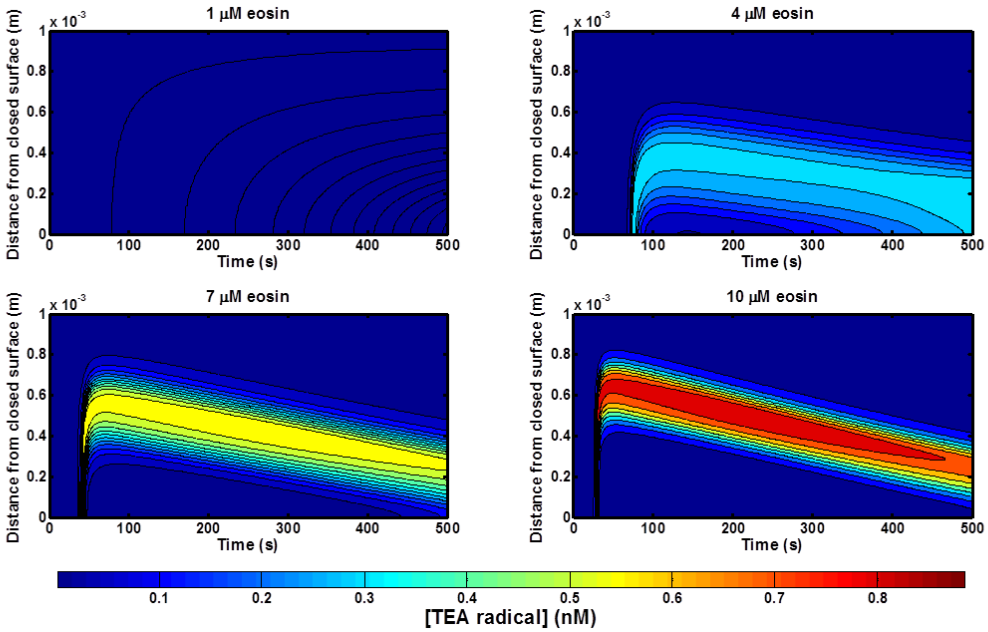

Figure 3-3. Contour plots of TEA radical concentrations as the contours with time as the x-axis and distance from the surface open to air as the y-axis at different initial eosin concentrations.

In our model, eosin is unable to be regenerated in the absence of oxygen, thus new TEA radicals cannot be generated near the closed surface after all the oxygen has been consumed. With termination and propagation reactions consuming TEA radicals, the

regions near the closed surface are therefore unable to sustain high TEA radical concentrations. On the other hand, TEA· concentrations close to the open surface with continuous oxygen diffusing into the system also remain low due to the fast kinetics of the oxygen inhibition reaction. Due to this dual role of oxygen in our reaction scheme, the peak TEA radical concentration thus takes place around the diffusion front where some oxygen is present for eosin regeneration to occur while still having a low enough oxygen concentration for the oxygen inhibition rate to be slow.

3.3.3 Propagation and regeneration rates

Figure 3-4 shows the spatial and temporal distribution of the total rates of propagation whereby monomers are added onto the ends of propagating radicals. The contour plots show initial bursts of propagation activity some distance away from the closed surface, with the maximum propagation rates at each time point gradually decreasing in magnitude and moving towards the closed surface as time progresses. This trend follows the movement of the TEA· concentration front as the diffusion of oxygen from the open air surface results in competition between inhibition and propagation reactions both of which have propagating radicals as a reactant. Having a higher initial eosin concentration results in higher peak propagation rates that are further away from the closed surface due to the faster consumption of oxygen at higher eosin concentrations as more radicals are generated and the diffusion of oxygen from air is unable to penetrate far from the open surface before reacting.

One unique aspect of the model is the inclusion of a reaction that regenerates eosin after it has reacted to produce a TEA radical. This provides a mechanism for the ability of low concentrations of photoinitiator to polymerize acrylate monomers in the presence of much larger concentrations of an inhibitor; regenerated eosin molecules can undergo further initiation reactions to produce free radicals that may propagate. Thus, the regeneration rate profiles are also plotted at various initial eosin concentrations in Figure 3-5. The contour plots all show similar regeneration rate profiles, with high regeneration rates during the initial stages across the whole spatial dimension as the initially dissolved oxygen is being consumed and a slowly decreasing rate nearer the open surface moving towards the closed surface as time goes on. These plots suggest

that regeneration is continuously occurring in regions where oxygen is replenished by dissolution into the polymerization mixture from the open air.

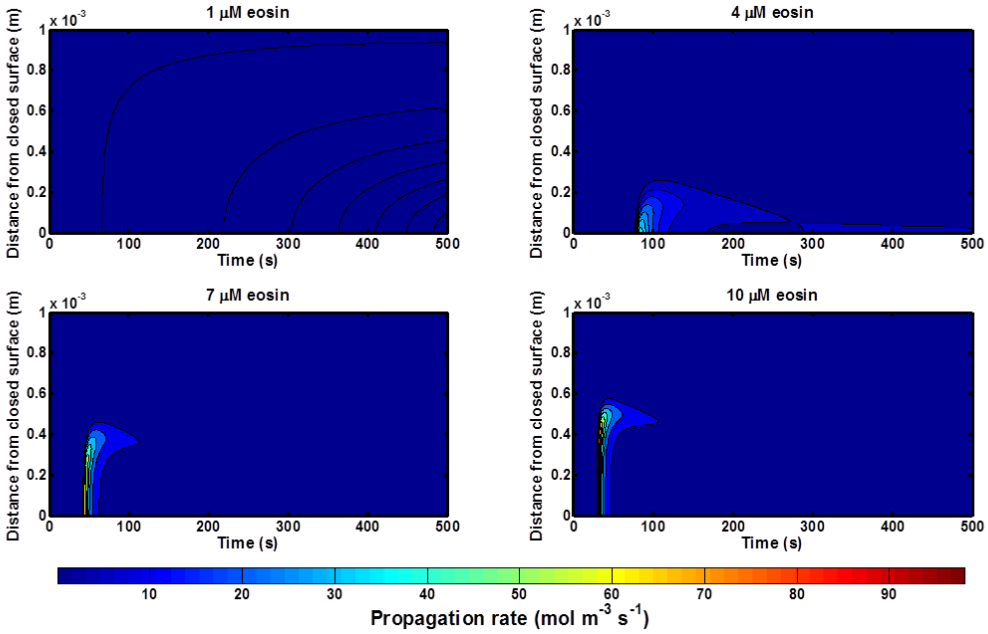

Figure 3-4. Contour plots of the total rate of propagation as the contours with time as the x-axis and distance from the surface open to air as the y-axis at different initial eosin concentrations.

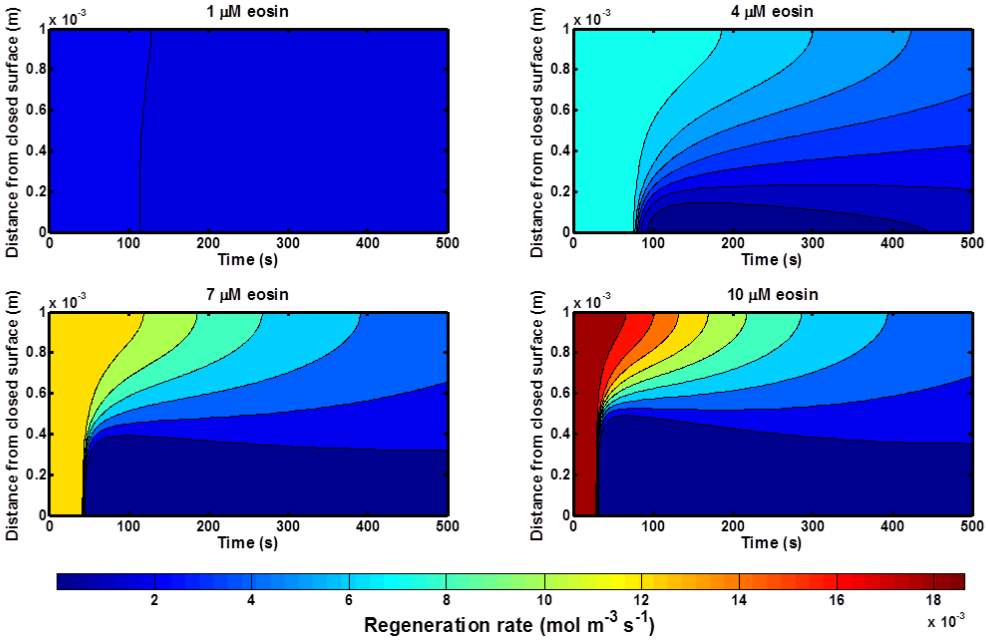

Figure 3-5. Contour plots of regeneration rates as the contours with time as the x-axis and distance from the surface open to air as the y-axis at different initial eosin concentrations.

3.3.4 Double bond conversion

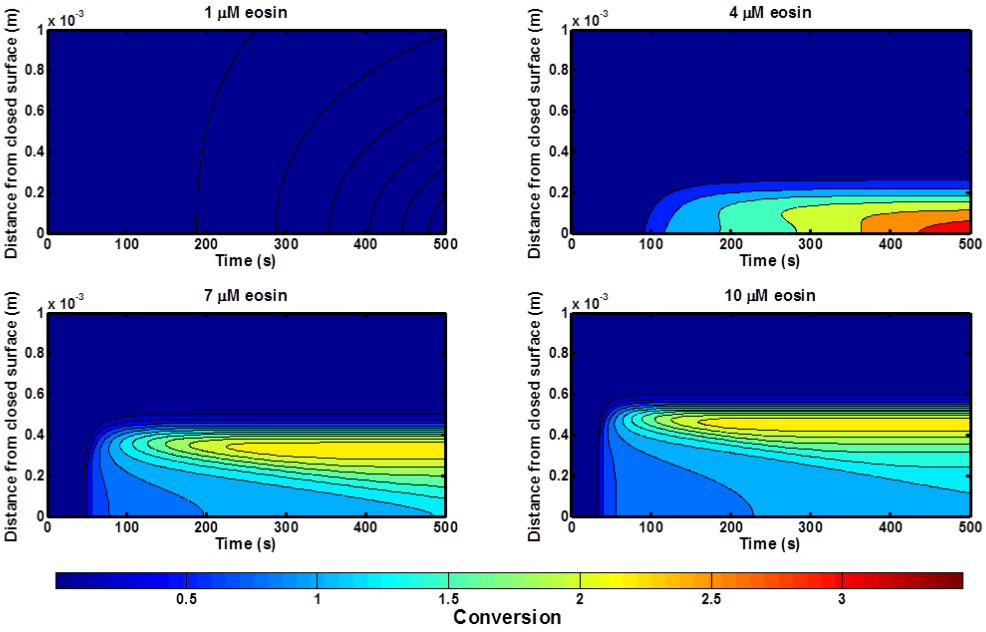

Figure 3-6. Contour plots of conversion, the total concentration of double bonds reacted at each position scaled to the initial total double bond concentration, as the contours with time as the x-axis and distance from the surface open to air as the y-axis at different initial eosin concentrations.

Conversion, which is the amount of double bonds reacted scaled to its initial total amount, is one property that denotes the extent of polymerization. Its value commonly ranges between zero and one, but for our reaction-diffusion model whereby monomers can diffuse into other spatial positions, the value of conversion can exceed the conventional limit of one as monomer molecules are able to move to regions of space with lower concentrations and react there. Consequently, the contour plots of conversion as a function of time and space in Figure 3-6 have contours with values that are above one as those are regions where propagation rates were the highest and therefore consumed more monomers as they diffused from the regions of higher concentrations to these regions of large propagation rates. The thickness of the polymer film that is formed can be taken to be the furthest distance from the closed surface with conversion of at least 0.2, and the plots show a trend of increasing thickness as the initial eosin concentration was increased from 4 μM to 10 μM. Further propagation reactions can still occur within these regions after the initial burst of reactivity with a

greater increase in conversion closer to the closed surface as time progresses, matching the trends of the moving TEA· concentration front. In addition, higher initial eosin concentrations result in a more rapid onset of polymerization as the time required for conversion to reach one decreases as the initial eosin concentration is increased.

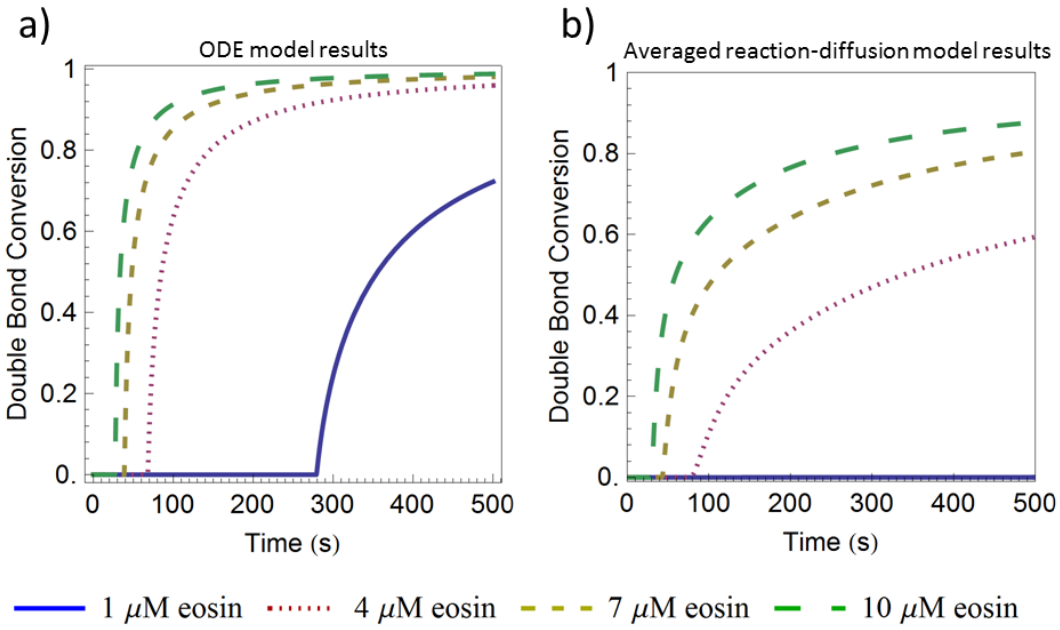

Figure 3-7. Plots of conversion obtained a) from an ODE model[78] that excludes diffusion effects and continuous flux of oxygen from the open surface, and b) from the reaction-diffusion model averaged over the whole spatial dimension at each time step.

Another property of interest is the average conversion achieved over the whole polymerization mixture as it signifies the extent of reaction of the monomers. The plot of conversion in Figure 3-7 tracks the overall amount of monomer reacted with time, indicating the progress of polymerization. Both figures show that a higher initial eosin concentration requires a shorter period of time before polymerization starts while also resulting in a higher overall averaged conversion. This trend matches that of the results obtained experimentally[73,78], whereby the conversion, as measured using spectroscopic techniques, follows a similar shape with experiments at higher initial eosin concentrations polymerizing faster. Furthermore, comparing both conversion profiles also indicate that the continuous flux of oxygen into the system as in the reaction-diffusion case slows down the overall polymerization process as inhibition times are

increased. This can be explained by the addition of a greater amount of oxygen into the reaction system that further inhibits the propagation reaction when the open air boundary is considered in the reaction-diffusion system.

3.3.5 Inhibition (t_{inh}) and gelation ($t_{0.2}$) times

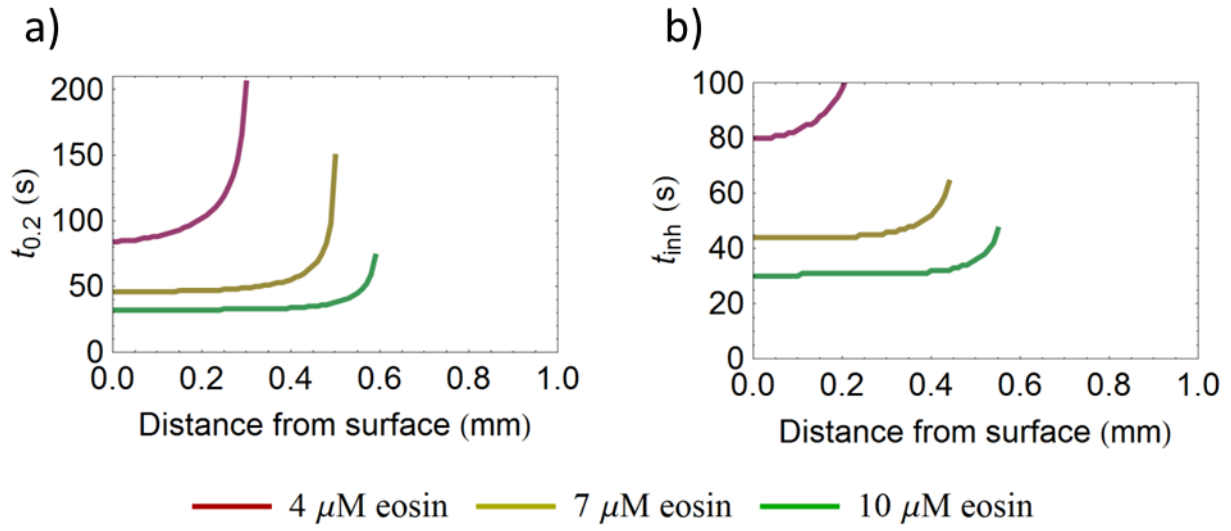

Figure 3-8. Plots of (a) time required for oxygen concentration to drop to 10^{-6} M and (b) time required for scaled amount of reacted monomer to reach 0.2 as a function of distance from the surface open to air. The 1 μM eosin case is not plotted due to negligible reaction predicted by the model.

With a continuous flow of oxygen from the surface open to air diffusing into the reaction mixture, it is of interest to determine how long it takes for the initial oxygen concentration to drop to concentrations where propagation is comparable to inhibition (t_{inh}) and the scaled amount of monomer reacted to reach 0.2 ($t_{0.2}$) at various positions in space as it provides an idea of the time period required for polymerization to begin and a hydrogel to form, respectively. As shown in Figure 3-8, both t_{inh} and $t_{0.2}$ show a drastic increase as the distance from the closed surface is increased, with a higher initial eosin concentration leading to lower values and penetrating further way from the closed surface as well. This can be explained by the diffusion of oxygen from the air inhibiting the polymerization reactions, with higher initial eosin concentrations able to produce more radicals quickly and therefore reaching further away from the closed surface and having shorter times. In addition, the maximum distance away from the

closed surface that $t_{0.2}$ is able to reach is further than that for t_{inh}. This suggests that it is not necessary for the local oxygen concentration to go below 10^{-6} M in order for propagation and consumption of monomer to occur, and that diffusion allows for the broadening of the propagation front.

3.4 Conclusions

The trends obtained from the reaction-diffusion simulations indicate that the addition of a boundary condition modeling the surface open to air as a source of oxygen continuously diffusing into the reaction system introduces spatial variations to the overall polymerization process. In the initial stages when the light is first turned on, the inhibition reactions are much faster than the oxygen flux into the system due to the dissolution of atmospheric oxygen into the aqueous reaction mixture, resulting in an oxygen gradient where oxygen diffuses from the surface representing the open air to the closed solid surface. Due to the dual roles of oxygen as both a free radical inhibitor and an oxidizing agent that reacts to form peroxy radicals which regenerate eosin radicals, there is a broad reaction front that moves in space with time whereby most of the reactive free radicals that can propagate are generated. The initial eosin concentration present in the reaction system is found to have a large influence on the time required for the formation of this front as well as the furthest distance away from the closed surface that this front can reach, and the resulting effects of polymerization such as the conversion profile and t_{inh} and $t_{0.2}$ are also strongly dependent on the initial eosin concentration. These findings signify that oxygen plays a nuanced role in this overall polymerization process as it both inhibits the propagation reactions while also being required to regenerate eosin for further production of free radicals. This is in contrast with more traditional polymerization reactions where oxygen acts only as an inhibitor that slows down the rate of polymerization and where peroxy radicals or other oxygen-containing species do not participate in any regeneration reactions that could initiate further propagation reactions. Without any eosin regeneration reaction, polymerization is unable to proceed at such low initiator concentrations in the presence of a large excess of oxygen, but the inclusion of regeneration of eosin diminishes the influence of oxygen inhibition and allows for the buildup of free radicals to polymerize

the reaction system. The continuous oxygen flux condition thus creates a moving reaction front as the rates of inhibition and regeneration are both dependent on the flow of oxygen.

Chapter 4. Effect of amine chain peroxidation

4.1 Introduction

As demonstrated in Chapter 2, the peroxy-mediated eosin-regeneration mechanism alone has been shown to be inadequate to explain the ability of eosin-tertiary amine to initiate photopolymerizations in the presence of oxygen. Preliminary experimental studies performed in-house showed that the choice of tertiary amines to include in the amplification solution had a substantial impact on polymerization times. This suggests that the tertiary amine should participate in a significant reaction that reduces the effect of oxygen inhibition. Previous studies have proposed amine chain peroxidation[84–86] as a possible reaction that explains the faster consumption of oxygen when amines are present in certain photopolymerization conditions. The full mechanism behind reactions of amines with oxygen is poorly understood, with many other possible reactions other than hydrogen transfers and radical-radical reactions proposed, but resolving the full complexity of this chemistry is beyond the scope of this thesis.

Amine chain peroxidation involves the reaction between a less reactive peroxy radical formed by the inhibition reaction between oxygen and a reactive free radical, which is mainly the TEA radical before propagation can proceed at significant rates. The amine chain peroxidation is modeled as the following reaction with a rate constant k_{amine}:

$$P_nOO\bullet + TEA \xrightarrow{k_{amine}} P_nOOH + TEA\bullet \quad (1)$$

where $P_nOO\bullet$ is a peroxy radical of any length, TEA is triethanolamine, TEA• is a reactive TEA radical and P_nOOH is an unreactive hydroperoxide. The net effect of this reaction is to directly convert a less reactive peroxy radical to a reactive free radical which can further consume more oxygen. The addition of this amine chain peroxidation reaction is thus anticipated to reduce the model-predicted polymerization times, thereby bringing it closer to experimental values. On the other hand, amine chain peroxidation

also competes with the regeneration of eosin for peroxy radicals as both reactions require it as an oxidizing reactant, potentially delaying the onset of polymerization.

4.2 Modifications to ODE Model

A summary schematic of the updated model incorporating amine chain peroxidation is shown in Scheme 4-1. The amine chain peroxidation reaction (Eq. 1) is added onto the basic model framework as previously mentioned in Chapter 2, creating an additional closed loop between peroxy radicals and TEA radicals. The full reaction scheme is shown in Scheme 4-2, with the rate equation for amine chain peroxidation shown in Eq. 21. The default value of k_{amine} was set to 10^4 $mM^{-1}s^{-1}$ as that is in the middle of the range of experimental values[87] for hydrogen abstraction by peroxy radicals. The other parameters utilized in the model were the same as those in Tables 2-2, 2-3 & 2-4.

Scheme 4-1. Summary of important reactions incorporating amine chain peroxidation.

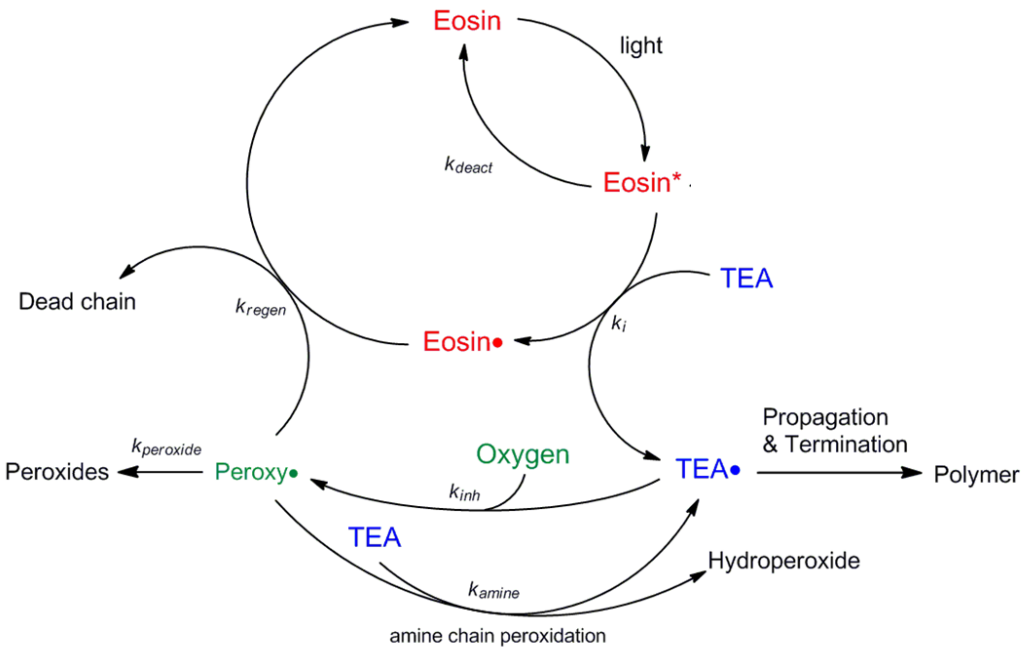

Scheme 4-2. Overall reaction scheme utilized in the kinetic rate model including the amine chain peroxidation reaction.

Photogeneration of radicals:

$$E \xrightarrow{h\nu} E^* \qquad \text{Rate} = \frac{\varepsilon I_0 [E]}{E'} \qquad (2)$$

$$E^* \xrightarrow{k_{deact}} E \qquad \text{Rate} = k_{deact}[E^*] \qquad (3)$$

$$E^* + TEA \xrightarrow{k_i} EH\bullet + TEA\bullet \qquad \text{Rate} = k_i[E^*][TEA] \qquad (4)$$

Initiation:

$$TEA\bullet + PEGDA \xrightarrow{k_{p,A}} P_n\bullet \qquad \text{Rate} = k_{p,A}[TEA\bullet][PEGDA] \qquad (5)$$

$$TEA\bullet + VP \xrightarrow{k_{p,B}} P_n\bullet \qquad \text{Rate} = k_{p,B}[TEA\bullet][VP] \qquad (6)$$

$$P_nO\bullet/TEA-O\bullet + PEGDA \xrightarrow{k_{p,A}} P_n\bullet \qquad \text{Rate} = k_{p,A}[P_nO\bullet][PEGDA] \qquad (7)$$

$$P_nO\bullet/TEA-O\bullet + VP \xrightarrow{k_{p,B}} P_n\bullet \qquad \text{Rate} = k_{p,B}[P_nO\bullet][VP] \qquad (8)$$

Propagation:

$$P_n\bullet + PEGDA \xrightarrow{k_{p,A}} P_n\bullet \qquad \text{Rate} = k_{p,A}[P_n\bullet][PEGDA] \qquad (9)$$

$$P_n\bullet + VP \xrightarrow{k_{p,B}} P_n\bullet \qquad \text{Rate} = k_{p,B}[P_n\bullet][VP] \qquad (10)$$

Radical terminations:

$$P_n\bullet + TEA\bullet \xrightarrow{k_t} P_{n+1} \qquad \text{Rate} = k_t[P_n\bullet][TEA\bullet] \qquad (11)$$

$$P_n\bullet + P_n\bullet \xrightarrow{k_t} P_{n+n} \qquad \text{Rate} = k_t[P_n\bullet][P_n\bullet] \qquad (12)$$

$$P_n\bullet + P_nO\bullet/TEA-O\bullet \xrightarrow{k_t} P_{n+n} \qquad \text{Rate} = k_t[P_n\bullet][P_nO\bullet] \qquad (13)$$

Radical quenching:

$$P_nO\bullet/TEA-O\bullet + TEA\bullet \xrightarrow{k_t} P_{n+n} \qquad \text{Rate} = k_t[P_nO\bullet][TEA\bullet] \qquad (14)$$

$$2P_nO\bullet/TEA-O\bullet \xrightarrow{k_t} P_{n+n} \qquad \text{Rate} = k_t[P_nO\bullet][P_nO\bullet] \qquad (15)$$

Inhibition by oxygen:

$$TEA\bullet + O_2 \xrightarrow{k_{inh}} P_nOO\bullet \qquad \text{Rate} = k_{inh}[TEA\bullet][O_2] \qquad (16)$$

$$P_n\bullet + O_2 \xrightarrow{k_{inh}} P_nOO\bullet \qquad \text{Rate} = k_{inh}[P_n\bullet][O_2] \qquad (17)$$

Regeneration of eosin:

$$P_nOO\bullet + EH\bullet \xrightarrow{k_{regen}} POOH + E \qquad \text{Rate} = k_{regen}[P_nOO\bullet][EH\bullet] \qquad (18)$$

Peroxy radical reactions:

$$P_nOO\bullet + TEA\bullet \xrightarrow{k_{peroxide}} POO-TEA \qquad \text{Rate} = k_{peroxide}[P_nOO\bullet][TEA\bullet] \qquad (19)$$

$$P_nOO-TEA \xrightarrow{k_{dis}} P_nO\bullet + TEA-O\bullet \qquad \text{Rate} = k_{dis}[P_nOO-TEA] \qquad (20)$$

Amine chain peroxidation:

$$P_nOO\bullet + TEA \xrightarrow{k_{amine}} POOH + TEA\bullet \qquad \text{Rate} = k_{amine}[P_nOO\bullet][TEA] \qquad (21)$$

4.3 Results and Discussion

After the addition of the amine chain peroxidation reaction into the overall photopolymerization reaction scheme, we first examined its effects on the conversion profiles at various eosin concentrations. The previous experimental data (Chapter 2) is

compared with the updated model predictions in Figure 4-1. The updated model results show a similar conversion profile as with previous results, with an almost immediate onset of polymerization and rapid change from no conversion to almost full conversion. The trend where increasing the eosin concentration results in faster polymerizations still holds in the updated model, but inhibition times are now almost negligible for most of the concentrations when amine chain peroxidation is incorporated.

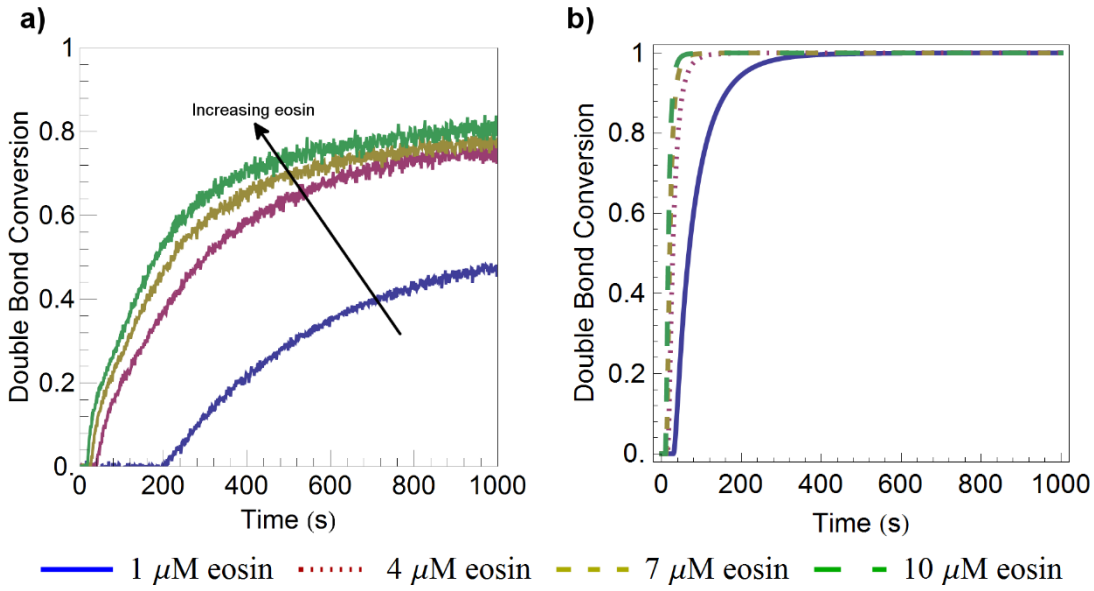

Figure 4-1. Comparison of representative conversion profiles as a function of time for various starting eosin concentrations obtained (a) experimentally and (b) from simulations including the amine chain peroxidation reaction.

A similar plot of $t_{0.2}$ against eosin concentration was also plotted to compare model predictions with experimental results. Figure 4-2 shows that the updated model predicts that $t_{0.2}$ decreases according to a power law of slope -0.54, with a magnitude much smaller than both the experiments and what was predicted previously in Figure 2-15. This reduction in magnitude of the slope suggests that the addition of amine chain peroxidation has resulted in eosin concentration being a less limiting factor in starting the polymerization process, and that the amine chain peroxidation reaction has diminished the effects of oxygen inhibition resulting in much shorter inhibition times.

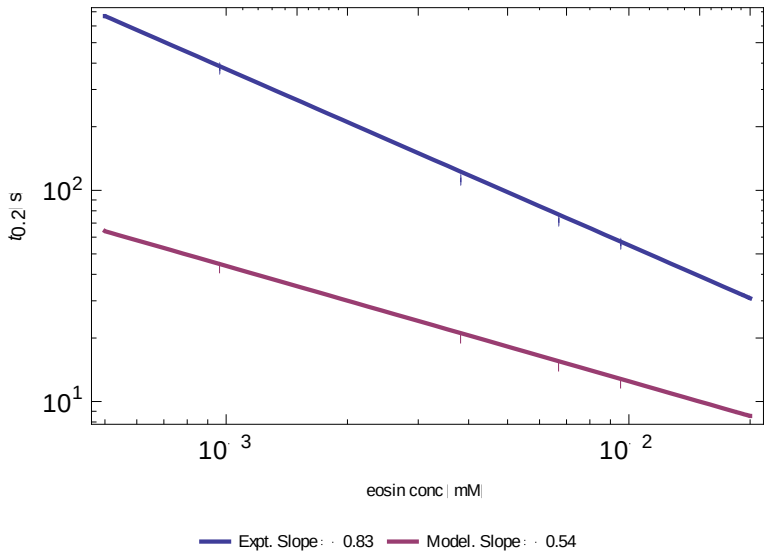

Figure 4-2. Log-log plot comparing $t_{0.2}$ obtained from model simulations including the amine chain peroxidation reaction with experimental data.

The model's sensitivity to the value of k_{amine} when the system has 0.5 mM of dissolved oxygen initially present with 0.4 μM eosin or 4 μM eosin is plotted in Figure 4-3. At both eosin concentrations, the contour plots show that when the value of k_{amine} is close 10^0 $mM^{-1}s^{-1}$, the onset of polymerization is very sensitive to the exact value of k_{amine}, with almost an order of magnitude changes in time required before polymerization occurs when value of k_{amine} is varied by an order of magnitude. However, if the value of k_{amine} is below ~10^{-2} $mM^{-1}s^{-1}$ or above ~10^2 $mM^{-1}s^{-1}$, the effects of an inaccurate estimate of k_{amine} become less significant, indicating that some other reaction becomes the rate-limiting step. This sensitivity analysis demonstrates that amine chain peroxidation in combination with regeneration greatly influences the conversion profile for very low concentrations of eosin. On the other hand, the sensitivity range of k_{amine} becomes smaller at the higher starting eosin concentration of 4 μM, suggesting that the amine chain peroxidation and regeneration reactions become less important when more eosin is present in the system.

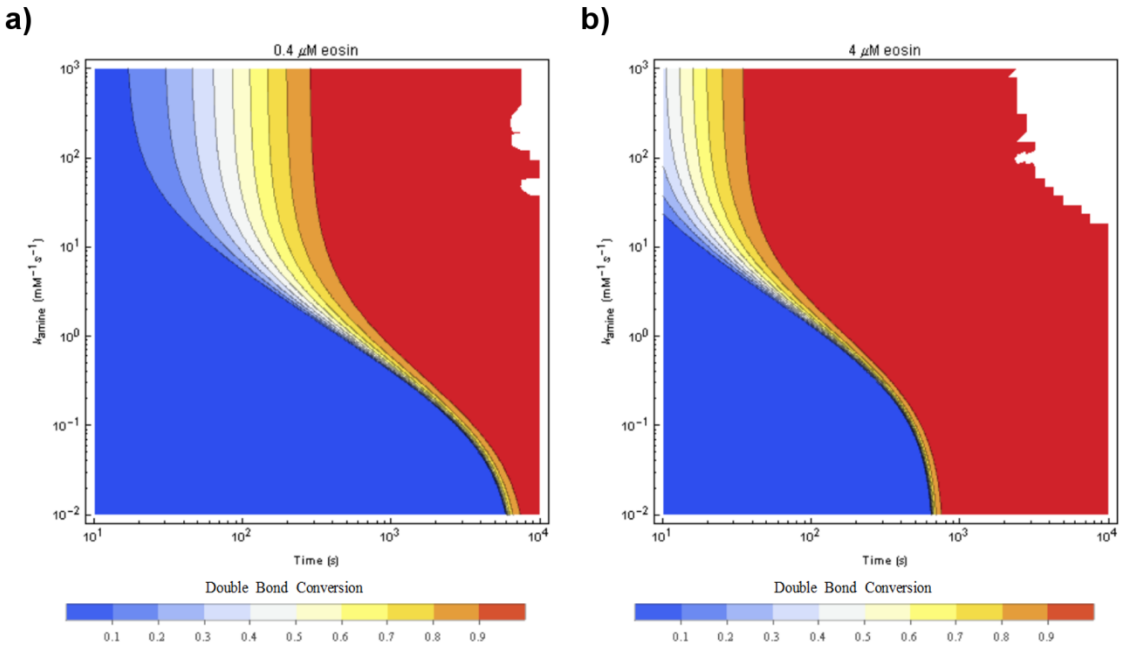

Figure 4-3. Contour plots on a log-log scale from model simulations showing how the value of k_{amine} affects conversion, with time as x-axis, k_{amine} as y-axis and conversion as the contours. Two different starting eosin concentrations are shown: (a) 0.4 µM eosin; (b) 4 µM eosin.

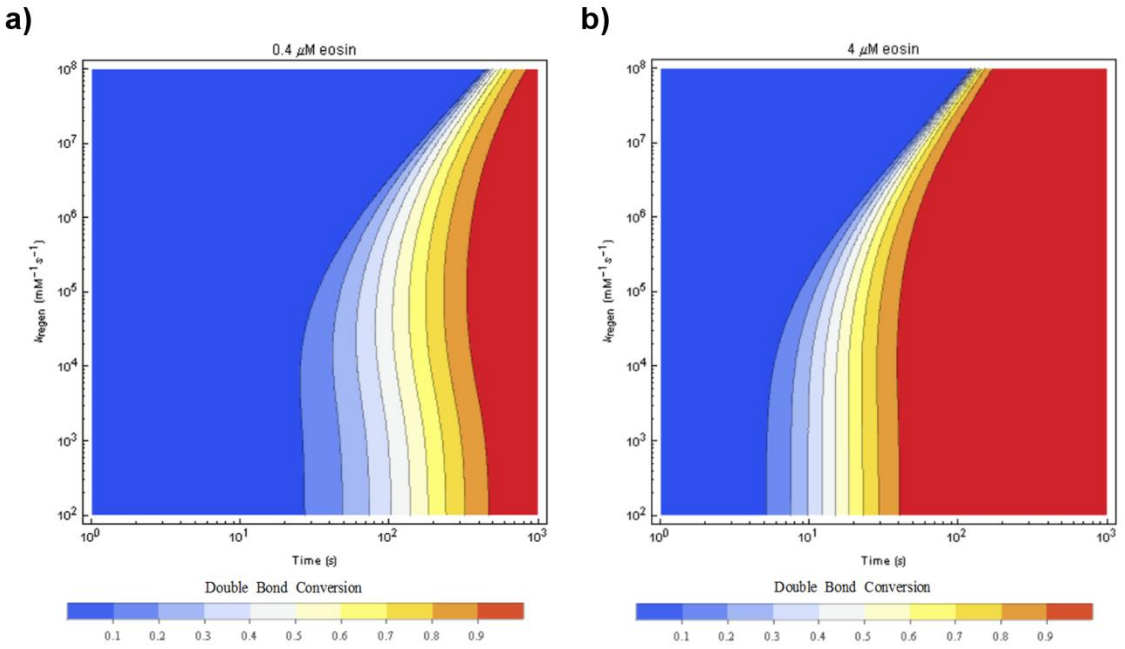

Figure 4-4. Contour plots on a log-log scale from model simulations showing how the value of k_{regen} affects conversion, with time as x-axis, k_{regen} as y-axis and conversion as the contours. Two different starting eosin concentrations are shown: (a) 0.4 µM eosin; (b) 4 µM eosin.

Figure 4-4 shows a similar sensitivity analysis performed for k_{regen}. The contour plots show that when the value of k_{regen} is reduced from a large value, the onset of polymerization occurs earlier, with about an order of magnitude decrease in inhibition time when k_{regen} is reduced by 2 orders of magnitude from ~10^8 $mM^{-1}s^{-1}$ to ~10^6 $mM^{-1}s^{-1}$. However, even if k_{regen} is decreased to less than ~10^5 $mM^{-1}s^{-1}$, there is no longer any reduction in inhibition times. This suggests that there is a competition between the eosin regeneration and amine chain peroxidation reactions as peroxy radicals are critical reactants that participate in both of these reactions. A faster regeneration reaction actually results in a slower onset of polymerization as regenerating eosin is a slower indirect pathway to generate free radicals that react with oxygen as compared to direct hydrogen transfer between peroxy radicals and TEA during amine chain peroxidation.

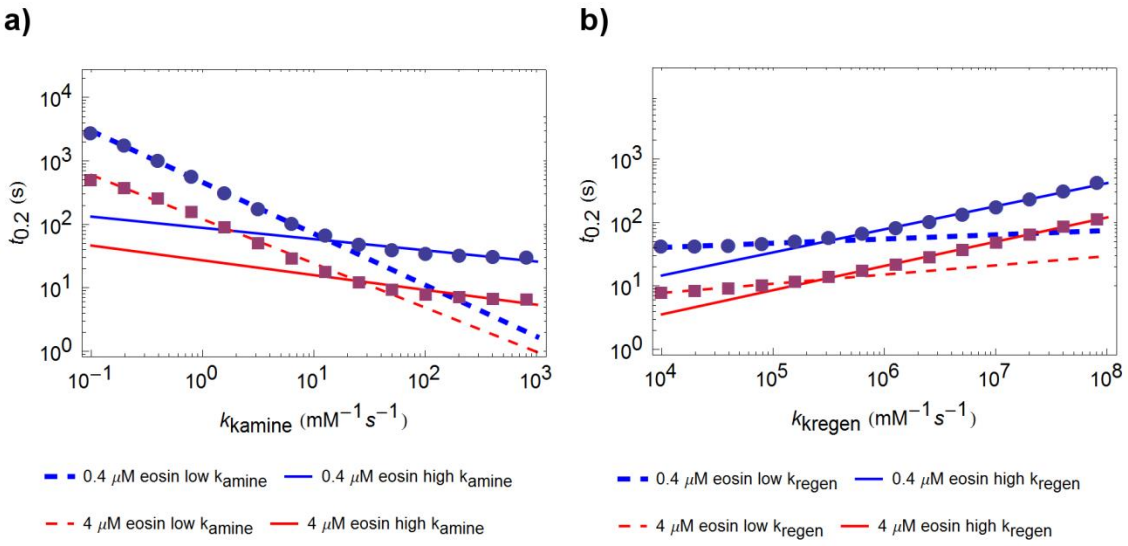

Figure 4-5. Log-log plot obtained from model simulations comparing $t_{0.2}$ obtained at two different eosin concentrations. The lines are best-fit lines to their corresponding data points.

The model-predicted $t_{0.2}$ as a function of k_{amine} and k_{regen} obtained from the model simulations presented in Figure 4-3 and Figure 4-4 are plotted on a log scale in Figure 4-5. These results more clearly showcase the competing effects that eosin regeneration and amine chain peroxidation has on polymerization times; increasing k_{amine} below 10^1 $mM^{-1}s^{-1}$ generally decreases $t_{0.2}$ while increasing k_{regen} above 10^6 $mM^{-1}s^{-1}$ generally increases $t_{0.2}$. However, the diffusion-limited value for second-order rate constants in

water is about 10^5–10^6 $mM^{-1}s^{-1}$, so the effects of an inaccurate value of k_{regen} is less significant.

The effect of varying eosin concentration in tandem with either k_{amine} or k_{regen} on model predictions of $t_{0.2}$ is plotted in Figure 4-6. Taken together, both plots show that $t_{0.2}$ is predicted to decrease by increasing eosin concentration, increasing k_{amine} or decreasing k_{regen}. In the whole range of k_{regen} simulated, the sensitivity of $t_{0.2}$ towards eosin concentration is almost uniform, however, at values of k_{amine} ragning between ~10^0 $mM^{-1}s^{-1}$ and ~10^1 $mM^{-1}s^{-1}$, the sensitivity of $t_{0.2}$ towards eosin concentration is greatly reduced. This implies that the value of k_{regen} is a more influential factor in predicted polymerization times as it seems to determine which reactions are limiting in the overall reaction scheme.

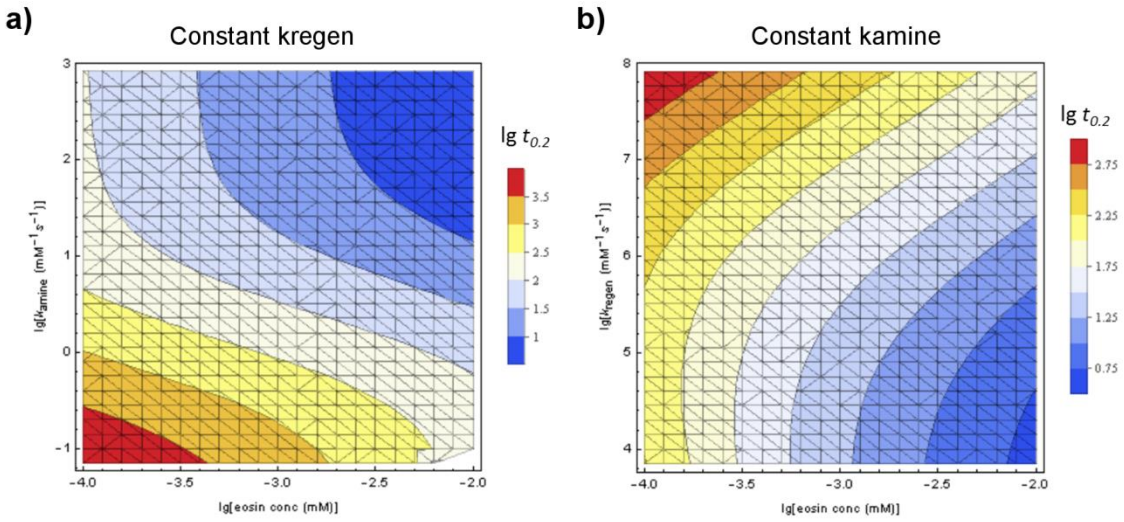

Figure 4-6. Contour plots from model simulations showing how the eosin concentration affects $t_{0.2}$ as k_{amine} and k_{regen} are varied as the other is held constant, with $t_{0.2}$ as the contours and eosin concentration as x-axis. (a) k_{amine} as y-axis and; (b) k_{regen} as y-axis.

As the unknown rate constants are expected to be invariant with concentrations at a constant temperature, it was anticipated that an estimate of k_{amine} and k_{regen} might be possible by comparing the model simulation results with experimental data. The values of $t_{0.2}$ obtained from the experiments at two different eosin concentrations in Chapter 2 are represented as black dotted lines in Figure 4-7, where the model predictions of $t_{0.2}$ are plotted as contours while k_{amine} and k_{regen} are varied. The sets of combinations for

the values of k_{amine} and k_{regen} that match the experimental values were then extracted and plotted as line plots in Figure 4-8. It was expected that if the overall reaction scheme was complete with all the pertinent reactions included, there would be a single set of combinations of rate constants that would remain the same even when different concentrations of reactant were used. In the case of our model, the two line plots are almost parallel with an intersection point located at very low physically unfeasible values, indicating that we would require different values of rate constants at different eosin concentrations in order to get a match between experiments and model. This inconsistency between parameter sets implies that the updated model with amine chain peroxidation is still incomplete, and that some other reaction(s) would need to be incorporated into the reaction scheme.

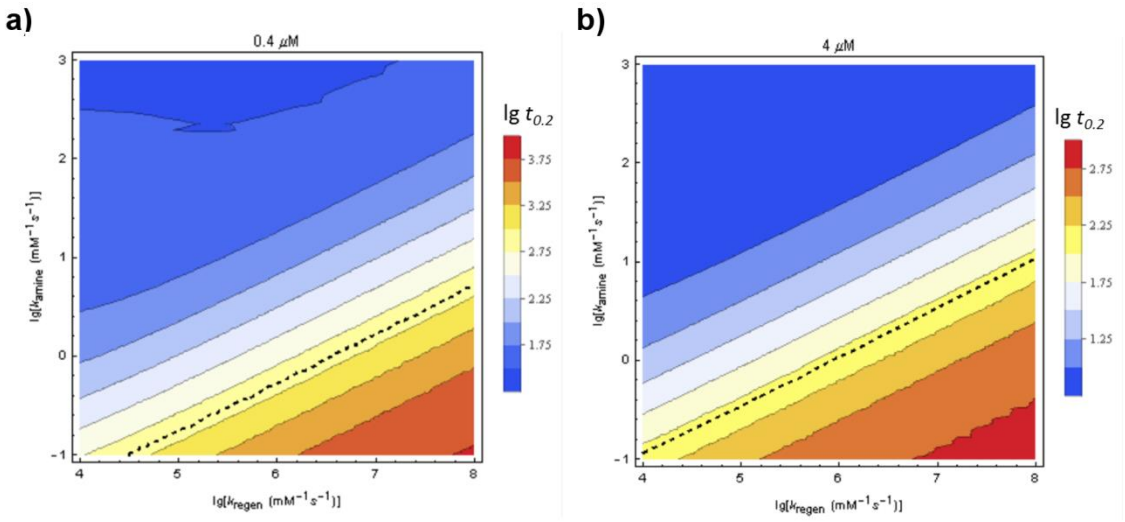

Figure 4-7. Contour plots from model simulations showing how the predicted $t_{0.2}$ changes as k_{amine} and k_{regen} are varied. Two different starting eosin concentrations are shown: (a) 0.4 μM eosin; (b) 4 μM eosin. The black dotted lines represent the experimental values of $t_{0.2}$ from Chapter 2.

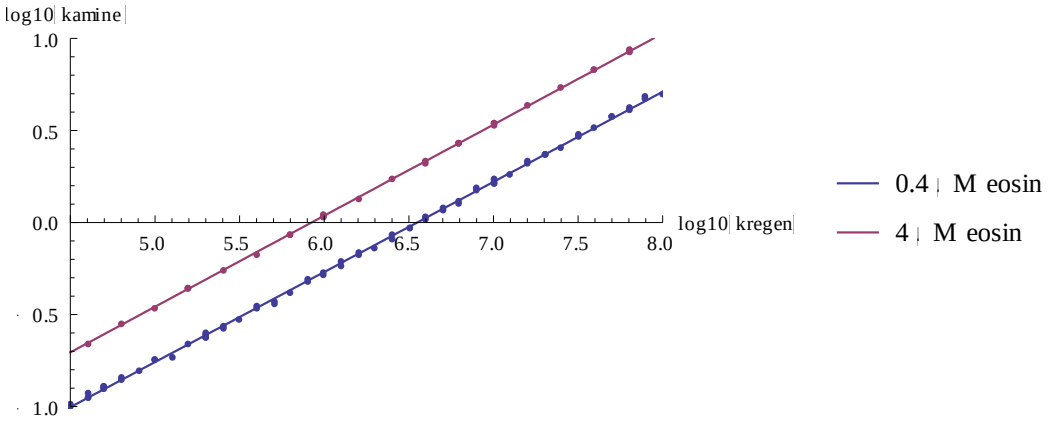

Figure 4-8. Plots of sets of values of (k_{amine}, k_{regen}) obtained from Figure 4-7 that result in predicted values of $t_{0.2}$ matching the experimental values at 0.4 & 4 μM eosin with the corresponding best-fit lines.

4.4 Conclusions

The addition of amine chain peroxidation into the overall reactions scheme has drastically reduced the model-predicted polymerization times. The rate of consumption of oxygen is greatly increased due to the creation of a cycle that produces reactive free radicals from less reactive peroxy radicals through the transfer of hydrogen from the plentiful TEA present in the reaction system. This cyclical reaction pathway involving TEA and its derived species is now the main method whereby oxygen becomes rapidly consumed, resulting in greatly decreased inhibition times. Comparison between the model predictions and experiments suggest that the model is still incomplete as inconsistencies in the estimated value of rate constants become apparent when different eosin concentrations are considered.

Chapter 5. Impacts of amine chain peroxidation and higher surface concentration of eosin on the reaction-diffusion model

5.1 Introduction

In polymerization-based amplification (PBA), the presence of the analyte of interest is detected by the formation of a polymer film after a set duration of illumination of light, while a negative result produces no polymer within that same period of time. The difference between these two cases is the binding events which occur only when the target analyte is present in the test sample. The specific and selective binding interactions between the target analyte and the functionalized surface results in an increased concentration of eosin on the solid surface as the bioconjugated eosin that is subsequently added is then able to sandwich the analyte of interest without being removed during the ensuing washing steps before the amplification process. A small discrepancy between the surface and bulk eosin concentration is enough to distinguish between the presence or absence of the target analyte in the sample, with prior experimental results[10] demonstrating that a minimum of about 15 biotin molecules per square micrometer on the surface is adequate.

Many model simulations have previously been performed in order to investigate the process of polymers growing from a solid surface as in free radical graft polymerization[88] or surface-initiated controlled radical polymerizations such as Atom Transfer Radical Polymerizations[89,90] and photoiniferter-mediated polymerizations[75,91], but these models only considered initiators present only on the solid surface without any other initiating radicals present in the bulk solution. On the other hand, Turgman-Cohen & Genzer have simulated controlled living polymerizations that concurrently occur in both the bulk and on the surface[76,92] and obtained useful trends comparing the resultant surface versus bulk polymers, but their models utilized Monte Carlo methods that has no direct correlation to actual reaction kinetics and polymerization times.

In this chapter, we explore the effects of both amine chain peroxidation and a higher surface eosin concentration on the kinetics of polymerization at the micromolar eosin concentrations studied in previous chapters. A reaction-diffusion model incorporating the overall reaction scheme including amine chain peroxidation as proposed in Chapter 4 and the oxygen flux boundary condition as presented in Chapter 3 was developed. The option of having an increased surface eosin concentration was also added to model the binding events occurring for positive results during PBA, with the consequential trends resulting from having a higher surface eosin concentrations also examined and compared against the model with a uniform eosin concentration.

5.2 Model Development

Scheme 5-1. Overview of reaction-diffusion model incorporating the amine chain peroxidation reaction and a 1 nm surface region to model higher surface eosin concentrations.

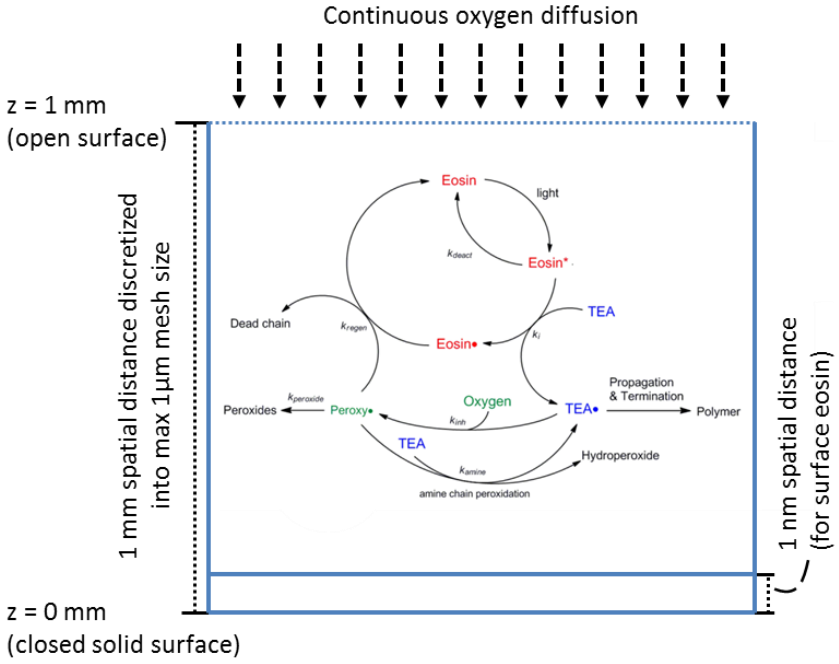

The reaction-diffusion model was further modified by including the amine chain peroxidation reaction as described in Chapter 4. In addition, a surface region of 1 nm in length near the closed surface was also created in the reaction-diffusion model to simulate the consequence of binding events creating a higher localized surface concentration of eosin (Scheme 5-1). Thus, in combination with the additional surface

region spatial mesh points, the full reaction scheme in Scheme 4-2 along with the corresponding values of the kinetic and diffusion parameters in Tables 3-1, 3-2, 3-3 & 3-4 and a default value of k_{amine} set to 10^4 $mM^{-1}s^{-1}$ was utilized in numerically solving this new reaction-diffusion model. In this model, a total eosin concentration of 1 mM was assumed to be in the surface region if a higher surface eosin concentration was present, corresponding to about 600 molecules of total eosin molecules per square micrometer averaged over the 1 nm deep surface region. The eosin in this surface region was unable to diffuse, simulating the strong binding between the biomolecules.

With the shorter amounts of time required for the onset of polymerizations when amine chain peroxidation is included in the reaction scheme as presented in Chapter 4, the reaction-diffusion model was run up to a total of 100 seconds with a maximum time step of 0.1 seconds. The system of reaction-diffusion equations and its boundary conditions were numerically solved using BDF and PARDISO solvers in COMSOL, with the resulting reaction rates and species concentrations exported at 0.1 second intervals and subsequently plotted.

5.3 Results and Discussion

This section explores the effects of adding the amine chain peroxidation reaction into the overall photopolymerization reaction scheme in an updated reaction-diffusion model, both with and without a surface region at a higher eosin concentration of 1 mM that models the effect of binding events occurring in the presence of target analyte in the sample causing additional bioconjugated eosin to attach to the closed surface.

5.3.1 The effect of oxygen diffusing in from the open surface

The oxygen concentration contour plots as a function of time and distance from the closed surface at various initial eosin concentrations without and with the extra surface eosin are plotted in Figure 5-1 and Figure 5-2 respectively. Both figures are very similar with no noticeable difference and show an oxygen profile whereby oxygen is rapidly depleted closer to the closed surface while regions close to the open surface do not show complete depletion of oxygen as a result of the continuous flux of oxygen diffusing from the air into the modeled system. This diffusion of oxygen from the open air also

results in oxygen concentrations at all regions of space increasing with time after the initial burst of oxygen consumption. In addition, the initial eosin concentration has a large effect on the duration required for the initial rapid consumption of oxygen as well as the depth of penetration of the regions of low oxygen concentration away from the closed surface, with increased eosin concentrations resulting in shorter times and further distances.

Comparing Figure 5-1 and Figure 5-2 with the corresponding oxygen profiles without amine chain peroxidation in Figure 3-1 and noting the difference in the time scales on the x-axis of these figures, we find that oxygen consumption is much more rapid even at 1 μM eosin, with the regions of low oxygen concentrations reaching further away from the closed surface when amine chain peroxidation is included. With the amine chain peroxidation reaction acting as an additional reaction that consumes oxygen, the onset of polymerization occurs much earlier, while the competition between amine chain peroxidation and eosin regeneration for peroxy radicals results in the oxygen replenishment reaching further towards the closed surface as less eosin gets regenerated and produce more free radicals.

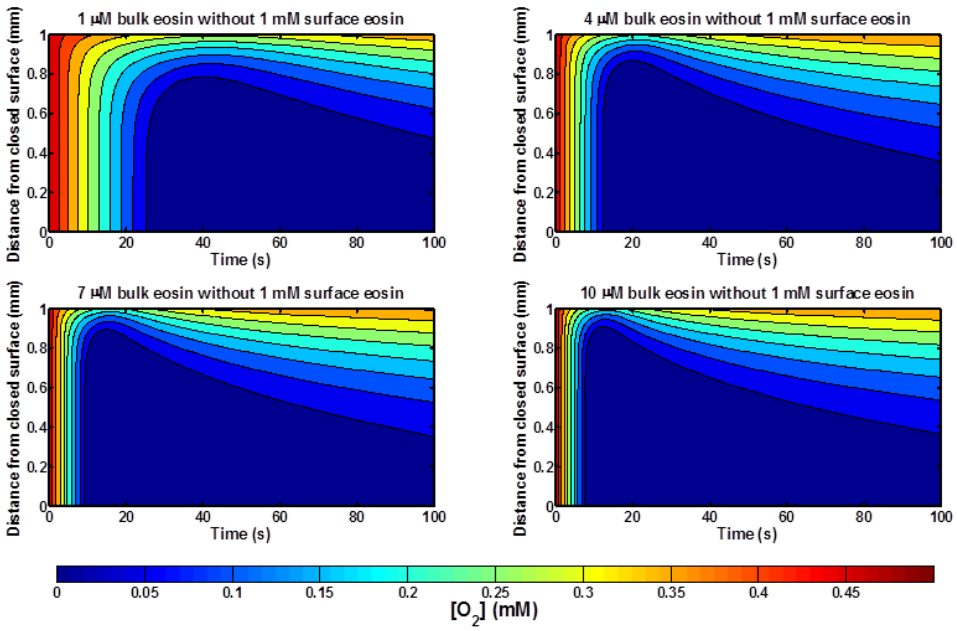

Figure 5-1. Contour plots of oxygen concentrations as the contours with time as the x-axis and distance from the surface open to air as the y-axis at different initial eosin concentrations without a higher eosin concentration at the closed surface.

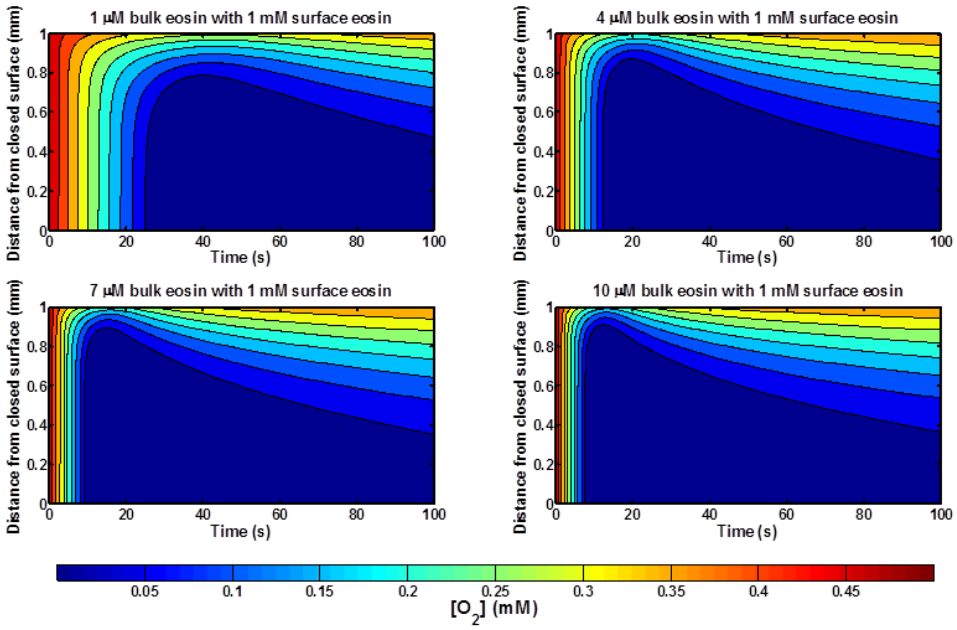

Figure 5-2. Contour plots of oxygen concentrations as the contours with time as the x-axis and distance from the surface open to air as the y-axis at different initial eosin concentrations with 1 mM of eosin at the closed surface region modeling the effects of prior surface binding events.

The contour plots of Da_{O2} as a function of time and space obtained from reaction-diffusion models without and with 1mM extra surface eosin are shown in Figure 5-3 and

Figure 5-4 respectively. In both cases, the profiles are very similar, with Da_{O2} gradually increasing until the onset of polymerization where a region of higher Da_{O2} reaches away from the closed surface, after which a very thin band of the highest values of Da_{O2} forms which slowly reaches towards the closed surface as time progresses. Furthermore, most of the values of Da_{O2} stay above 10^0 except for the enclosed region between the closed surface and the front that moves towards the closed surface with time as well as the areas close to the open surface at longer times, with a larger initial eosin concentration resulting in the faster onset of front formation and a smaller enclosed region of Da_{O2} with values below 10^0. Comparing these results with the corresponding reaction diffusion model results without amine chain peroxidation in Figure 3-2 suggests that the amine chain peroxidation reaction causes oxygen to be consumed more rapidly, resulting in the higher peak Da_{O2} and a thinner moving front as oxygen is able to be reacted away before being able to diffuse through the moving front into the inner regions.

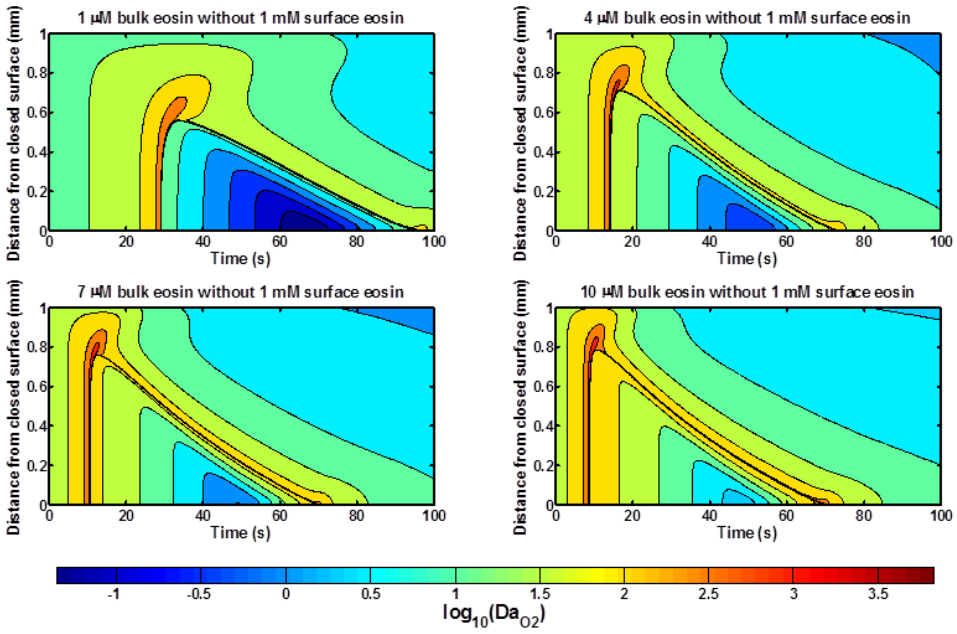

Figure 5-3. Contour plots of $\log_{10}$ of the Damkohler number of oxygen as the contours with time as the x-axis and distance from the surface open to air as the y-axis at different initial eosin concentrations without a higher eosin concentration at the closed surface.

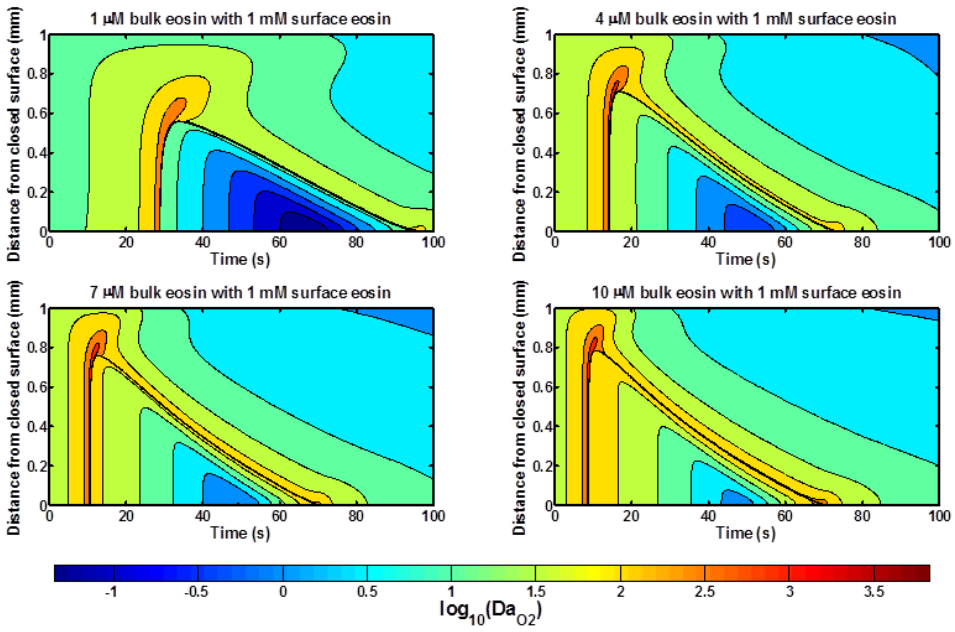

Figure 5-4. Contour plots of $\log_{10}$ of the Damkohler number of oxygen as the contours with time as the x-axis and distance from the surface open to air as the y-axis at different initial eosin concentrations with 1 mM of eosin at the closed surface region modeling the effects of prior surface binding events.

5.3.2 Tertiary amine (TEA) radical concentrations

Following the analysis of Da_{O2} presented earlier, the TEA radical profiles at various initial eosin concentrations both without and with the extra surface eosin are plotted in Figure 5-5 and Figure 5-6 respectively. Due to the very thin front where most of the highest TEA radicals are concentrated, the contours and colors have been plotted using a $\log_{10}$ scale for the TEA radical concentrations. Both figures show a very thin front of peak TEA radical concentrations that match the regions of peak Da_{O2} at each time point, with a higher initial eosin concentration resulting in a faster onset and further reach away from the closed surface for the TEA radical front as well as a higher peak TEA radical concentration. As eosin cannot be regenerated without oxygen, new TEA radicals cannot be generated near the closed surface after all the oxygen has been depleted while termination and propagation reactions consume TEA radicals. Conversely, with a continuous oxygen flux from the open surface, the TEA radicals react away quickly due to the fast oxygen inhibition reaction. A moving front is thus formed between these two competing regions where some oxygen is present for eosin

regeneration to occur while still being low enough for the rate of oxygen inhibition to be slow.

These very thin bands in Figure 5-5 and Figure 5-6 are in contrast with the results obtained from the reaction-diffusion model without amine chain peroxidation where a broad band of high TEA radical concentrations is observed (Figure 3-3), suggesting that when the overall rate of consumption of oxygen becomes very fast, the region where oxygen inhibition and eosin regeneration is comparable becomes narrower as the effects of oxygen being able to diffuse becomes less important. However, the presence of a front that moves in space and time implies that regeneration of eosin still plays an important role in initiating polymerization through the production of free radicals as only the dual role of oxygen as an inhibitor and oxidizing agent for eosin regeneration can account for this moving front.

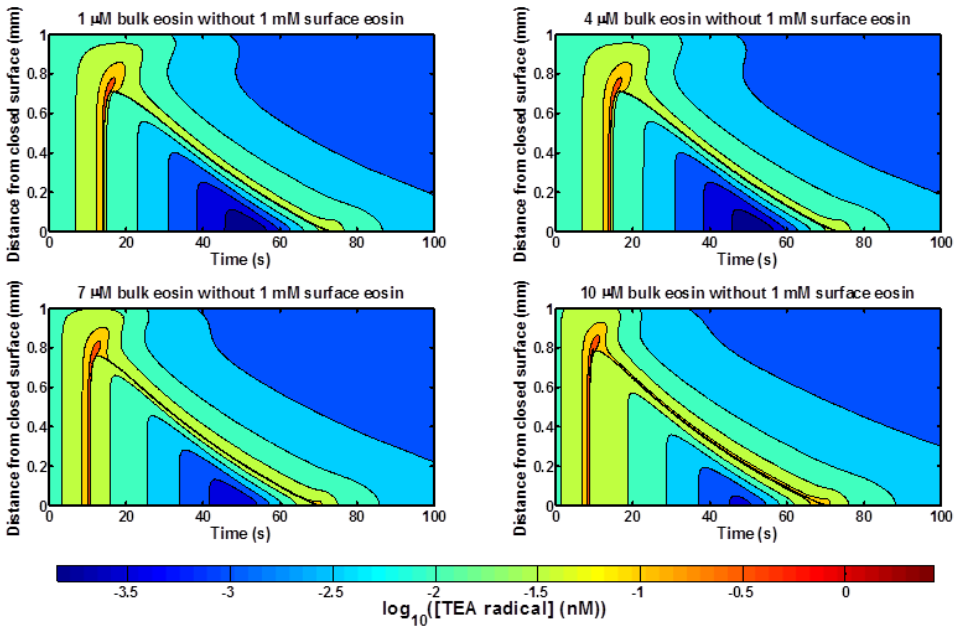

Figure 5-5. Contour plots of $\log_{10}$ of TEA radical concentrations as the contours with time as the x-axis and distance from the surface open to air as the y-axis at different initial eosin concentrations without a higher eosin concentration at the closed surface.

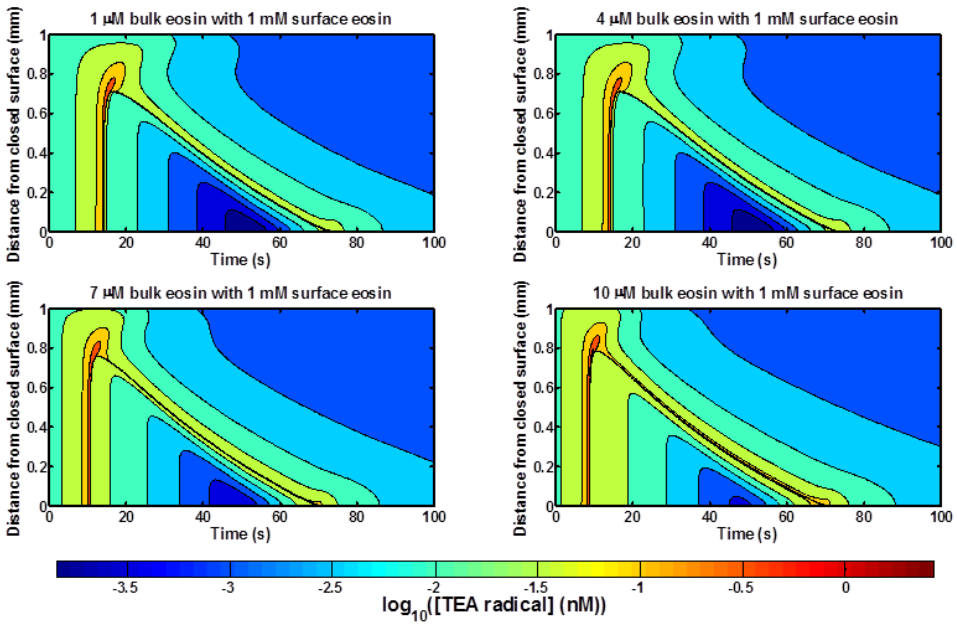

Figure 5-6. Contour plots of $\log_{10}$ of TEA radical concentrations as the contours with time as the x-axis and distance from the surface open to air as the y-axis at different initial eosin concentrations with 1 mM of eosin at the closed surface region modeling the effects of prior surface binding events.

5.3.3 Propagation and regeneration rates

The contour plots of the total rates of propagation at various initial eosin concentrations for both without and with the extra surface eosin are plotted in Figure 5-7 and Figure 5-8 respectively. The figures are quite similar, with most of the propagation activity occurring in the enclosed region between the moving front and the closed surface and gradually decreasing in magnitude with time. This stands in contrast with the corresponding results from the reaction-diffusion model without amine chain peroxidation (Figure 3-4) where an initial burst of propagation occurs away from the closed surface before rapidly decaying off. Furthermore, faster onset of propagation and higher peak rates are predicted at higher initial eosin concentrations as the consumption of oxygen is faster when more eosin is present. Similarly, the formation of an enclosed region near the closed surface where propagation rates remain high is because oxygen diffusion is unable to penetrate past the moving front due to the amine chain peroxidation reaction rapidly recycling peroxy radicals back into reactive TEA radicals that can undergo propagation.

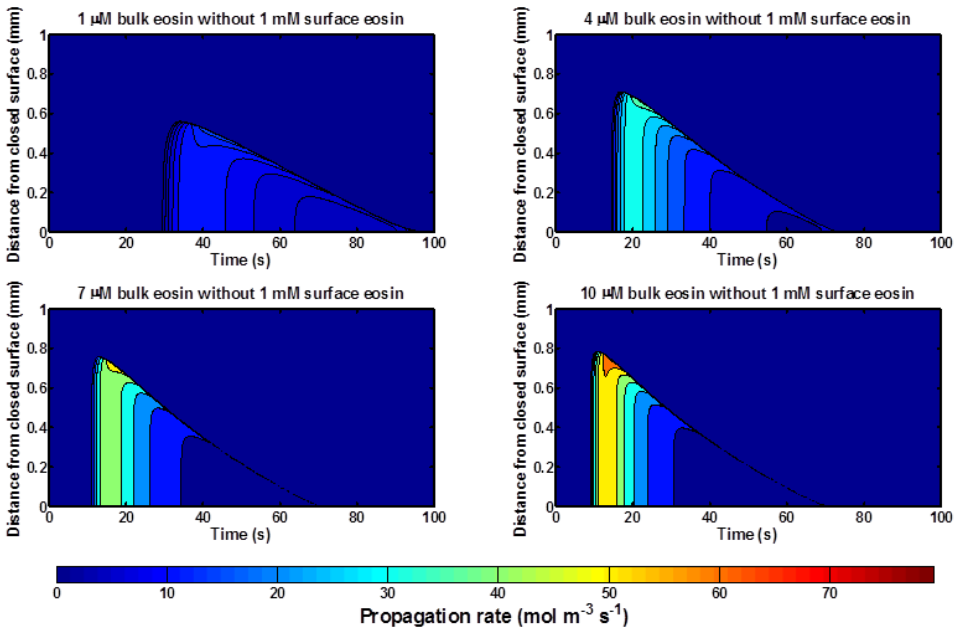

Figure 5-7. Contour plots of the total rate of propagation as the contours with time as the x-axis and distance from the surface open to air as the y-axis at different initial eosin concentrations without a higher eosin concentration at the closed surface.

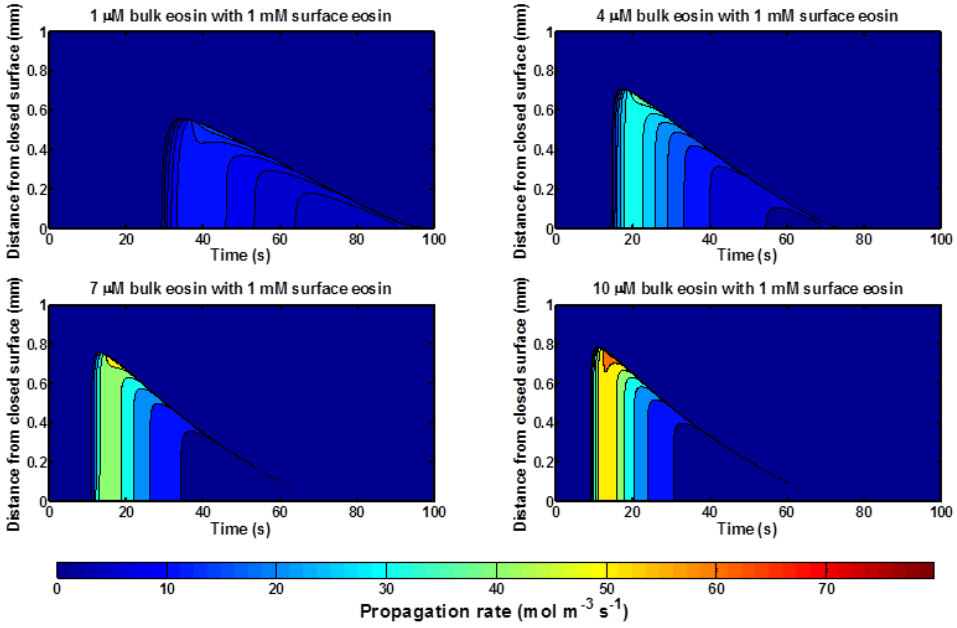

Figure 5-8. Contour plots of the total rate of propagation as the contours with time as the x-axis and distance from the surface open to air as the y-axis at different initial eosin concentrations with 1 mM of eosin at the closed surface region modeling the effects of prior surface binding events.

5.3.4 Double bond conversion

The contour plots showing double bond conversions for the amine chain peroxidation reaction-diffusion models both without and with the extra surface eosin are presented in Figure 5-9 and Figure 5-10 respectively. The two figures are somewhat similar, with the model including the 1 mM surface eosin region having a slightly faster onset of polymerization and higher maximum conversion attained. Comparing these results with the corresponding reaction-diffusion model results without amine chain peroxidation (Figure 3-6), we find that the trends whereby increasing eosin concentration results in shorter inhibition times and thicker polymer films still hold. On the other hand, the inhibition times are much shorter and that the regions of at least 0.2 conversion reach even further away from the closed surface when amine chain peroxidation is included in the reaction scheme. Furthermore, the maximum conversions achieved by the amine chain peroxidation reaction-diffusion models do not exceed 1.0, which is in contrast with the previous model where conversions above 2.0 were predicted. This suggests that because the eosin regeneration reaction is slower than the kinetics of amine chain peroxidation and inhibition, the effects of diffusion of monomer become less important.

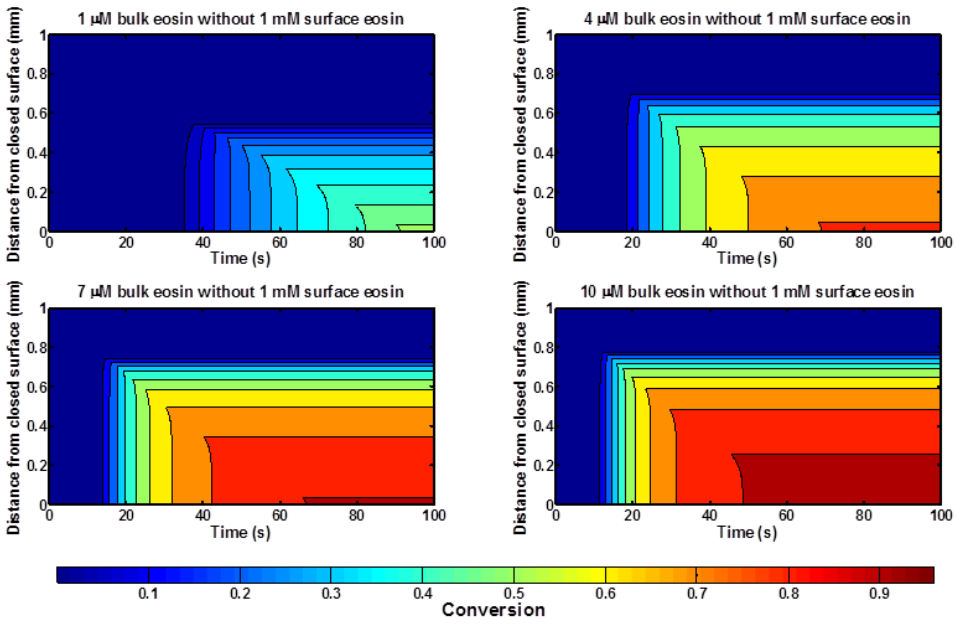

Figure 5-9. Contour plots of conversion, the total concentration of double bonds reacted at each position scaled to the initial total double bond concentration, as the contours with time as the x-axis and distance from the surface open to air as the y-axis at different initial eosin concentrations without a higher eosin concentration at the closed surface.

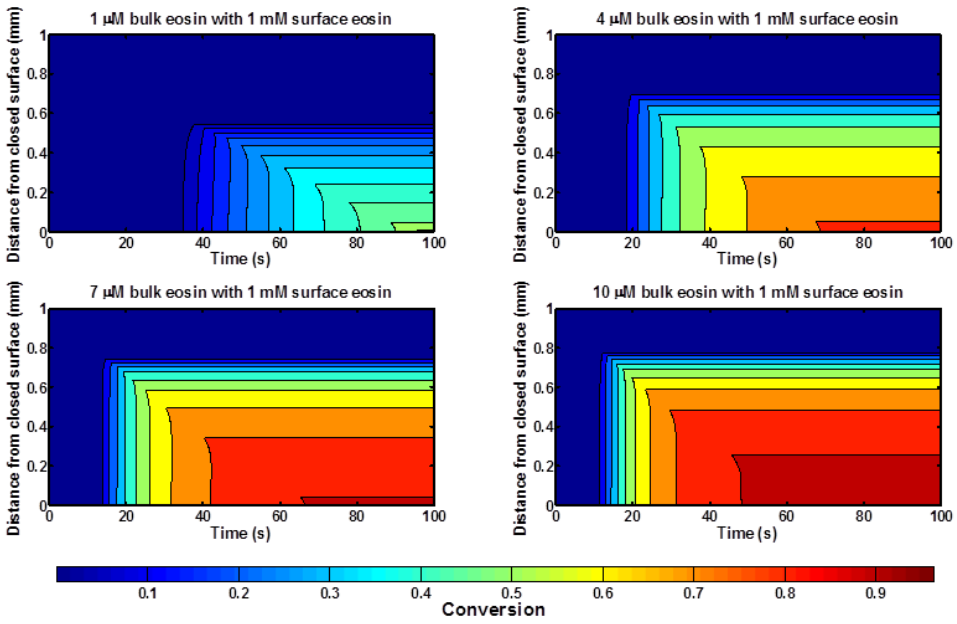

Figure 5-10. Contour plots of conversion, the total concentration of double bonds reacted at each position scaled to the initial total double bond concentration, as the contours with time as the x-axis and distance from the surface open to air as the y-axis at different initial eosin concentrations with 1 mM of eosin at the closed surface region modeling the effects of prior surface binding events.

The overall double bond conversion plots for models including the amine chain peroxidation reaction as obtained from the ODE model as well as the reaction-diffusion models without and with surface eosin are presented in Figure 5-11. All three plots exhibit the previously observed trend whereby higher initial eosin concentrations results in a shorter inhibition times and a higher overall averaged conversion, with a similar shape as the profiles obtained experimentally[73,78]. On the other hand, although incorporating continuous oxygen flux in the reaction-diffusion models had minor effects on the inhibition times, the profiles plateaued at a lower maximum conversion, with the addition of a 1 mM eosin surface region resulting in a higher conversion as compared to the reaction-diffusion model without it. This suggests that despite the close similarities in the contour plots, there is still a quantifiable difference in the overall results between the presence and absence of a higher surface eosin concentration.

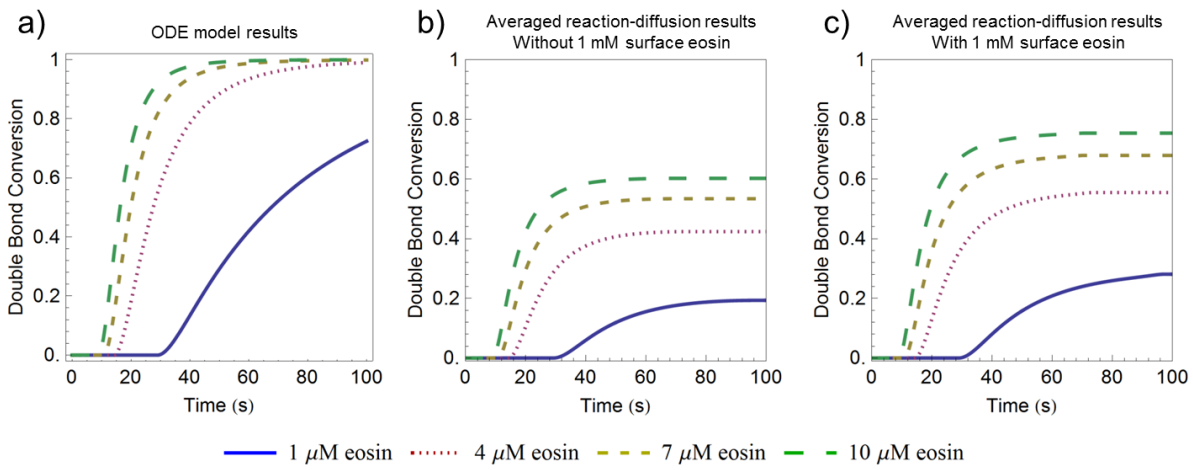

Figure 5-11. Plots of conversion obtained a) from an ODE model[78] that excludes diffusion effects and continuous flux of oxygen from the open surface, as well as conversions averaged over the whole spatial dimension at each time step from the reaction-diffusion model b) without a higher eosin concentration at the closed surface and c) with 1 mM of eosin at the closed surface region modeling the effects of prior surface binding events.

5.3.5 Inhibition (t_{inh}) and gelation ($t_{0.2}$) times

The local spatial distribution of t_{inh} and $t_{0.2}$ for the four different bulk eosin concentrations after including amine chain peroxidation into the reaction-diffusion model both with and without the 1 mM surface eosin region was plotted in Figure 5-12. Compared to the previous reaction-diffusion model without amine chain peroxidation (Figure 3-8), there is still the similar trend of increasing t_{inh} and $t_{0.2}$ with increasing distance away from the closed surface. On the other hand, we find that t_{inh} and $t_{0.2}$ both do not change as much with position and extend further away from the closed surface, with much smaller values of t_{inh} and $t_{0.2}$ than before at all of the bulk eosin concentrations simulated. This suggests that as amine chain peroxidation consumes oxygen so rapidly, the effect of oxygen diffusion near the closed surface becomes less important during the initial stages of polymerization, with the continuous oxygen flux mainly affecting the thickness of the final polymer product by creating an inhibition zone where oxygen concentration remains high enough such that polymerization cannot proceed.

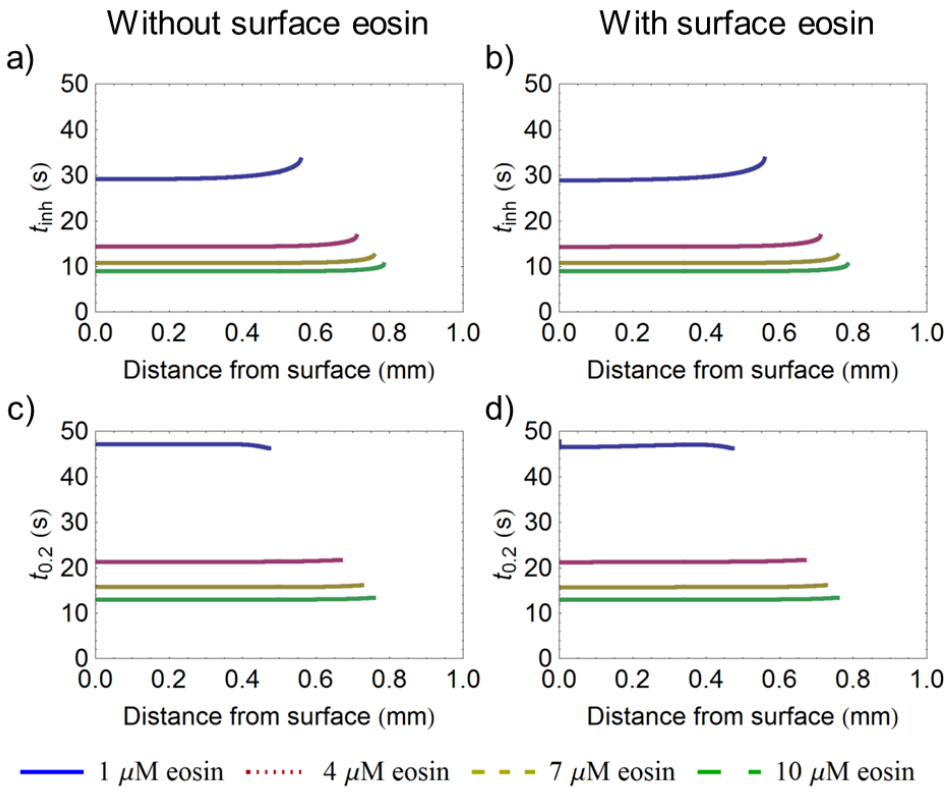

Figure 5-12. Plots of time required for oxygen concentration to drop to 10^{-6} M for the reaction-diffusion model (a) without and (b) with extra surface eosin as well as time required for scaled amount of reacted monomer to reach 0.2 for the reaction-diffusion model (c) without and (d) with extra surface eosin as a function of distance from the surface open to air.

A first glance at Figure 5-12 seems to indicate no detectable differences between the plots of reaction-diffusion model with and without the 1 mM surface eosin, but a closer look comparing t_{inh} and $t_{0.2}$ in Figure 5-13 and Figure 5-14 respectively shows that the extra surface eosin does have some effect on the inhibition and polymerization times, especially at lower bulk eosin concentrations. With 1 μM of bulk eosin, having the surface eosin results in about 0.3 seconds shorter t_{inh} near the closed surface, with there being at least a 0.1 second discrepancy reaching about 0.4 mm away from the closed surface. Similarly, there is a 0.1 second difference at 4 μM of bulk eosin which reaches about 0.15 mm away from the closed surface. On the other hand, when 7 and 10 μM of bulk eosin is simulated, there seems to be no difference between having surface eosin and not. Looking at $t_{0.2}$ also gives similar trends with there being the largest discrepancy at 1 μM bulk eosin and no difference for 10 μM of bulk eosin. In the

case of $t_{0.2}$, the magnitude of the discrepancies are much larger, with about 0.6 seconds difference at 1 μM bulk eosin and 0.1 seconds for both 4 and 7 μM bulk eosin. These results suggest that having a higher surface eosin concentration does spatially and temporally affect the progress of polymerization, resulting in a slightly faster production of polymer next to the closed surface, similar to the PBA process where a surface polymer is first formed after which the drop of solution polymerizes.

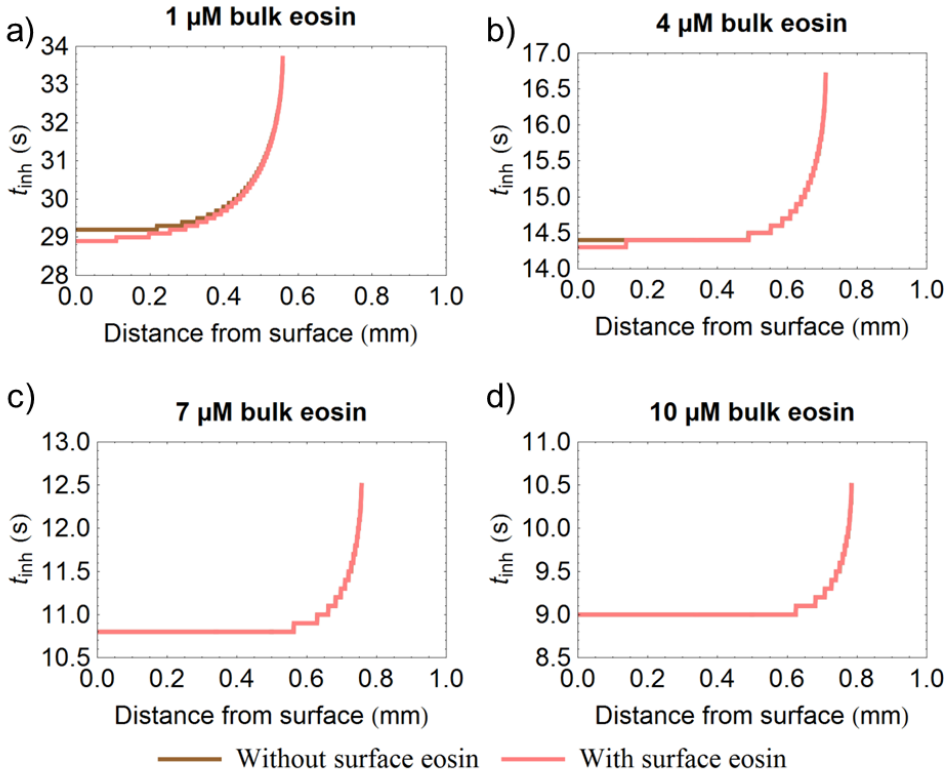

Figure 5-13. Plots comparing the time required for oxygen concentration to drop to 10^{-6} M for reaction-diffusion models without and with higher surface eosin at different initial bulk eosin concentrations. (a) 1 μM bulk eosin; (b) 4 μM bulk eosin; (c) 4 μM bulk eosin; (d) 10 μM bulk eosin.

Another unusual trend for 1 μM of bulk eosin predicted by the model is that $t_{0.2}$ actually decreases when moving away from the closed surface when around the middle region. This suggests that there at lower bulk eosin concentrations, eosin regeneration becomes more important in generating free radicals for polymerization as oxygen replenishment is occurring more rapidly in the middle region than at the closed surface and it is only when there is oxygen present that eosin regeneration can proceed. This is to be expected as after the initial rapid consumption of oxygen by amine chain

peroxidation reactions, any remaining free radicals can then participate in propagation and termination reactions, but for lower eosin concentrations, any additional radicals produced from eosin regeneration reactions would thus have a larger proportionate effect on the propagation rates.

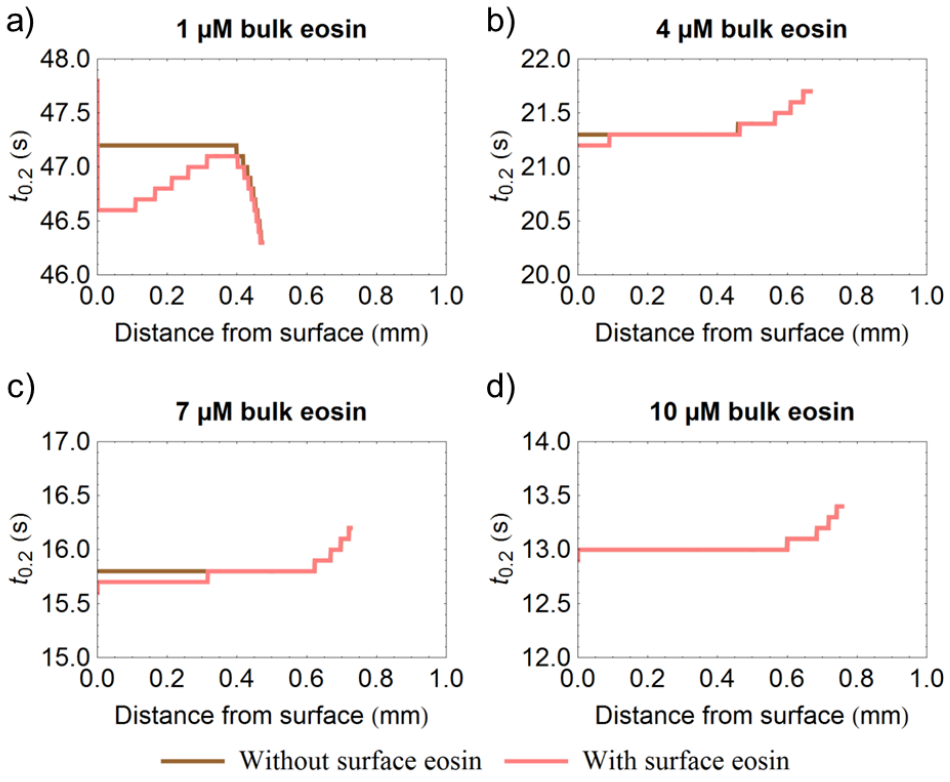

Figure 5-14. Plots comparing the time required for scaled amount of reacted monomer to reach 0.2 for reaction-diffusion models without and with higher surface eosin at different initial bulk eosin concentrations. (a) 1 μM bulk eosin; (b) 4 μM bulk eosin; (c) 4 μM bulk eosin; (d) 10 μM bulk eosin.

With the increased rate of oxygen consumption due to amine chain peroxidation, simulations performed at the lower bulk eosin concentration of 0.1 μM and 0.5 μM predicted considerable conversions attained within 200 seconds, which the previous reaction-diffusion model did not even after running until 1000 seconds in simulation time. From these simulations, the spatial profiles of t_{inh} and $t_{0.2}$ are plotted in Figure 5-15. The plots continue to show the trend of increasing difference in polymerization times as bulk eosin concentration is decreased when comparing between the models with and without surface eosin, with the values of $t_{0.2}$ near the closed surface for 0.5 μM bulk eosin comparable to the value from experiments[10]. Furthermore, the difference in

$t_{0.2}$ for regions next to the closed surface are now about 10 seconds for 0.1 μM bulk eosin and 2 seconds for 0.5 μM bulk eosin, durations that can easily be measured experimentally.

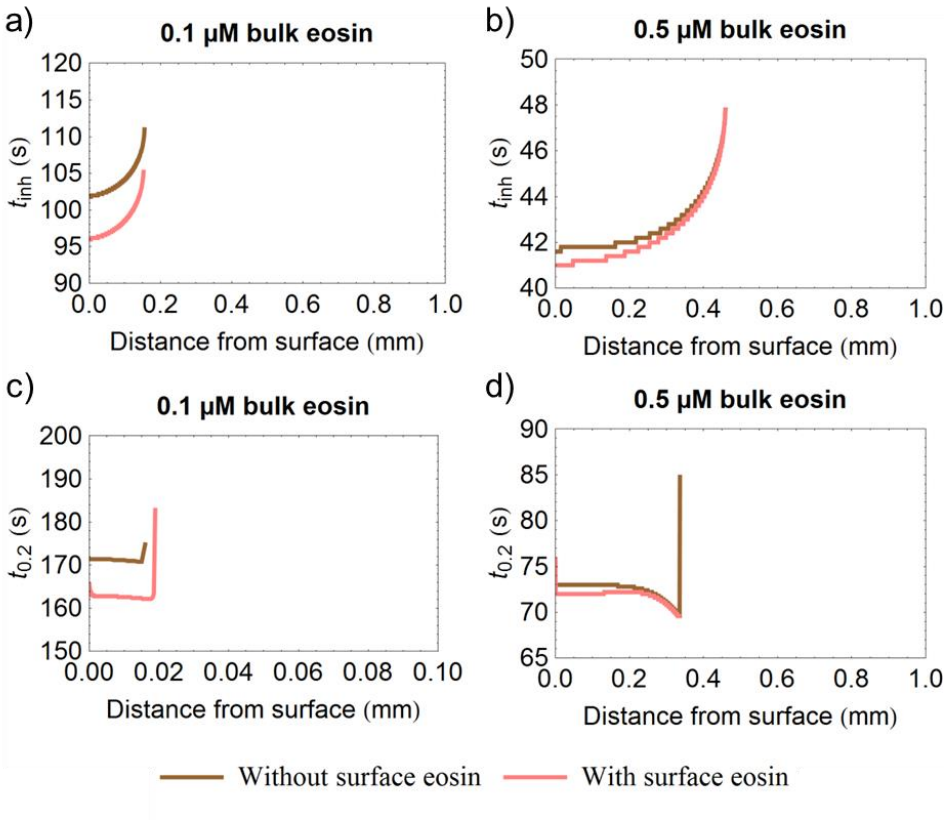

Figure 5-15. Plots comparing time required for oxygen concentration to drop to 10^{-6} M for (a) 0.1 μM bulk eosin; (b) 0.5 μM bulk eosin, and the time required for scaled amount of reacted monomer to reach 0.2 for (c) 0.1 μM bulk eosin; (d) 0.5 μM bulk eosin. Note that for easier visualization, the x-axis for (c) is only up to 0.10 mm.

5.4 Conclusions

Having oxygen replenishment at the open surface boundary in the reaction-diffusion model incorporating amine chain peroxidation is predicted to have a smaller influence on the polymerization times when compared to the corresponding ODE model even though lower final conversions were attained. The continuous oxygen flux resulted in the formation of a moving front during the polymerization process, but spatial variations in the reaction-diffusion model were also diminished as the higher rate of consumption

of inhibiting oxygen through amine chain peroxidation resulted in the reduced impact of molecular diffusion on the overall polymerization kinetics.

Nevertheless, the models predicted that the onset of polymerization occurred earlier in the region near the closed surface when there was a higher concentration of eosin on the closed surface. The additional eosin allowed for a slightly quicker depletion of oxygen and thus faster t_{inh} and $t_{0.2}$, while also causing a higher final conversion to be achieved as well, similar to experimental observations.

Chapter 6. Investigation of two possible reactions that slow down the rate of oxygen consumption

6.1 Introduction

As expounded in Chapter 4 and Chapter 5, including amine chain peroxidation into the overall reaction scheme resulted in the simulations predicting polymerization times that are much faster than those observed from experiments. The formation of a cycle whereby radicals shuttle between the less reactive peroxy radical formed from oxygen reacting with free radicals in the inhibition reactions and a reactive TEA radical created from peroxy radicals reacting with the excess amine through amine chain peroxidation results in an increased rate of consumption of oxygen and thus a shorter time for polymerization to occur. Furthermore, inconsistencies when comparing results obtained from the model at different eosin concentrations to experimental data suggest that there are missing reactions in the model's reaction scheme. As such, this chapter serves to introduce two probable reactions that were expected to slow down oxygen consumption as well as its effects on polymerization when they were separately incorporated into the reaction scheme.

The first reaction that was studied was the first order self-decomposition of peroxy radicals into inert products. As amine chain peroxidation was previously shown to have a large effect on the overall consumption rate of oxygen, one of the most direct ways expected to slow down oxygen consumption was to reduce the amount of peroxy radicals available to participate in the amine chain peroxidation reaction. Hence, self-decomposition of peroxy radicals, which have been tracked experimentally[87], was incorporated into the reaction scheme. The self-decomposition of peroxy radicals was modeled using the following equation with a rate constant $k_{PO2radSelf}$:

$P_nOO\bullet \xrightarrow{k_{PO2radSelf}}$ Inert species Rate = $k_{PO2radSelf}$ [$P_nOO\bullet$] (6-1)

where $P_nOO\bullet$ is a peroxy radical of any length.

The other probable reaction that was investigated was the direct quenching of activated triplet eosin by oxygen to form singlet oxygen and ground state eosin[93,94], with the singlet oxygen produced assumed to be unreactive and unable to participate in further reactions. This reaction thereby reduces the amount of TEA radicals initially generated as oxygen competes with TEA for activated eosin, resulting in fewer radicals in the system which can undergo amine chain peroxidation. This reaction was modeled as the following equation with a rate constant k_{quench}:

$O_2 + E^* \xrightarrow{k_{quench}} O_2^* + E$ Rate = k_{quench} [O_2] [E*] (6-2)

where E* is triplet eosin, O_2* is singlet oxygen and E is ground state eosin.

6.2 Modifications to ODE Model

The two additional proposed reactions were independently incorporated into the overall reaction scheme including amine chain peroxidation (Scheme 4-2), with the ODE model simulations incorporating Eqs. 6-1 and 6-2 separately in order to explore the effects of each reaction by itself.

As the rate constant for the self-decomposition of peroxy radicals ranges from 10^0 s^{-1} to 10^6 s^{-1} depending on the structure of the specific peroxy radical[87], a value of 10^2 s^{-1} was used for $k_{PO2radSelf}$ in the model as it was the most common order of magnitude among the tabulated data and in the middle of the whole range. Sensitivity analyses were then also performed in order to determine its effect on the polymerization reaction. On the other hand, the rate constant for the quenching reaction of oxygen with activated triplet eosin was taken to be 10^6 $mM^{-1}s^{-1}$ as obtained from literature[93].

6.3 Results and Discussion

6.3.1 Self-decomposition of peroxy radicals

With a large range of values for $k_{PO2radSelf}$ published in the literature, the model's sensitivity to $k_{PO2radSelf}$ at 1 μM eosin or 10 μM eosin was first investigated and subsequently plotted in Figure 6-1. Both contour plots show that polymerization is greatly slowed down when the self-decomposition of peroxy radicals is included in the reaction scheme. The slowdown in polymerization rate is especially pronounced at lower eosin concentrations, where negligible conversion is attained even after 1000 seconds when 1 μM eosin is used. Even at the higher eosin concentration of 10 μM, negligible conversion is predicted within 1000 seconds when $k_{PO2radSelf}$ is set to a value of more than ~10^2 s^{-1}, as observed by the sharp bend in the contours above that value. This sensitivity analysis thus suggests that if the rate of self-decomposition of peroxy radicals is too fast, amine chain peroxidation and regeneration of eosin is unable to proceed, resulting in the total inhibition of polymerization.

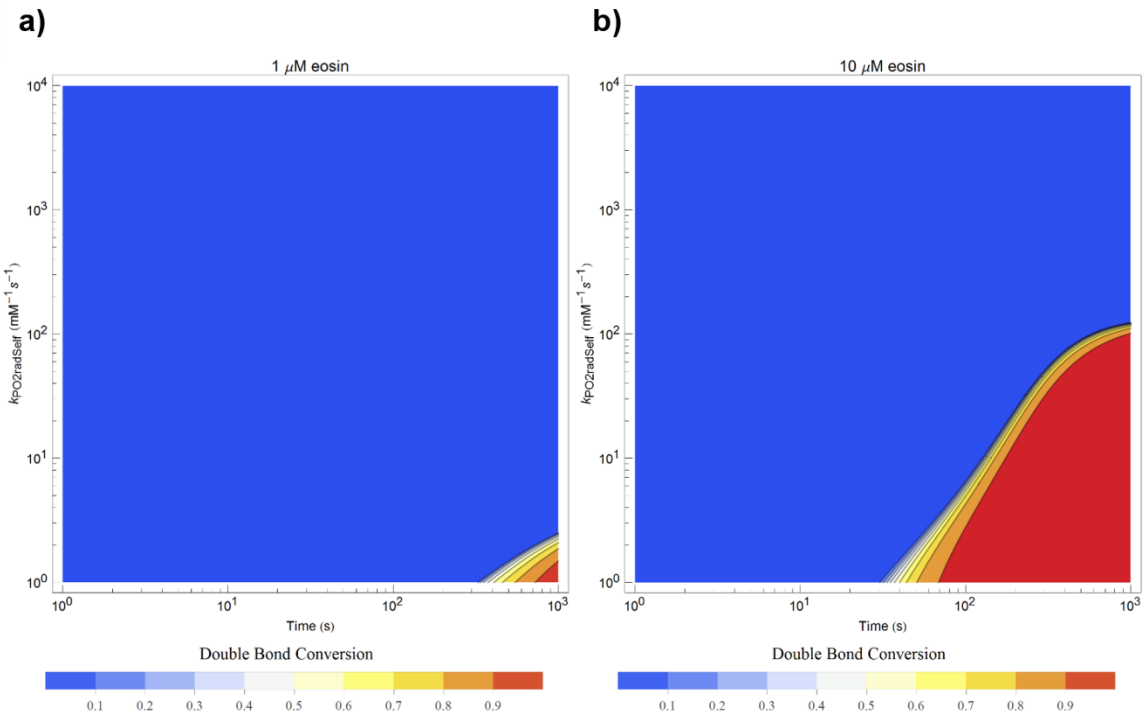

Figure 6-1. Contour plots on a log-log scale from model simulations showing how the value of $k_{PO2radSelf}$ affects conversion, with time as x-axis, $k_{PO2radSelf}$ as y-axis and conversion as the contours. Two different starting eosin concentrations are shown: (a) 1 μM eosin; (b) 10 μM eosin.

The effect of a faster rate of eosin regeneration was also explored in Figure 6-2, with k_{regen} varied by a few orders of magnitude while $k_{PO2radSelf}$ stayed at a default value of

10^2 s^{-1}. The contour plots show that increasing the eosin regeneration rate did not decrease the inhibition times below 1000 seconds for the lower eosin concentration of 1 µM, while there was a noticeable reduction in polymerization times up to a fastest time of ~200 seconds as k_{regen} is increased from 5×10^5 $mM^{-1}s^{-1}$ for the higher 10 µM eosin case. This result implies that the faster rate constant for regeneration of eosin alone is not enough to overcome the inhibition of oxygen when there is another reaction competing for peroxy radicals.

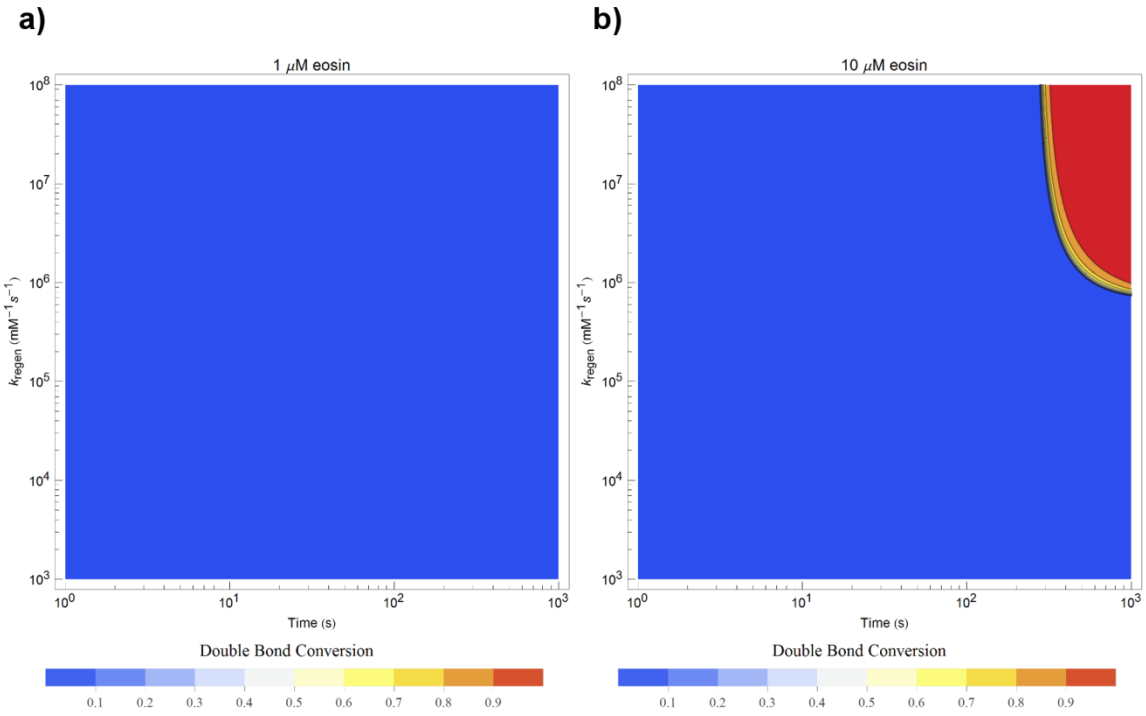

Figure 6-2. Contour plots on a log-log scale from model simulations showing how the value of k_{regen} affects conversion, with time as x-axis, k_{regen} as y-axis and conversion as the contours. Two different starting eosin concentrations are shown: (a) 1 µM eosin; (b) 10 µM eosin.

As no conversion was predicted by the model at the default values used, a sensitivity analysis for k_{amine} with $k_{PO2radSelf}$ at a default value of 10^2 s^{-1} was also performed (Figure 6-3). The model results show that at the lower eosin concentration of 1 µM, a minimum value of ~4×10^2 $mM^{-1}s^{-1}$ for k_{amine} is required before any polymerization is predicted to occur at all within 1000 seconds. On the other hand, for the higher eosin concentration of 10 µM, a wider range of values for k_{amine} starting from ~3 $mM^{-1}s^{-1}$ is predicted to reach conversions more than 0.2 in less than 1000 seconds,

with a larger value resulting in a faster onset of polymerization. Taking all the sensitivity analyses together, the results suggest that there is strong competition for peroxy radicals among eosin regeneration, amine chain peroxidation and self-decomposition that is heavily dependent on the relative ratios of the respective rate constants. The effects of these reactions competing with regeneration of eosin for peroxy radicals on polymerization times are especially significant at lower initiator concentrations, with narrower window of sets of values of rate constants where polymerization is predicted to occur within 1000 seconds.

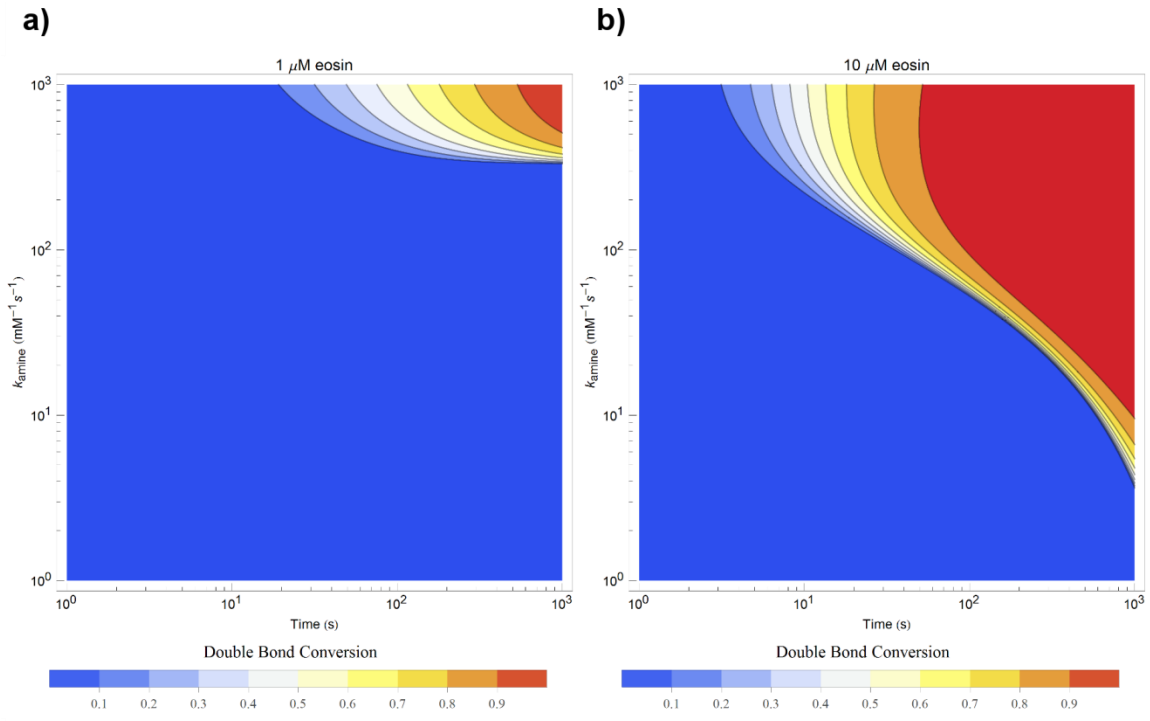

Figure 6-3. Contour plots on a log-log scale from model simulations showing how the value of k_{amine} affects conversion, with time as x-axis, k_{amine} as y-axis and conversion as the contours. Two different starting eosin concentrations are shown: (a) 1 μM eosin; (b) 10 μM eosin.

6.3.2 Oxygen quenching of triplet eosin

Results from simulations including the oxygen quenching of triplet eosin reaction in the reaction scheme indicated that there was insignificant impact on the polymerization times upon adding the oxygen quenching reaction. As shown in Figure 6-4, there is no noticeable difference in model-predicted values of $t_{0.2}$ when oxygen quenching is

incorporated into the overall reaction scheme, with the similar trend of higher eosin concentrations requiring less time for polymerization to occur.

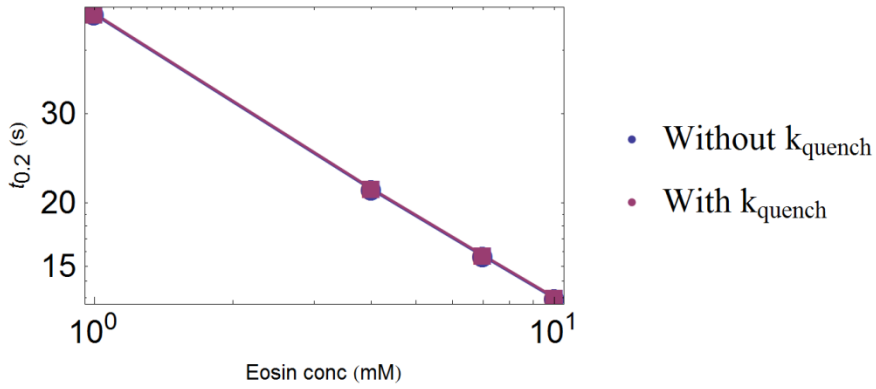

Figure 6-4. Log-log plot comparing $t_{0.2}$ obtained from simulations with and without oxygen quenching at default parameter values as eosin concentration is varied.

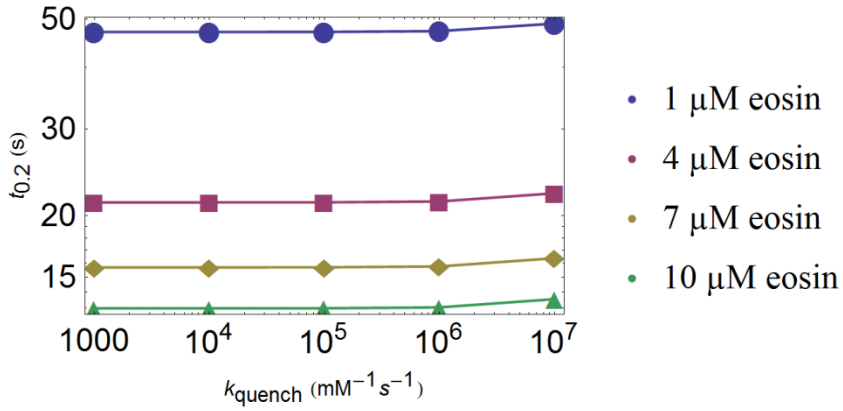

Figure 6-5. Log-log plot comparing $t_{0.2}$ obtained at different eosin concentrations as k_{quench} is varied by four orders of magnitude.

In addition, the model simulations predict only minor changes to the values of $t_{0.2}$ even when the rate constant k_{quench} was varied over four orders of magnitude (Figure 6-5). This implies that even with large values of the k_{quench} rate constant, oxygen quenching is still happening too slowly as compared to hydrogen transfer reactions between activated eosin and TEA to slow down the production of free radicals which can then undergo inhibition and amine chain peroxidation reactions. As such, the reaction of oxygen with triplet eosin is not expected to play a large role in the overall reaction scheme.

6.4 Conclusions

The addition of peroxy radical self-decomposition, another reaction competing for peroxy radicals, resulted in much slower predicted polymerization times while direct quenching of triplet eosin by oxygen has a negligible effect on polymerization times. As amine chain peroxidation is the major reaction for the consumption of inhibiting oxygen, any additional reaction that competes with it at a comparable rate while not producing more free radicals is thus predicted to have a large effect on the polymerization times. Conversely, the model simulations show that quenching of triplet eosin by oxygen is largely ineffective at slowing down polymerization, mainly because amine chain peroxidation is fast enough to compensate for the reduced production of free radicals from TEA.

Chapter 7. Conclusions and Future Directions

7.1 Conclusions

A better understanding of the mechanistic complexity underlying the unique combination of eosin and tertiary amines in photoinitiation reactions has been achieved through the modeling efforts outlined in this thesis. The mechanism behind eosin-tertiary amine initiated photopolymerizations in the context of PBA has been investigated using a combination of chemical kinetic models and reaction-diffusion models. Additional details and trends that would affect the photopolymerization were also obtained by performing sensitivity analyses on uncertain kinetic parameters instead of trying to fit experimental results to the proposed reaction schemes.

Chapter 2 established that the addition of an eosin regeneration reaction did account for the ability of smaller amounts of photoinitiator to initiate polymerization even in the presence of three orders of magnitude larger concentrations of inhibiting oxygen. Furthermore, trends obtained from the model as eosin concentrations were varied were similar to that of experiments, indicating that regeneration of eosin plays an important part in the overall reaction scheme. However, the model predictions for polymerization times were much larger than the experimental values, suggesting that peroxy radical mediated regeneration of eosin alone is insufficient to fully explain the short polymerization times observed from experiments and that additional reactions were probably missing in the reaction scheme.

Chapter 3 showed that for photopolymerizations in open air where replenishment of oxygen is possible, spatial variations during the polymerization process are to be expected when regeneration of eosin is included in the reaction scheme. A reaction front that moves in both space and time is also predicted by the model incorporating an oxygen flux coming from one end due to continuous oxygen dissolution into the reaction mixture from the open air. This interesting result could be due to the dual roles of oxygen as both an inhibitor of free radicals as well as an oxidizing agent required for the

regeneration of eosin. The model-predicted spatial and temporal profiles at different eosin concentrations also suggest that a difference in local surface eosin concentrations due to binding events could be a possible explanation why the surface polymerization occurs some time before bulk polymerization of the monomer droplet during PBA.

Chapter 4 demonstrated that amine chain peroxidation plays an important role in being the main mode of oxygen consumption. The presence of large amounts of excess TEA in the reaction system coupled with the direct transfer of hydrogen between less reactive peroxy radicals and TEA to form reactive radicals result in the rapid onset of polymerization as oxygen gets depleted more quickly. On the other hand, inconsistencies in the parameter sets upon comparison with experimental results indicate that the reaction scheme is still incomplete.

Chapter 5 indicated that incorporating the amine chain peroxidation reaction in Chapter 4 into the reaction-diffusion model with oxygen replenishment in Chapter 3 resulted in a diminished effect of diffusion on the polymerization times due to the more rapid rate of consumption of oxygen. The effect of a higher surface eosin concentration was also modeled, with the simulation results showing a slight decrease in t_{inh} and $t_{0.2}$ nearer the closed surface, similar to experimental observations where a surface polymer is first formed before the bulk solution polymerizes.

Chapter 6 showed that of the two proposed reactions that are expected to slow down polymerization, the self-decomposition of peroxy radicals have the most impact on polymerization times as it competes with amine chain peroxidation for peroxy radicals. With less peroxy radicals, amine chain peroxidation is slowed down and the rate of oxygen consumption reduced.

In summary, the models have helped advance the understanding of the eosin-tertiary amine photoinitiation system step-by-step. The combination of regeneration of eosin together with TEA's ability to reduce effects of oxygen inhibition has been shown to be vital for rapid polymerizations in a few minutes; the models predict that only one without the other results in much longer polymerization times and that the two reactions complement each other in a synergistic manner to produce such a unique effect of

allowing photopolymerizations in open air at such low photoinitiator concentrations. A higher surface eosin concentration was also shown to create a noticeable difference in polymerization times near the closed surface, similar to experimental observations during PBA where a surface polymer is formed first before the whole bulk polymerizes.

As such, when deciding what modifications to make in order to improve PBA, the choices of both photoinitiators and tertiary amines being used are expected to have the largest effects on polymerization times. The type of photoinitiator used is anticipated to greatly affect the regeneration rate as its structure is believed to influence the rate of electron and hydrogen transfer during the regeneration and free radical generation reactions. In addition, the choice of tertiary amine would affect the chain peroxidation rate as using triethylamine, where the alcohol functional groups on TEA are substituted with hydrogen, has been found experimentally to result slower polymerizations.

7.2 Future Directions

The model simulations have provided predictions that qualitatively match trends observed from experiments. Following these preliminary studies, we can utilize this working model to investigate more thoroughly the various factors that affect the polymerization times without too many time-consuming trial-and-error experiments in order to further optimize PBA. A working knowledge of many trends has been amassed from various experimental studies, but these have not been measured quantitatively Model predictions can thus provide some guidance on the expected times required for polymerizations to begin, while further experimental data can be used to further refine the details of the model. Comparison studies between model and experiments would thus be a fruitful endeavor in our attempts to understand the polymerization process during PBA.

The thicknesses of the bulk and surface polymer formed during the PBA process as well as the minimum time required for polymerization to occur are variables that can be easily obtained from experiments and the model. Initial quantitative experimental measurements were previously performed[10] with the lowest value bulk eosin of 0.1 μM, but the duration of illumination in that study were kept to a reasonable maximum value

of 150 seconds as it is not practical to keep running the experiment without knowing if polymerization would proceed at all. Using the model, predictions about whether polymerization would even begin along with the expected durations required could be obtained at even lower eosin concentrations, further increasing the range of values to be experimentally studied. The experimental trends can then be compared with the model results as further verification of the model.

As shown in Chapter 5, the current model is able to make predictions on the spatial variation of polymerization times. With an estimate of the required durations obtained from model simulations, we can systematically study the effects of varying bulk and surface eosin concentrations. It is difficult to distinguish between t_{pBA} and $t_{0.2}$ for experiments if the time difference is too short, so the models can be used to guide the set of experimental conditions to be studied by choosing it only if the estimated time difference is more than a few seconds long. The difference in times between t_{pBA} and $t_{0.2}$ when bulk eosin concentration is varied as the surface concentration is held constant or when surface concentration is varied as the bulk eosin concentration is held constant can thus be more easily obtained from experiments with this prior information. Comparisons between the results obtained from experiments and model can also then be performed.

References

(1) Decker, C. *Acta Polym.* **1994**, *347* (43), 333–347.
(2) Decker, C. *Macromol. Rapid Commun.* **2002**, *23* (18), 1067–1093.
(3) Andrzejewska, E. *Prog. Polym. Sci.* **2001**, *26* (4), 605–665.
(4) Neckers, D. C. *Polym. Eng. Sci.* **1992**, *32* (20), 1481–1489.
(5) Valdes-Aguilera, O.; Pathak, C. P.; Shi, J.; Watson, D.; Neckers, D. C. *Macromolecules* **1992**, *25* (2), 541–547.
(6) Gruber, H. F. *Prog. Polym. Sci.* **1992**, *17* (6), 953–1044.
(7) Denisov, E. T.; Khudyakov, I. V. *Chem. Rev.* **1987**, *87* (6), 1313–1357.
(8) O'Brien, A. K.; Bowman, C. N. *Macromolecules* **2006**, *39* (7), 2501–2506.
(9) Sikes, H. D.; Hansen, R. R.; Johnson, L. M.; Jenison, R.; Birks, J. W.; Rowlen, K. L.; Bowman, C. N. *Nat. Mater.* **2008**, *7* (1), 52–56.
(10) Kaastrup, K.; Sikes, H. D. *Lab Chip* **2012**, *12* (20), 4055–4058.
(11) Ligon, S. C.; Husár, B.; Wutzel, H.; Holman, R.; Liska, R. *Chem. Rev.* **2014**, *114* (1), 557–589.
(12) George, M. H.; Ghosh, A. *J. Polym. Sci. Polym. Chem. Ed.* **1978**, *16* (5), 981–995.
(13) Odian, G. G. *Principles of Polymerization*, 4th ed.; Wiley-Interscience, 2004.
(14) Shultz, A. R.; Joshi, M. G. *J. Polym. Sci. Polym. Phys. Ed.* **1984**, *22* (10), 1753–1771.
(15) Decker, C. *Prog. Polym. Sci.* **1996**, *21*, 593–650.
(16) Bowman, C.; Kloxin, C. *AIChE J.* **2008**, *54* (11), 2775–2795.
(17) O'Brien, A. K.; Bowman, C. N. *Macromol. Theory Simulations* **2006**, *15* (2), 176–182.
(18) Tobita, H.; Hamielec, A. E. *Polymer (Guildf).* **1991**, *32* (14), 2641–2647.
(19) Wen, M.; McCormick, A. V. *Macromolecules* **2000**, *33* (25), 9247–9254.
(20) Anseth, K. S.; Wang, C. M.; Bowman, C. N. *Macromolecules* **1994**, *27* (3), 650–655.
(21) Johnson, P. M.; Stansbury, J. W.; Bowman, C. N. *Macromolecules* **2008**, *41* (1), 230–237.
(22) Lovestead, T. M.; O'Brien, A. K.; Bowman, C. N. *J. Photochem. Photobiol. A Chem.* **2003**, *159* (2), 135–143.
(23) Kizilel, S.; Pérez-Luna, V. H.; Teymour, F. *Macromol. React. Eng.* **2009**, *3* (5-6), 271–287.
(24) Goodner, M. D.; Bowman, C. N. *Chem. Eng. Sci.* **2002**, *57* (5), 887–900.
(25) Kizilel, S.; Pérez-Luna, V. H.; Teymour, F. *Macromol. Theory Simulations* **2006**, *15* (9), 686–700.
(26) Hansen, R. R.; Sikes, H. D.; Bowman, C. N. *Biomacromolecules* **2008**, *9* (1), 355–362.
(27) Sikes, H. D.; Jenison, R.; Bowman, C. N. *Lab Chip* **2009**, *9* (5), 653–656.
(28) Avens, H. J.; Berron, B. J.; May, A. M.; Voigt, K. R.; Seedorf, G. J.; Balasubramaniam, V.; Bowman, C. N. *J. Histochem. Cytochem.* **2011**, *59* (1), 76–87.
(29) Avens, H. J.; Bowman, C. N. *Acta Biomater.* **2010**, *6* (1), 83–89.

(30) Berron, B. J.; Johnson, L. M.; Ba, X.; McCall, J. D.; Alvey, N. J.; Anseth, K. S.; Bowman, C. N. *Biotechnol. Bioeng.* **2011**, *108* (7), 1521–1528.
(31) Pathak, C. P.; Sawhney, A. S.; Hubbell, J. A. *J. Am. Chem. Soc.* **1992**, *114* (21), 8311–8312.
(32) Kizilel, S.; Pérez-Luna, V. H.; Teymour, F. *Langmuir* **2004**, *20* (20), 8652–8658.
(33) Cruise, G. M.; Hegre, O. D.; Scharp, D. S.; Hubbell, J. A. *Biotechnol. Bioeng.* **1998**, *57* (6), 655–665.
(34) Avens, H. J.; Bowman, C. N. *J. Polym. Sci. Part A Polym. Chem.* **2009**, *47* (22), 6083–6094.
(35) Lee, J. K.; Heimer, B. W.; Sikes, H. D. *Biomacromolecules* **2012**, *13* (4), 1136–1143.
(36) Kaastrup, K.; Chan, L.; Sikes, H. D. *Anal. Chem.* **2013**, *85* (17), 8055–8060.
(37) Kuck, L.; Taylor, A. *Biotechniques* **2008**, *45* (2), 179–186.
(38) Heimer, B. W.; Shatova, T. A.; Lee, J. K.; Kaastrup, K.; Sikes, H. D. *Analyst* **2014**, *139* (15), 3695–3701.
(39) Badu-Tawiah, A. K.; Lathwal, S.; Kaastrup, K.; Al-Sayah, M. H.; Christodouleas, D. C.; Smith, B. S.; Whitesides, G. M.; Sikes, H. D. *Lab Chip* **2014**.
(40) Lathwal, S.; Sikes, H. D. *Lab Chip* **2016**.
(41) Decker, C.; Lorinczova, I. *J. Coatings Technol. Res.* **2004**, *1* (4), 247–256.
(42) Stansbury, J. W. *J. Esthet. Restor. Dent.* **2000**, *12* (6), 300–308.
(43) Nguyen, K. T.; West, J. L. *Biomaterials* **2002**, *23* (22), 4307–4314.
(44) Lin, C.-C.; Anseth, K. S. *Pharm. Res.* **2009**, *26* (3), 631–643.
(45) Chung, B. G.; Lee, K.-H.; Khademhosseini, A.; Lee, S.-H. *Lab Chip* **2012**, *12* (1), 45–59.
(46) Fuchs, Y.; Soppera, O.; Haupt, K. *Anal. Chim. Acta* **2012**, *717*, 7–20.
(47) Fuchs, Y.; Soppera, O.; Mayes, A. G.; Haupt, K. *Adv. Mater.* **2013**, *25* (4), 566–570.
(48) Lee, J.; Bisso, P. W.; Srinivas, R. L.; Kim, J. J.; Swiston, A. J.; Doyle, P. S. *Nat. Mater.* **2014**, *13* (5), 524–529.
(49) Fisher, J. P.; Dean, D.; Engel, P. S.; Mikos, A. G. *Annu. Rev. Mater. Res.* **2001**, *31* (1), 171–181.
(50) Rohr, T.; Hilder, E. F.; Donovan, J. J.; Svec, F.; Fréchet, J. M. J. *Macromolecules* **2003**, *36* (5), 1677–1684.
(51) Scott, T. F.; Kowalski, B. A.; Sullivan, A. C.; Bowman, C. N.; McLeod, R. R. *Science* **2009**, *324* (5929), 913–917.
(52) Khire, V. S.; Benoit, D. S. W.; Anseth, K. S.; Bowman, C. N. *J. Polym. Sci. Part A Polym. Chem.* **2006**, *44* (24), 7027–7039.
(53) Avens, H. J.; Randle, T. J.; Bowman, C. N. *Polymer (Guildf).* **2008**, *49* (22), 4762–4768.
(54) Matyjaszewski, K.; Dong, H.; Jakubowski, W.; Pietrasik, J.; Kusumo, A. *Langmuir* **2007**, *23* (8), 4528–4531.
(55) Hoyle, C. E.; Lee, T. Y.; Roper, T. *J. Polym. Sci. Part A Polym. Chem.* **2004**, *42* (21), 5301–5338.
(56) Qian, H.; He, L. *Anal. Chem.* **2009**, *81* (11), 4536–4542.
(57) Qian, H.; He, L. *Anal. Chem.* **2009**, *81* (23), 9824–9827.
(58) Kasche, V.; Lindqvist, L. *Photochem. Photobiol.* **1965**, *4* (5), 923–933.

(59) Encinas, M. V.; Rufs, a. M.; Bertolotti, S. G.; Previtali, C. M. *Polymer (Guildf).* **2009**, *50* (13), 2762–2767.
(60) Beuermann, S.; Paquet, D. A.; McMinn, J. H.; Hutchinson, R. A. *Macromolecules* **1996**, *29* (12), 4206–4215.
(61) Stach, M.; Lacík, I.; Chorvát, D.; Buback, M.; Hesse, P.; Hutchinson, R. A.; Tang, L. *Macromolecules* **2008**, *41* (14), 5174–5185.
(62) Maillard, B.; Ingold, K. U.; Scaiano, J. C. *J. Am. Chem. Soc.* **1983**, *105* (15), 5095–5099.
(63) Huyser, E. S.; VanScoy, R. M. *J. Org. Chem.* **1968**, *33* (9), 3524–3527.
(64) Korolev, G. V.; Mogilevich, M. M. *Three-Dimensional Free-Radical Polymerization*; Springer Berlin Heidelberg: Berlin, Heidelberg, 2009.
(65) Penzkofer, A.; Beidoun, A.; Daiber, M. *J. Lumin.* **1992**, *51* (6), 297–314.
(66) Penzkofer, A.; Beidoun, A.; Speiser, S. *Chem. Phys.* **1993**, *170* (1), 139–148.
(67) Dunsbach, R.; Schmidt, R. *J. Photochem. Photobiol. A Chem.* **1995**, *85* (3), 275–279.
(68) Hari, D. P.; König, B. *Chem. Commun. (Camb).* **2014**, *50* (51), 6688–6699.
(69) Majek, M.; Filace, F.; Wangelin, A. J. Von. *Beilstein J. Org. Chem.* **2014**, *10*, 981–989.
(70) Kasche, V. *Photochem. Photobiol.* **1967**, *6* (9), 643–650.
(71) CS Bahney, TJ Lujan, CW Hsu, M Bottlang, JL West, B. J. *Eur. Cells Mater.* **2011**, *22*, 43–55.
(72) Popielarz, R.; Vogt, O. *J. Polym. Sci. Part A Polym. Chem.* **2008**, *46* (11), 3519–3532.
(73) Kaastrup, K.; Aguirre-Soto, A.; Wang, C.; Bowman, C. N.; Stansbury, J. W.; Sikes, H. D. *Polym. Chem.* **2016**, *7* (3), 592–602.
(74) Genzer, J. *Macromolecules* **2006**, *39* (20), 7157–7169.
(75) Rahane, S. B.; Kilbey, S. M.; Metters, A. T. *Macromolecules* **2008**, *41* (24), 9612–9618.
(76) Turgman-Cohen, S.; Genzer, J. *Macromolecules* **2012**, *45* (4), 2128–2137.
(77) Shenoy, R.; Bowman, C. N. *Macromolecules* **2010**, *43* (19), 7964–7970.
(78) Wong, J.; Kaastrup, K.; Aguirre-Soto, A.; Sikes, H. D. *Polymer (Guildf).* **2015**, *69*, 169–177.
(79) Kizilel, S.; Sawardecker, E.; Teymour, F.; Pérez-Luna, V. H. *Biomaterials* **2006**, *27* (8), 1209–1215.
(80) Papavasiliou, G.; Songprawat, P.; Pérez-Luna, V.; Hammes, E.; Morris, M.; Chiu, Y.-C.; Brey, E. *Tissue Eng. Part C. Methods* **2008**, *14* (2), 129–140.
(81) de Beer, D.; Stoodley, P.; Lewandowski, Z. *Biotechnol. Bioeng.* **1997**, *53* (2), 151–158.
(82) Yaws, C. L. *Yaws' Handbook of Thermodynamic and Physical Properties of Chemical Compounds*; Knovel, 2003.
(83) Han, P.; Bartels, D. M. *J. Phys. Chem.* **1996**, *100* (13), 5597–5602.
(84) Bartholomew, R. F.; Davidson, R. S. *J. Chem. Soc. C Org.* **1971**, 2342–2346.
(85) Decker, C.; Jenkins, A. D. *Macromolecules* **1985**, *18* (6), 1241–1244.
(86) Bhanu, V. A.; Kishore, K. *Chem. Rev.* **1991**, *91* (2), 99–117.
(87) Neta, P.; Huie, R. E.; Ross, A. B. *J. Phys. Chem. Ref. Data* **1990**, *19* (2), 413.
(88) Chaimberg, M.; Cohen, Y. *AIChE J.* **1994**, *40* (2), 294–311.

(89) Gao, X.; Feng, W.; Zhu, S.; Sheardown, H.; Brash, J. L. *Macromol. React. Eng.* **2010**, *4* (3-4), 235–250.
(90) Zhou, D.; Gao, X.; Wang, W.; Zhu, S. *Macromolecules* **2012**, 1198–1207.
(91) Rahane, S. B.; Kilbey, S. M.; Metters, A. T. *Macromolecules* **2005**, *38* (20), 8202–8210.
(92) Turgman-Cohen, S.; Genzer, J. *J. Am. Chem. Soc.* **2011**, *133* (44), 17567–17569.
(93) Redmond, R. W.; Gamlin, J. N. *Photochem. Photobiol.* **1999**, *70* (4), 391–475.
(94) DeRosa, M. C.; Crutchley, R. J. *Coord. Chem. Rev.* **2002**, *233-234*, 351–371.